NEUTRON SCATTERING STUDIES OF THE DYNAMICS OF IMPERFECT CRYSTALS

NEUTRON SCATTERING STUDIES OF THE DYNAMICS OF IMPERFECT CRYSTALS

by

WILLIAM ATSUSHI KAMITAKAHARA, B.Sc.

A Thesis

Submitted to the Faculty of Graduate Studies

in Partial Fulfilment of the Requirements

for the Degree

Doctor of Philosophy

McMaster University

August 1972

DOCTOR OF PHILOSOPHY (1972)
(Physics)

McMASTER UNIVERSITY
Hamilton, Ontario

TITLE: Neutron Scattering Studies of the Dynamics of Imperfect Crystals

AUTHOR: William Atsushi Kamitakahara, B.Sc. (University of Toronto)

SUPERVISOR: Professor B. N. Brockhouse

NUMBER OF PAGES: x, 246

SCOPE AND CONTENTS: The effect of random mass disorder on the vibrational properties of simple crystals has been investigated by inelastic neutron scattering. Phonon frequencies and natural widths have been measured in alloy crystals of copper and gold containing 1, 3, and 9 atomic percent gold, in order to study the vibrational properties of the heavy gold atoms in the predominantly copper host lattices. Similar measurements have been made on a crystal of Ni(55%)Pd(45%) in order to investigate the nature of the atomic vibrations in a crystal in which the concentration of the heavy (Pd) atoms is very high. Detailed discussions are given to interpret the results in the light of existing theories.

The phonon dispersion curves of several copper-nickel alloys have been measured as part of a research program on the lattice dynamics of transition metals and their alloys.

An experiment to measure the phonon dispersion curves of silver has also been carried out.

ACKNOWLEDGEMENTS

Above all, I would like to thank my research supervisor, Professor B.N. Brockhouse, F.R.S., for his advice and encouragement at all stages of this work. His depth of knowledge and high professional standards provided a constant reference point.

I am also grateful to Dr. E.C. Svensson, with whom I collaborated on part of the work described in this thesis. Particular thanks are due to Dr. D.W. Taylor for helpful discussions on points of theory, for expert assistance in some of the analysis of experiment, and for a critical reading of parts of the manuscript.

To my colleagues in the neutron scattering group at McMaster University: Mr. J. Couper, Mr. D.H. Dutton, Mr. R.R. Dymond, Dr. E.D. Hallman, Mr. A. Larose, Dr. A.P. Miiller, Dr. S.C. Ng, Dr. A.P. Roy, and Dr. H.C. Teh, go my sincere thanks for providing a congenial and stimulating atmosphere, and for the innumerable occasions on which they have assisted me.

I am sincerely grateful to Mrs. H. Coxall, who patiently and accurately typed this manuscript.

This work was made possible through the financial support of the National Research Council of Canada, and of the Province of Ontario, and by the provision of research facilities by Atomic Energy of Canada Limited, Chalk River.

TABLE OF CONTENTS

			Page
CHAPTER I.	INTRODUCTION		1
A.	GENERAL PERSPECTIVE		1
B.	OUTLINE OF THE THESIS		7
C.	NEUTRON SCATTERING		11
	(i)	Introduction	11
	(ii)	Scattering by Crystals	14
	(iii)	Scattering by a General System	19
	(iv)	The Triple-Axis Crystal Spectrometer	26
D.	THEORY OF THE DYNAMICS OF IMPERFECT CRYSTALS		34
	(i)	Historical Survey	34
	(ii)	Basic Equations for the Imperfect Crystal	42
	(iii)	Results for Low Impurity Concentrations	52
	(iv)	Results for High Impurity Concentrations	55
CHAPTER II.	LATTICE VIBRATIONS AND RESONANT MODES IN CU(AU) ALLOYS		59
A.	INTRODUCTION		59
	(i)	Techniques for the Spectroscopy of Impurity Vibrations	59
	(ii)	Neutron Scattering Experiments on Impurity Vibrations	63
	(iii)	Choice of the Cu(Au) System	72

			Page
B.	EXPERIMENT		79
	(i)	The Specimen Crystals	79
	(ii)	Neutron Scattering Measurements	83
	(iii)	Results for Cu(9%Au)	86
	(iv)	Results for Cu(3%Au)	94
	(v)	Results for Cu(1%Au)	101
C.	DISCUSSION		104
	(i)	Important Features of the Experimental Results	104
	(ii)	Inclusion of Force Constant Changes	117
	(iii)	Other Factors	121
	(iv)	Other Experiments on Phonons and Magnons in Disordered Alloys	122
	(v)	Summary	124
CHAPTER III.	DYNAMICS OF AN IMPERFECT CRYSTAL WITH HIGH IMPURITY CONCENTRATION: NI(55%)PD(45%)		126
A.	INTRODUCTION		126
	(i)	General Remarks	126
	(ii)	Choice of the Ni-Pd System	131
B.	EXPERIMENT		138
	(i)	The Specimen Crystal	138
	(ii)	Neutron Scattering Measurements	139
	(iii)	Treatment of Resolution	144
C.	RESULTS AND DISCUSSION		149
	(i)	General Description of Experimental Results	149
	(ii)	Important Features of the Experimental Results	155

			Page
	(iii)	Comparison with Theory	163
		1) Perturbation Theory	163
		2) Self-Consistent Theory	171
		3) Low Concentration Theory	181
	(iv)	Factors other than Force Constant Changes	185
	(v)	Summary	190
CHAPTER IV.	CRYSTAL DYNAMICS OF COPPER-NICKEL ALLOYS		192
A.	INTRODUCTION		192
B.	EXPERIMENT		196
	(i)	The Specimen Crystals	196
	(ii)	Neutron Scattering Measurements	197
C.	RESULTS AND DISCUSSION		200
	(i)	General Description of Results	200
	(ii)	Absence of Disorder Broadening	200
	(iii)	Interpretation of Results	207
APPENDIX I	CRYSTAL DYNAMICS OF SILVER		212
APPENDIX II.	DATA TABLES		220
BIBLIOGRAPHY			237
REPRINTS OF PUBLISHED ARTICLES			

CRYSTAL DYNAMICS OF SILVER by W. A. Kamitakahara and B. N. Brockhouse, Physics Letters 29A, 639(1969).

RESONANT PERTURBATION OF PHONONS IN CU(AU) ALLOYS STUDIED BY NEUTRON SCATTERING by E. C. Svensson and W. A. Kamitakahara, Canadian Journal of Physics 49, 2291(1971).

LIST OF FIGURES

		Page
Fig. I-1	Schematic diagram of the McMaster (E2) triple-axis spectrometer at Chalk River	27
Fig. I-2	The constant-Q method	31
Fig. II-1	Characterization of Cu(Au) and Cu single crystals by neutron diffraction as described in the text.	82
Fig. II-2	Impurity-induced widths in Cu(9% Au) plotted against the frequency of the corresponding mode in pure copper	87
Fig. II-3	Impurity-induced frequency shifts for Cu(9% Au)	88
Fig. II-4	Widths Γ, and frequency shifts Δ, for three transverse branches in Cu(3% Au)	95
Fig. II-5	Impurity-induced widths for the $[00\zeta]T$ and $[\zeta\zeta 0]T_1$ branches in Cu(3% Au)	98
Fig. II-6	Impurity-induced frequency shifts for two transverse branches in Cu(1% Au)	102
Fig. II-7	Concentration dependence of resonances from Cu(3% Au) to Cu(9% Au)	109
Fig. II-8	The calculations of Svensson (1967) for the line shapes in Cu(3% Au) and Cu(9% Au) from mass defect theory	113
Fig. II-9	Neutron groups for the $[\zeta\zeta\zeta]T$ branch in Cu(9% Au)	114
Fig. II-10	Representative neutron groups for the $[\zeta\zeta 0]T_1$ branch in Cu(3% Au) and Cu(9% Au), and for $[00\zeta]T$ in Cu(3% Au)	116
Fig. III-1	Reciprocal space diagram illustrating a double scattering process	142

		Page
Fig. III-2	A pair of neutron groups for Ni(55%) Pd(45%) showing the dependence of a spurious 'tranverse' peak on the mode of spectrometer operation	142
Fig. III-3	Effect of resolution extraction procedure on widths	148
Fig. III-4	Dispersion curves (bottom) and natural widths (top) observed along three symmetry directions in Ni(55%) Pd(45%)	150
Fig. III-5	Observed neutron groups for the $[\zeta\zeta\zeta]T$ branch of Ni(55%)Pd(45%)	152
Fig. III-6	Typical neutron groups used in obtaining the data points of Fig. III-4, showing modes of low and higher wave vector in three different branches	153
Fig. III-7	The natural widths for Ni(55%)Pd(45%) plotted for each branch as a function of the reference lattice frequency	158
Fig. III-8	Widths for Ni(55%)Pd(45%) predicted by perturbation theory	168
Fig. III-9	Line shapes of the coherent neutron scattering cross section predicted for Ni(55%)Pd(45%) by the self-consistent mass defect theory of Taylor	177
Fig. III-10	Neutron groups for the $[\zeta\zeta 0]T_1$ branch in Ni(55%)Pd(45%)	179
Fig. III-11	Line shapes predicted for Ni(55%)Pd(45%) by low concentration mass defect theory	183
Fig. IV-1	Characterization of three Cu-Ni alloy crystals by neutron diffraction	198
Fig. IV-2	Measured dispersion curves of Cu(59%) Ni(41%) compared with those of copper (Svensson et al, 1967)	201
Fig. IV-3	The dispersion curves for the $[\zeta\zeta 0]T_2$ and $[\zeta\zeta 0]L$ branches of Cu(95%)Ni(5%) and Cu(80%)Ni(20%)	202
Fig. IV-4	Neutron groups for $[0\zeta 1]\Pi$, $\zeta=0.5$, in three Cu-Ni alloys	206

		Page
Fig. IV-5	Composition dependence of first and second neighbour force constants for Fe-Ni, Cu-Ni, and Cu-Zn alloys	208
Fig. AI-1	The phonon dispersion curves of silver at room temperature	216

LIST OF TABLES

		Page
Table II-1	Characteristics of copper and copper-gold crystals	80
Table III-1	Properties of nickel and palladium	132
Table III-2	Force constants of Pd, Ni and a mean crystal model of Ni(55%)Pd(45%)	135
Table IV-1	Characterization of Cu-Ni alloy crystals	197
Table AI-1	Properties of copper, silver and gold	213
Table AI-2	Atomic force constants of silver and copper	217
Table AII-1	Phonon frequency shifts Δ and widths Γ in Cu(9% Au)	221
Table AII-2	Phonon frequency shifts Δ and widths Γ in Cu(3% Au)	223
Table AII-3	Phonon frequency shifts in Cu(1% Au)	226
Table AII-4	Phonon frequencies ν and natural widths Γ in Ni(55%)Pd(45%)	227
Table AII-5	Phonon frequencies in Cu-Ni alloys	231
Table AII-6	Phonon frequencies in silver at 296°K	236

CHAPTER I

INTRODUCTION

A. GENERAL PERSPECTIVE

During the twelve years that have passed since the first spectroscopic experiments on impurity vibrations, there has been an increasing interest in the nature of elementary excitations in imperfect crystals. The term 'imperfect crystal' in the following refers only to substitutional disorder, although it is more usually taken to include crystals containing other types of defects. In substitutionally disordered crystals, the lattice sites of the system still form a periodic array, although the type of atom present at a particular site varies randomly. Many aspects of the lattice vibrational, magnetic, and electronic excitations in such systems have been intensively studied in interrelated theoretical and experimental investigations. Of the three basic types of excitations, the problem of describing the lattice vibrations in imperfect crystals is conceptually the simplest and also the most readily accessible to experiment. The purpose of this thesis is to describe some experiments in which are investigated some fundamental aspects of the dynamics in systems containing both fairly low (1, 3, and 9 atomic percent Au in Cu) and very high (45 atomic percent Pd in Ni) concentrations of heavy atoms. The constituents in these face-centred cubic alloys have masses that differ by a factor of two or three,

but are chemically analogous; they are noble and transition metals whose lattice dynamics in perfect crystals are particularly simple. The method that is used in the experiments is coherent inelastic neutron scattering, which to date has revealed the most detailed information on the dynamics of perfect crystals, but has been applied to imperfect crystals in only a few cases.

In any solid, crystalline or not, the constituent atoms are vibrating about their equilibrium positions. Even at the absolute sero of temperature, there is zero-point motion, which in the case of very light atoms (H, He) may be substantial. The study of these oscillatory motions and their origin in the microscopic physical forces in the solid, as well as their influence on macroscopic physical properties, constitute the subject of lattice dynamics. In a perfectly periodic array of atoms connected by harmonic (Hooke's Law) forces, each normal mode of the system is a plane wave whose frequency is dependent on the wave vector. The connection between frequency and wave vector (the dispersion relation) and the amplitude, relative phase, and direction of vibration (polarization vector) for each type of atom in any particular normal mode, are determined by the interatomic forces.

If the translational symmetry is destroyed by the introduction of substitutional disorder, the plane waves are no longer true normal modes of the system. Phonons, the quanta of the waves, then do not propagate without scattering, but

have a definite lifetime, or equivalently, a frequency or energy width. In addition, modes of special character can be formed in certain cases. The occurrence of high frequency localized modes for sufficiently light or strongly bound impurities, and of quasi-localized resonance modes for sufficiently heavy or weakly bound impurities, probably represents the most thoroughly studied aspect of imperfect crystal dynamics.

In order to properly indicate the type of information that one hopes to gain in a neutron scattering experiment, perhaps it is instructive at this point to list, from the point of view of the neutron experimentalist, the most important questions that one can ask about the dynamics of imperfect crystals. The following come to mind:

1) What are the changes in the frequency spectrum of the lattice vibrations when impurities are introduced? This question is of particular interest when the impurity concentration becomes large.

2) How do the impurity atoms differ in their individual motions from the host atoms, and how are the motions of the host atoms affected by the presence of the impurities? Are there any localized states formed?

3) What are the widths and frequency shifts of the formerly sharp states labelled with wave vector $\underline{q}$ and frequency ν?

4) How do the answers to 1), 2), and 3) depend on mass

and force constant differences, and on the defect concetration and the amount of order present?

5) What are the miscroscopic physical characteristics of different types of impurities in real physical systems, and how do these influence the defect vibrations?

6) How do the vibrational properties of the imperfect crystal influence measurable physical properties, notably thermal, electrical, optical, and scattering properties?

Coherent neutron scattering allows one to directly answer question 3) above. The impurity concentrations in the experiments described in the following chapters range from 1 atomic percent to 45 atomic percent, and the mass differences from 8 percent to a factor of three, enabling significant information to be obtained about question 4). In the experiment on Cu(Au), described in Chapter II, and in the experiment on Ni-Pd, Chapter III, the quasi-localized 'resonance modes' associated with the heavy atoms are considered in detail; this concerns us with question 2). As has been mentioned, the experiments reported here deal with face-centred cubic noble and transition metal alloys. Neutron scattering, in contrast to optical spectroscopy, allows one to study metals and, concurrently, disorder effects in simple monatomic structures. The experiments on Cu(Au) and Ni-Pd indicate the presence of sizable force constant changes. Since detailed information about the behaviour of individual modes is revealed in these experiments, it is possible that fitting to the measurements will allow significant

information to be obtained about the nature of the force constant changes (question 5))for the case of an impurity atom in a simple metal.

The disorder, from the lattice dynamics point of view, has two aspects. The first is that the substitutional impurity has a mass different from that of the atom it replaces. The second aspect is that the force constants connecting the impurity to its neighbours may be different from the force constants connecting two host atoms, and the latter may themselves differ from those that existed in the pure host crystal. The changes produced in the host-host force constants merit expecially careful consideration when the defects are present in finite concentration. In fact, when one goes to very high impurity concentrations, the force constant changes may depend on the local environment of the pair of atoms involved. In this thesis, we investigate primarily the effects of mass disorder, since this aspect of the problem leads to more interesting effects, and is also theoretically much easier to treat. However, from a large number of experiments by means of optical and neutron techniques, it now seems that mass and force constant changes, although conceptually separable, probably occur together in most real physical systems. A substituted atom that differs substantially in mass from the one it replaces will almost certainly have important force constant changes associated with it.

In the Cu(Au) and Ni-Pd experiments, we find this to be the case. Apart from this, concentration effects on going from 3 to 9 atomic percent Au in Cu are also observed. The detailed investigation of lattice dynamics in a crystal with a very large impurity concentration is an area in which the coherent neutron scattering method reveals information available by no other means. The Ni-Pd experiment represents the first detailed investigation by coherent scattering of a monatomic imperfect crystal with a very high degree of mass disorder. The results indicate that although the phonons in such a system are strongly broadened, the behaviour of the broadening as a function of frequency and wave vector bears considerable qualitative similarity to that found at much lower impurity concentrations. This gives hope that the dynamics of such crystals may be understandable from a reasonably simple point of view.

B. OUTLINE OF THE THESIS

In the remainder of this chapter, the background material necessary to understand and appreciate the experimental work in the thesis, and its analysis, is presented. None of this background material is original. Included are a section on the technique of inelastic neutron scattering, and one on the theory of the dynamics of imperfect crystals. The latter section consists of a brief historical survey of the subject, emphasizing material directly relevant to the thesis topic, followed by an introduction to the theoretical material used in later chapters.

Chapter II presents the results of a neutron scattering experiment on the crystal dynamics of dilute Cu(Au) alloys. The purpose of this experiment was to observe, at fairly low impurity concentrations (1, 3, and 9 atomic percent), the perturbation of the lattice vibrational modes produced by the presence of the impurity Au atoms. A gold atom is 3.1 times as heavy as one of copper, but has similar chemical and electronic properties. It was thus hoped that the gold atom would simulate, as well as possible, the case of a substitutional impurity which differs from the atom it replaces only through its much larger mass. If such an assumption were valid, the existing theories of crystals containing such impurities ('mass-defect' theories) could be tested by the experiment. In particular, specific calculations by Elliott and Maradudin (1965) predicted a strong resonant

perturbation of the phonon dispersion curves would be observable by neutron scattering, arising from a well-developed 'resonance mode' of the heavy gold atom in the predominantly copper lattice.

The Cu(Au) experiment was initiated by Svensson and Brockhouse as part of the Ph.D. work of E.C. Svensson (thesis, McMaster University, 1967). There have been two publications, prior to the author's involvement, in connection with Cu(Au) (Svensson, Brockhouse and Rowe, 1965, Svensson and Brockhouse, 1967). The experiments described in Chapter II below are a continuation of this work, involving extensive further measurements and analysis. The tentative conclusions of the earlier experiments have been strongly modified as a consequence of these results. Most of the data presented in Chapter II, and their analysis, have already been described in a paper published in the Canadian Journal of Physics (Svensson amd Kamitakahara, 1971). However, a considerable amount of new and unpublished material, consisting of further neutron measurements as well as a more detailed discussion, has also been included.

Chapter II begins with a brief description of other experimental techniques used for the spectroscopy of impurity vibrations, followed by a survey of neutron scattering experiments reported to date on this topic. A detailed description of the experiment on Cu(Au) is then given, and finally the results are discussed with reference to calculations based on mass defect theory. Some of the material presented in Chapter

II is the work of E.C. Svensson, including most of the calculations. Most of the measurements were taken by the author.

If, in a two-component random alloy, the heavy atoms are present in such a high concentration that they can in no way be considered to be impurities, the theoretical description of the dynamics becomes much more complicated and uncertain. The problem is conceptually a simple and important one, and yet is basically unsolved mathematically. All of the theories extant involve highly questionable assumptions necessitated by the complexity of the calculations. In order to improve the understanding of such systems, the phonon dispersion curves and disorder-induced widths were measured in a crystal of the face-centred cubic random alloy Ni(55 at.%) Pd(45 at.%). (Pd is 1.8 times as heavy as Ni.) These measurements are presented and discussed in Chapter III. Because of the substantial amount of disorder present in this alloy, the width for a phonon of higher wave vector is often found to be a large fraction of the mean frequency of the mode. Thus we were able to carry out a more accurate and complete determination of natural widths than has been done in previous experiments by coherent neutron scattering. Behaviour characteristic of resonance modes was found to persist into the high concentration regime. In fact, the results show a good deal of similarity to those obtained for Cu(Au). The experiment is compared with calculations based on the theory of D.W. Taylor (1967), whose treatment of the dynamics of mass-disordered

crystals is probably the most realistic attempt to date on this topic, for which detailed calculations have been made. Simpler models are considered as well.

In Chapter IV are presented the results of a more straightforward type of lattice dynamics experiment, in which are measured the dispersion curves of random binary metallic alloys whose constituents do not differ greatly in mass, but have dissimilar chemical properties and electronic structure. Experience has shown that the phonons in such materials do not in general possess large widths. The dispersion curves are thought to reflect the average electronic structure. Complete dispersion curve measurements for four copper-nickel alloys, containing 20,40, 80, and 90 at. % Ni, are described in Chapter IV. Some measurements were also made on a copper-nickel crystal containing 5 at.% Ni.

Appendix I contains a description of an experiment to determine the phonon dispersion curves of silver (Kamitakahara and Brockhouse, 1969).

Appendix II contains tables of the phonon frequencies and widths for the experiments of Chapters II, III, IV, and Appendix I.

C. NEUTRON SCATTERING

(i) Introduction

Neutrons have several properties that make them ideal probes for the study of structure and dynamics in condensed matter. These may be listed as follows:

1) There are two important interactions of a thermal neutron with the atoms of the scatterer, both of which take a simple form. The first is with the nuclei, and produces absorption and isotropic scattering by each nucleus in an amount determined by the type of nucleus and the orientation of the nuclear spin with respect to the spin of the neutron. For nuclei with low energy neutron resonances, the absorption cross-section may show a dependence, but usually not a strong one, on the neutron energy. The second is a purely magnetic interaction of the neutron moment with the magnetic moments of unpaired electrons or with atomic orbital moments.

2) Because they are neutral particles, neutrons penetrate deeply into condensed matter and have a low probability of scattering in a volume that can be considered to be macroscopic.

3) The wavelength of a thermal neutron (usually in the range 0.5 to 10 Å) is of the order of interatomic distances in condensed matter, while its energy is comparable with the energies of two of the most important types of excitations, namely phonons and magnons in ordered structures, or their analogues in liquids and paramagnetics. In the following,

only non-magnetic scattering is discussed.

The scattering from condensed matter is usually treated in the first Born approximation, which is basically justified in the second property listed above. The approximation refers not to the nuclear potential, whose exact form is not even known, but to the fact that one can have a macroscopic scatterer in which the probability of multiple scatterings is very small. The nuclear potential is customarily replaced by the so-called Fermi pseudopotential, which has the form

$$V(\underline{r}) = \frac{2\pi\hbar^2}{m} b\, \delta(\underline{r}) \qquad (I\text{-}1)$$

where m is the mass of the neutron. The scattering length b is chosen so as to give the correct cross-section for a single bound atom, $\sigma = 4\pi|b|^2$, and is allowed to be complex in order to account for the possible phase change of the neutron wave in the scattering. In practice, b can almost always be considered to be a real number, but may be positive or negative.

In most cases, the scattering from an assembly of atoms can be separated into two parts: the coherent and the incoherent scattering. These may be roughly described as the interferent and non-interferent parts of the scattered-neutron waves. Whenever there is an uncertainty in the scattering length associated with a particular type of site or position within the scatterer, the scattered waves from atoms located at different positions will be partially non-interferent,

giving rise to incoherent scattering. The differing scattering lengths may be caused by the presence of different elements, or by different isotopes of the same element, or by different nuclear spin states for the same isotope. (As mentioned above, the scattered amplitude can depend on the orientation of the nuclear spin with respect to the spin of the incident neutron.)

The natural variables to describe a neutron scattering experiment are the wave vector transfer to the scatterer

$$\underline{Q} = \underline{k}_o - \underline{k}' \qquad \text{(I-2a)}$$

and the energy transfer

$$\hbar\omega = \frac{\hbar^2}{2m} (k_o^2 - k'^2) = E_o - E' \quad . \qquad \text{(I-2b)}$$

The neutron has a wave vector $\underline{k}_o$ before the scattering and $\underline{k}'$ afterwards. E_o and E' are the incident and scattered neutron energies respectively. The direction as well as the magnitude of the wave vector transfer is important for experiments in which the specimen has directional properties. The angle of scattering ϕ is given by

$$Q^2 = k_o^2 + k'^2 - 2k_o k' \cos\phi \quad . \qquad \text{(I-3)}$$

(ii) Scattering by Crystals

If the neutron scatters inelastically with the creation or annihilation of a single phonon of angular frequency $\omega_j(\underline{q})$, the scattering is governed by the conservation conditions

$$\underline{Q} = 2\pi\underline{\tau} - \underline{q} \qquad \text{(I-4a)}$$

and

$$\hbar\omega = \pm \hbar\omega_j(\underline{q}) \qquad \text{(I-4b)}$$

where $\underline{\tau}$ is a reciprocal lattice vector. The upper sign indicates a process in which a phonon is created, and the lower sign one in which a phonon is annihilated. Thus the energy spectrum of initially monochromatic neutrons scattered from a single crystal with a particular wave vector transfer $\underline{Q}$, has several very sharp peaks at the energies $E_o \pm \hbar\omega_j(\underline{q})$. Measurement of the position of these peaks determines experimentally the dispersion relation $\omega_j(\underline{q})$. The unambiguous and detailed nature of the information thus obtained should be noted. A quasi-continuous spectrum of excitations is being characterized in a very detailed manner, through the ability to simultaneously measure, in addition to the phonon energy, another important quantum number, the phonon wave vector.

In principle, the conservation conditions expressed in Eqs. I-4 are all one needs to know in order to measure dispersion curves. With these in mind, neutron inelastic

scattering experiments on crystal dynamics had already been initiated in the early 1950's when the experiments were put on a firm theoretical base.

Placzek and Van Hove (1954) first calculated the cross section to be expected for one-phonon inelastic scattering from crystals. By one-phonon scattering is meant that part of the inelastic scattering obtained by making the approximation of small displacements of the scatterers from their equilibrium positions, so that

$$\langle \exp\{-i\underline{Q}\cdot\underline{u}(\ell,0)\}\exp\{i\underline{Q}\cdot\underline{u}(\ell',t)\}\rangle$$

$$\simeq \exp(-2W)\,[1 + \langle \underline{Q}\cdot\underline{u}(\ell,0)\,\underline{Q}\cdot\underline{u}(\ell',t)\rangle] \qquad \text{(I-5)}$$

where $\underline{u}(\ell,t)$ is the operator for the displacement of the ℓth nucleus at time t, and $\exp(-2W)=\exp\{-\langle[\underline{Q}\cdot\underline{u}(\ell,0)]^2\rangle\}$ is the Debye-Waller factor. The term $\langle\underline{Q}\cdot\underline{u}(\ell,0)\underline{Q}\cdot\underline{u}(\ell',t)\rangle$ gives rise to one-phonon scattering. In the following subsection, I-C(iii), it will be shown how quantities like the left hand side of Eq. I-5 enter into the scattering cross sections. Placzek and Van Hove obtained, essentially, the following expression for the coherent scattering cross section, per nucleus, from a monatomic crystal.

$$\frac{d^2\sigma^{coh}}{d\Omega dE'} = \bar{b}^2\,\frac{(2\pi)^3}{VN}\,\frac{k'}{k_o}\,\frac{\hbar}{2M\omega}\sum_{j\underline{q}}[\underline{Q}\cdot\underline{\xi}_j(\underline{q})]^2\exp(-2W)$$
$$\times[n(\omega)+1]\,\delta(\underline{Q}-2\pi\underline{\tau}+\underline{q})\,\delta(\hbar\omega\pm\hbar\omega_j(\underline{q})) \qquad \text{(I-6)}$$

In the second delta function, the minus sign is taken for $\omega>0$ and the plus sign for $\omega<0$. $\bar{b}$ is the average scattering length

of a nucleus, V is the volume of a primitive unit cell, $n(\omega)$ is the Bose-Einstein distribution function $(\exp(\hbar\omega/k_B T)-1)^{-1}$, $\exp(-2W)$ is the Debye-Waller factor, M is the mass of a nucleus, and $\underline{\xi}_j(\underline{q})$ is the polarization vector associated with the normal mode of frequency $\omega_j(q)$. The delta functions imply conservation of energy and wave vector, as expressed in Eqs. I-4.

For a cubic monatomic crystal, the incoherent scattering cross section takes an equally simple and significant form.

$$\frac{d^2\sigma^{inc}}{d\Omega dE'} = (\overline{b^2} - \bar{b}^2)\ \frac{k'}{k_o}\ \frac{1}{2M\omega}\ Q^2\ \exp(-2W)\ [n(\omega)+1]g(\omega) \qquad (I-7)$$

The function $g(\omega)$ is the phonon frequency distribution of the crystal; for convenience we define $g(-\omega) = g(\omega)$. Thus for elements with body-centred cubic or face-centred cubic structures, the phonon frequency distribution can in principle be directly determined from the incoherent cross section in a fashion similar to the determination of dispersion curves from the coherent cross section.

These two equations contain a great deal of information about how an inelastic scattering experiment is to be done. Neutron experiments are inherently low intensity measurements compared with optical or X-ray methods because of the weakness of the source in terms of quanta per unit time. Therefore, some thought must be devoted to insuring adequate

counting rates. For example, it may be noted that the cross section in neutron energy loss ($\omega>0$, phonon creation) is proportional to $[n(\omega) + 1]$, while in energy gain ($\omega<0$, phonon annihilation), it is proportional* to $n(-\omega)$. The factor $[n(\omega) + 1]$ is always larger than $n(\omega)$ for positive ω and is much larger at higher frequencies and low temperatures. This means that experiments are usually done in neutron energy loss rather than in energy gain. This makes sense, since at low temperatures, the higher frequency states are unpopulated, and there are no phonons for the neutrons to annihilate. Each factor in Eqs. I-6 and I-7 is important, and each is carefully considered at some time during the course of an experiment.

The generalization of Eqs. I-6 and I-7 to the case of more than one atom per unit cell yields a form that is not much more complicated. For a polyatomic crystal, the cross section per unit cell is

$$\frac{d^2\sigma^{coh}}{d\Omega dE'} = \frac{k'}{k_o}\frac{\hbar}{2\omega}\frac{(2\pi)^3}{VN}\sum_{j\underline{q}} g_j(\underline{Q})\ [n(\omega)+1] \times \delta(\underline{Q}-2\pi\underline{\tau}+\underline{q})\,\delta(\hbar\omega\pm\hbar\omega_j(q)) \quad . \tag{I-8}$$

where $g_j(\underline{Q})$, called the 'inelastic structure factor', is given

---

* Equations I-6, 7, and 8 are valid for both energy loss. It is easily shown that $[n(\omega) + 1]/\omega = -n(-\omega)/\omega$.

by

$$g_j(\underline{Q}) = \left| \sum_s \bar{b}_s \, \underline{Q}\cdot\underline{\xi}_j(q) \, \exp(i\underline{Q}\cdot\underline{r}_s) M_s^{-1/2} \, \exp(-W_s) \right|^2 \qquad \text{(I-9)}$$

The last summation is over the atoms of the unit cell, located at positions $\underline{r}_s$ within the cell. The intensity of a one-phonon peak in the double-differential cross section, integrated over E', at a particular $\underline{Q}$, is proportional to $g_j(\underline{Q})$.

Experimentally, the measurement of the dispersion curves of simple polyatomic crystals differs little from the procedure for monatomic crystals, except that now one must take account of the modulating factor $g_j(\underline{q})$, instead of simply $\bar{b}^2 \, [\underline{Q}\cdot\underline{\xi}_j(\underline{q})]^2 \, M^{-1} \exp(-2W)$. The dispersion curves of very many crystalline substances have now been measured, ranging from such simple substances as the alkali metals to, in a few cases, fairly complicated molecular crystals. For crystals with many atoms per unit cell and low symmetry, the multiplicity of branches and the finite resolution of a neutron spectrometer make determination of complete dispersion relations much more difficult. (For example, see Powell et. al., 1972.)

One can write an expression similar to Eq. I-8 for tne one-phonon incoherent scattering from polyatomic crystals, but its experimental application is much more limited. The cross section is no longer proportional to $g(\omega)$, but generally still resembles it qualitatively, enabling useful information to be

obtained in many cases (Brockhouse et. al., 1964, pp. 595-9).

Phonons in perfect crystals are not the only excitations that can be studied by means of the scattering of slow neutrons. In fact, the technique can be applied quite generally to investigations of the structure and dynamics of interacting particle or spin systems in dense matter. The generality of the technique was first emphasized in the fundamental papers of Van Hove (1954a, 1954b).

(iii) Neutron Scattering by a General System

It is a well-known fact in crystallography that a measured diffraction pattern cannot be directly inverted into a structure. There is always an intermediate step in which physical principles and/or symmetry principles come into play. The difficulty arises because one measures the scattered neutron or X-ray intensity, and not the scattered amplitude, thereby losing knowledge of the phases of the scattered waves. What the crystallographer can, and usually does, obtain directly is the Fourier transform ($\underline{Q} \rightarrow \underline{r}$) of the elastically scattered intensity, which turns out to be proportional to the time-averaged pair correlation function of the scattering density.

Van Hove (1954a) was able to provide a quantum mechanical generalization of these concepts to systems in which the time dependence of the scattering density is considered. From the quantum viewpoint, the time dependence is equivalent to saying that the state of the system may change in the scattering, i.e., there is inelastic scattering.

The potential of the crystal as seen by a neutron can be written as

$$U(\underline{r}) = \sum_j V_j(\underline{r}-\underline{R}_j(t)) \qquad \text{(I-10)}$$

where V_j is the potential of the jth scatterer, located at the position $\underline{R}_j(t)$. If $U(\underline{r})$ is regarded as a time-dependent perturbation on the incident neutron wave, then the result for the scattering cross section in the first Born approximation is given by

$$\frac{d^2\sigma}{d\Omega dE'} = \frac{k'}{k_o} S(\underline{Q},\omega) \qquad \text{(I-11)}$$

where
$$S(Q,\omega) = \left(\frac{m}{2\pi\hbar^2}\right)^2 \sum_{if} g_i \left|\langle i \left| \sum_j V_j(\underline{Q}) \exp[i\underline{Q}\cdot\underline{R}_j(0)] \right| f\rangle\right|^2 \times \delta(E_o - E' + E_i - E_f) \qquad \text{(I-12)}$$

and
$$V_j(\underline{Q}) = \int V_j(\underline{r}) \exp(i\underline{Q}\cdot\underline{r})\, d\underline{r} \quad . \qquad \text{(I-13)}$$

The statistical weighting factor g_i, a Boltzmann factor, allows an average to be taken over the initial states $|i\rangle$ of the scattering system. E_i and E_f are the energies of the initial and final quantum states. The positions $\underline{R}_j$ are operators. These equations can be derived (Powell and Crasemann, 1961; Marshall and Lovesey, 1971) in a straightforward manner from time dependent perturbation theory and are the starting point of Van Hove's paper.

Van Hove defines a function which turns out to be the time-dependent generalization of the static or time-averaged pair correlation function. Assuming for the moment that all the scattering centres are identical, and replacing the neutron-nucleus potential by the Fermi pseudopotential of Eq. I-1, one can define

$$G(r,t) = \frac{\hbar}{(2\pi)^3 b^2} \int \exp\{-i(\underline{Q}.\underline{r}-\omega t)\} S(\underline{Q},\omega)\, d\underline{Q}\, d\omega \qquad \text{(I-14)}$$

or equivalently,

$$S(\underline{Q},\omega) = \frac{b^2}{(2\pi\hbar)} \int \exp\{i(\underline{Q}.\underline{r}-\omega t)\} G(\underline{r},t)\, d\underline{r}\, dt \qquad \text{(I-15)}$$

$G(\underline{r},t)$ is the probability (per unit volume and per unit time) that, given a scattering centre at the origin ($\underline{r}=\underline{0}$) at time zero, there will be another scattering center at position $\underline{r}$ at time t.

In cases where the particles of the scattering system can be regarded as distinguishable, $G(\underline{r},t)$ can be separated into two parts: $G(\underline{r},t)=G_s(\underline{r},t)+G_d(\underline{r},t)$. The s stands for 'self' and d for 'distinct'. G_s represents the probability that, given a particle at $(\underline{0},0)$, the <u>same</u> particle will be found at (r,t), whereas G_d is the probability that it will be a <u>different</u> particle.

Many of the properties of $G(\underline{r},t)$ and $S(\underline{Q},\omega)$ are derived and discussed by Van Hove (1954a, 1958). A comprehensive

account of these properties and of many other aspects of the theory of neutron scattering is contained in the monograph by Marshall and Lovesey (1971).

Direct manipulation of Eq. I-12 yields another useful form:

$$S(\underline{Q},\omega)= \frac{b^2}{2\pi\hbar N} \int \exp(-i\omega t) \sum_{\ell\ell'} \langle \exp\{-i\underline{Q}.\underline{R}_\ell(0)\} \exp\{i\underline{Q}.\underline{R}_{\ell'}(t)\} \rangle \, dt \qquad \text{(I-16)}$$

In this equation, $\underline{R}_\ell(t)$ is the Heisenberg operator for the position of the ℓth nucleus; $\underline{R}_\ell(t) = \exp(iHt/\hbar)\underline{R}_\ell(0)\exp(-iHt/\hbar)$, where H is the Hamiltonian of the scattering system. The brackets $\langle \ \rangle$ denote a thermal average.

For glasses and crystals, the exponentials can be expanded about the equilibrium positions of the atoms. Retaining only the first non-zero term in the product gives elastic scattering, the second gives one-phonon inelastic scattering, (as detailed in the preceding subsection for the case of crystals), the third gives two-phonon inelastic scattering, and so on. For future reference, we write down the one-phonon coherent contribution explicitly.

$$S^{(1)}_{coh}(\underline{Q},\omega)= \frac{b^2}{2\pi\hbar N} \int \exp(-i\omega t) \sum_{\ell\ell'} \exp\{i\underline{Q}.(\underline{R}_\ell-\underline{R}_{\ell'})\} \exp(-2W)$$

$$\times \langle \underline{Q}.\underline{u}_\ell(0)\underline{Q}.\underline{u}_{\ell'}(t) \rangle \, dt \qquad \text{(I-17)}$$

In section D of this chapter, an outline will be given

of the calculation of a correlation function similar to $\langle \underline{Q}.\underline{u}_{\ell}(0)\underline{Q}.\underline{u}_{\ell'}(t)\rangle$ for crystals containing defects.

If allowance is made for variation in the scattering length, then $b^2 G(\underline{r},t)$ in Eq. I-15 is replaced by

$$\Gamma(r,t) = \overline{b^2}\, G_s(\underline{r},t) + \overline{b}^2\, G_d(\underline{r},t) \qquad \text{(I-18)}$$

and the corresponding coherent and incoherent cross sections are given by the following expressions:

$$\frac{d^2\sigma^{coh}}{d\Omega dE'} = \frac{\overline{b}^2 N}{2\pi\hbar}\frac{k'}{k_o}\int \exp\{i(\underline{Q}.\underline{r}-\omega t)\}G(\underline{r},t)\,d\underline{r}\,dt \qquad \text{(I-19)}$$

$$\frac{d^2\sigma^{inc}}{d\Omega\, E'} = \frac{(\overline{b^2}-\overline{b}^2)N}{2\pi\hbar}\frac{k'}{k_o}\int \exp\{i(\underline{Q}.\underline{r}-\omega t)\}G_s(\underline{r},t)\,d\underline{r}\,dt \qquad \text{(I-20)}$$

The formalism which has been briefly described here is important for several reasons. In the first place, simply defining $S(\underline{Q},\omega)$ makes it clear that it is the wave vector and energy <u>transfers</u> that are important and not the incident and scattered neutron energies themselves. That is to say, in order to investigate the dynamics of a system, one does not have to study the dependence of the scattering on the six variables E_o, E', ϕ and α,β,γ (orientation variables of the specimen relative to the incident beam), but just on the four variables $\underline{Q},\omega$. With rare exceptions, all the information about the scatterer than can be obtained in a scattering experiment is contained in $S(\underline{Q},\omega)$. Even if the Fourier inversion cannot

be done, the formalism enables the experimenter to interpret his data (sometimes by Fourier transforming a model $G(\underline{r},t)$ to compare with the experimental $S(\underline{Q},\omega)$) with some degree of physical understanding.

For perfect crystals, the Van Hove formalism is not really so useful, since the cross section can be directly calculated (Placzek and Van Hove, 1954) in terms of phonons without its use. However, for anharmonic or imperfect crystals, the formalism does serve to emphasize that the observed cross section is related to a correlation function of a particularly simple form, and hence is amenable to calculation by the methods of thermodynamic Green's functions (Zubarev, 1960). For imperfect crystals, the separation of G into G_s and G_d also has some significance. G_s reflects the motion of individual atoms and G_d the relative motion of pairs of atoms. In low concentration mass defect theory (Elliott and Taylor, 1967), G_s turns out to be composed of parts that reflect whether the individual atoms are host or defect atoms, and G_d contains parts that reflect whether the two atoms are two host atoms, two defect atoms, or a host and a defect atom. In some cases, the qualitative behaviour of a particular component shows up particularly strongly in the neutron cross section. In particular, the large individual motion of a heavy mass defect in a resonance mode shows up as a pronounced peak in the incoherent inelastic cross section at the resonance mode frequency. More generally, it might be stated that in a disordered alloy in

which the characteristics of the atomic vibrations are expected to depend strongly on the type of atom, one should try to keep track of the physical sources of the coherent and incoherent inelastic scattering cross sections.

(iv) The Triple-Axis Crystal Spectrometer

In an inelastic scattering experiment, the production of the primary monochromatic beam and the energy analysis of the neutrons scattered from the specimen can each be done by one of two principal methods: either by neutron time-of-flight over a given path or by Bragg reflection from a single crystal. Polycrystalline filters, usually beryllium, which has a high transmission for neutron energies below a sharp cut-off at about 0.005 eV, are also commonly used in neutron spectroscopy. For discussions on the relative merits and areas of applicability of various types of spectrometers, see the review articles of Brockhouse (1961) and Brockhouse et. al. (1964), and the proceedings of a panel on instrumentation for neutron inelastic scattering research (IAEA, Vienna, 1970). The instrument that uses single crystals for both monochromator and analyser is the triple-axis crystal spectrometer. It has proven to be the most efficient instrument for the investigation of crystal dynamics.

Figure I-1 shows a schematic diagram of the crystal spectrometer used for all the phonon measurements contained in the thesis. This instrument was constructed primarily by E.D. Hallman and G.A. de Wit (Brockhouse, de Wit, Hallman, and Rowe, 1968) and is located at the E2 facility of the NRU reactor, Chalk River. A white neutron beam, with an approximately Maxwellian spectrum corresponding to the moderator temperature, is incident upon the monochromating crystals.

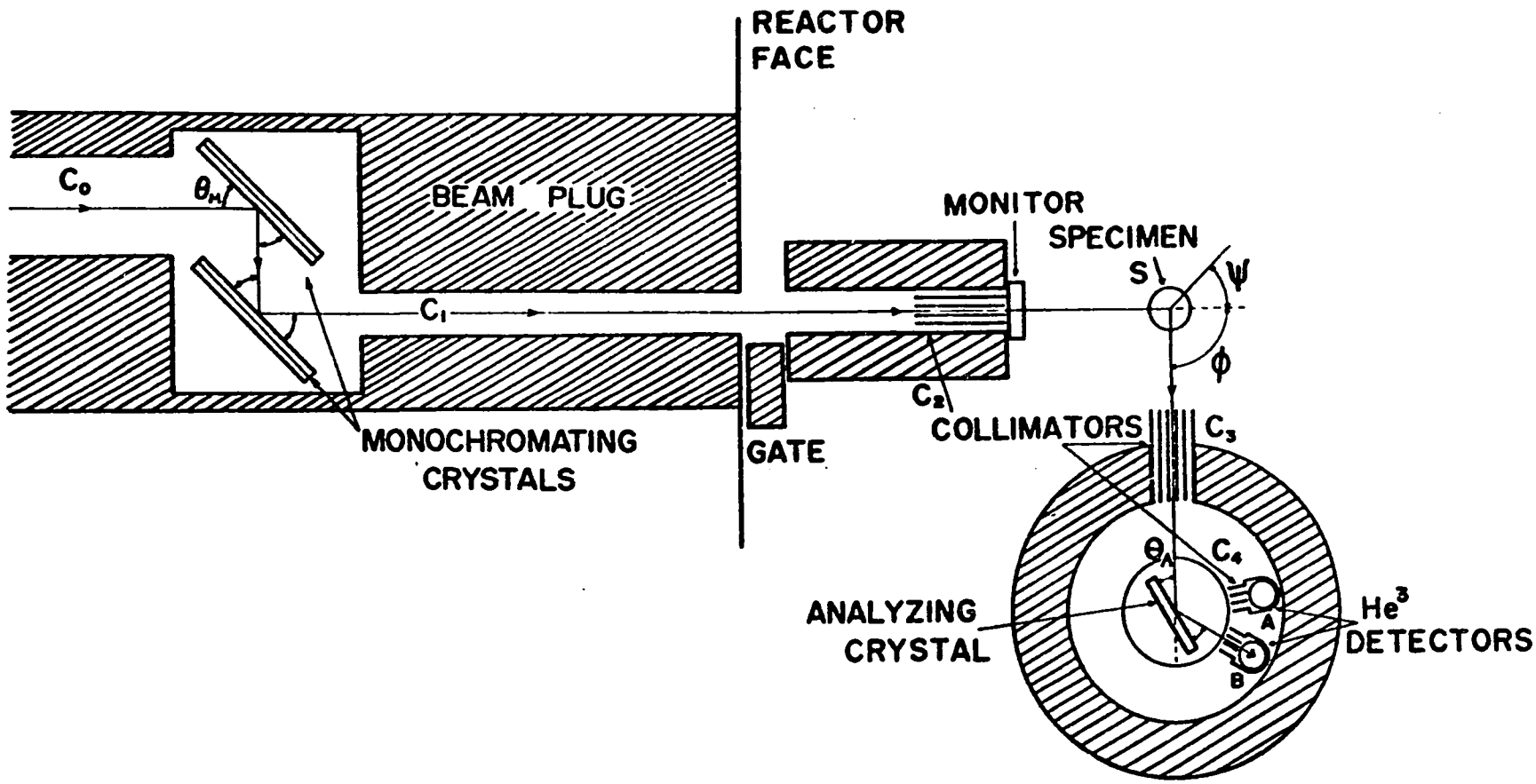

Fig. I-1. Schematic diagram of the McMaster (E2) triple-axis spectrometer at Chalk River.

A monochromatic beam is produced which then scatters from the specimen S, which has an orientation angle ψ. The neutrons scattered through an angle $\emptyset$ are energy analysed by means of Bragg reflection from the analyser crystal, and are detected by He^3 counter B. Counter A just measures background. The counting time is normalized to a constant number of incident neutrons by means of a beam monitor, which is a U^{235} fission counter with low efficiency and high transmission.

The only unusual feature of this spectrometer is the double crystal monochromator. In most crystal spectrometers, there is only one monochromator crystal, with the rest of the apparatus, including the specimen table, being rotatable about the monochromator axis. In this spectrometer, there are two monochromator crystals with their reflecting planes aligned parallel, allowing the monochromatic beam to exit in a fixed line, as shown, independent of the monochromator Bragg angle θ_M. The specimen table can therefore be fixed. Since neutron spectrometers are generally quite massive - the distance from the specimen table axis to the analyser table axis is about one metre in our spectrometer - this feature greatly reduces the cost of the apparatus and yet allows easy changing of all the spectrometer angles, including θ_M. If the monochromator crystals are well separated (not the case for our spectrometer), this design also results in very low background. The primary disadvantage of the double crystal monochromator

is, of course, the fact that about half of the incident neutrons are lost in the reflection from the second crystal.

A crystal spectrometer looks at one point in (Q,ω) space at a time. This is apparent if we consider that the incident beam is monochromatic with energy and wave vector $(E_o,\underline{k}_o)$ and that the analysing spectrometer accepts only one neutron energy and wave vector $(E',\underline{k}')$ at any particular setting. The wave vector transfer and the energy transfer are then uniquely specified through Eqs. I-2a and I-2b. Higher order reflections in the monochromator and analyser crystals do occur. That is to say, the wavelengths $\lambda/2$, $\lambda/3$,... are generally reflected from the crystals as well as the primary wavelength λ. However, the reflectivities of the crystals for these components usually drop off very quickly as one goes to higher orders. Also, in the case of the monochromator, the Maxwellian distribution of the incident neutrons means that the number of neutrons with the higher energies of the order contaminants is usually small. Nevertheless, spurious peaks in the scattered neutron distributions caused by order contamination sometimes occur in data taken with a crystal spectrometer.

The great advantage of the triple-axis spectrometer is its ability to operate in programmed modes. The most common and useful of these is the constant-$\underline{Q}$ mode (Brockhouse, 1961), in which the wave vector transfer $\underline{Q}$ is held fixed

during a particular scan and the energy transfer $\hbar\omega$ is varied. In terms of the mechanics of the instrument, this is usually accomplished by fixing one of θ_M or θ_A, thereby defining one of E_o or E', and varying the other to determine the energy transfer $(E_o - E')$. Meanwhile, the scattering angle ϕ and the specimen orientation angle ψ are varied to maintain constant the length and direction of the wave vector transfer $\underline{Q}$ in reciprocal space. This is illustrated in figure I-2, which shows schematically the reciprocal lattice of a specimen crystal (modulo 2π), and the orientation of the incident and scattered neutron wave vectors. The numbers 1 to n represent successive points in the scan, which is being done with E_o (and consequently $|\underline{k}_o|$) held fixed. $\underline{\tau}$ is a reciprocal lattice vector and $\underline{q}$ the phonon wave vector. When the energy transfer matches the phonon energy $\hbar\omega_j(\underline{q})$, a peak occurs in the observed intensity.

When the constant-$\underline{Q}$ method is used, the data that is obtained is gotten in its most useful form. One can preselect the wave vector of the phonon to be measured, and then scan the energy range where one suspects that it will occur. Usually one chooses the phonon wave vector along symmetry directions in the Brillouin zone, since the analysis of the measured dispersion curves is much simpler if this is done.

Intensity measurements of neutron groups are considerably easier when the constant-$\underline{Q}$ method is employed. If the cross section equation I-8 is integrated over E', the

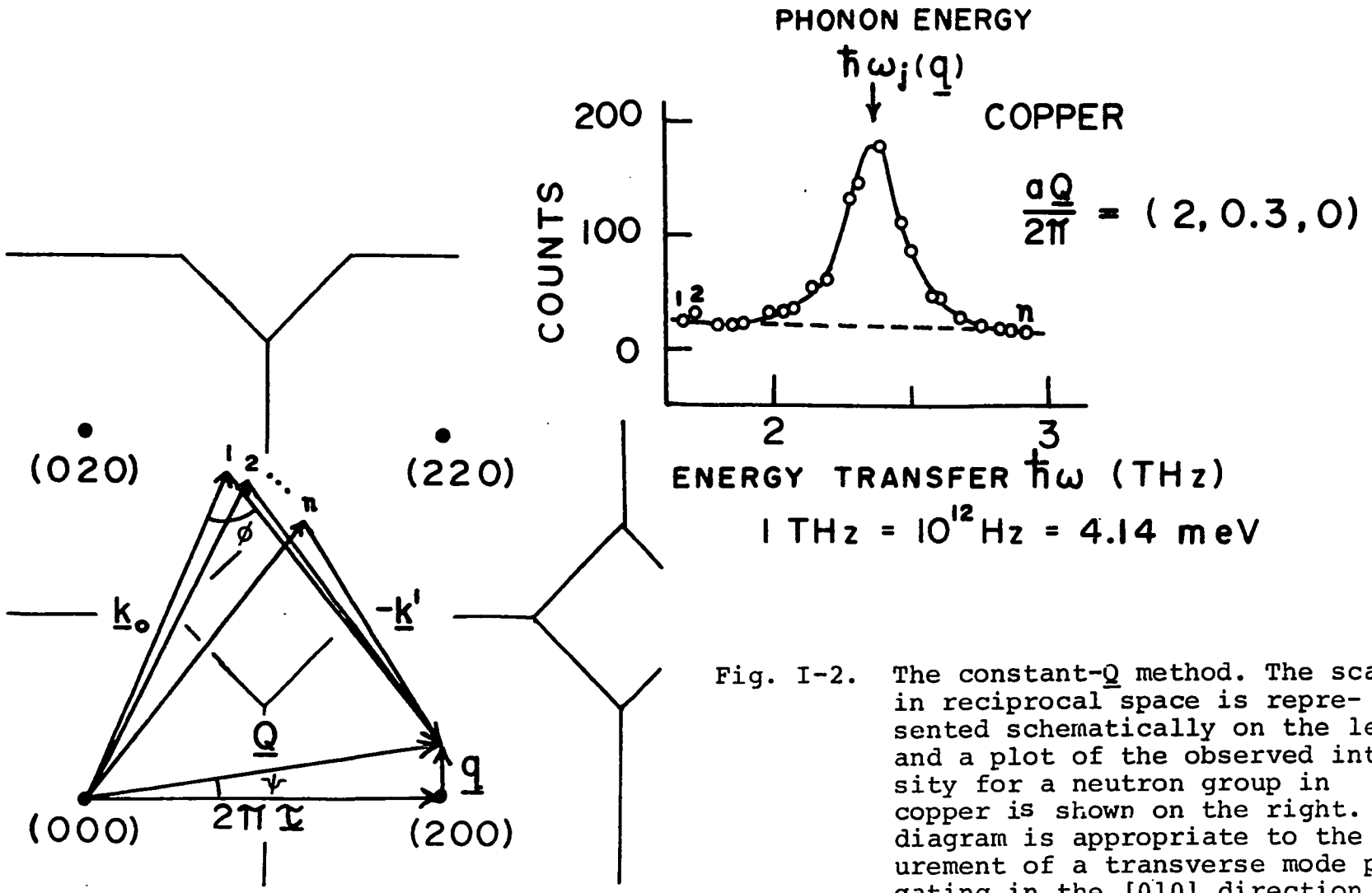

Fig. I-2. The constant-$\underline{Q}$ method. The scan in reciprocal space is represented schematically on the left and a plot of the observed intensity for a neutron group in copper is shown on the right. The diagram is appropriate to the measurement of a transverse mode propagating in the [010] direction of face-centred cubic crystal with a reduced wave vector ($a\underline{q}/2\pi$) = (0, 0.3, 0).

integration must be done over the path that the spectrometer follows in $(\underline{Q},\omega)$ space during the course of a scan. The integrated intensity of a neutron group becomes proportional to a Jacobian arising from the integration, the value of which depends on the path and on the form of the dispersion relation (e.g., see Brockhouse, 1966, pp. 120-121). In the constant-$\underline{Q}$ method, the Jacobian turns out to be unity (Brockhouse, 1961). With a crystal spectrometer, the scan can have an arbitrary path in $(\underline{Q},\omega)$ space, and often other programmed modes are used. In the constant-E mode, the energy transfer $\hbar\omega$ is fixed, and $\underline{Q}$ is varied along a preselected line in reciprocal space.

The resolution function of a crystal spectrometer is a fairly complicated quantity. Referring to Fig. I-1, it depends on the angles θ_M, θ_A, ϕ, the collimations C_o-C_4, the analyser and monochromator plane spacings, and the mosaic spreads of the analyser, monochromator and specimen crystals. In recent years, it has become possible to calculate the resolution function from the instrumental variables (Cooper and Nathans, 1967), if it is assumed that the mosaic spreads and the collimations are Gaussian. The constant sensitivity contours are ellipsoids in $(\underline{Q},\omega)$ space, with the sensitivity dropping off as a Gaussian away from the centre of the ellipsoid. For a spectrometer set to look at the position $(\underline{Q}_o,\omega_o)$, the resolution function is given by

$$R_{\underline{Q}_o,\omega_o}(\Delta\underline{Q},\Delta\omega)=R_o \exp\{-\frac{1}{2}\sum_{\ell=1}^{4}\sum_{k=1}^{4} X_k M_{k\ell} X_\ell\} \qquad \text{(I-21)}$$

where $X_1 = Q_x - Q_{xo} = \Delta Q_x$, $X_2 = \Delta Q_y$, $X_3 = \Delta Q_z$, and $X_4 = \omega$. The elements of the resolution matrix $M_{k\ell}$, which specifies the orientation of the ellipsoid, depend on the instrumental parameters listed above. R depends slowly on $\underline{Q}_o$ and ω_o. The resolution is highly correlated in the three variables Q_x , Q_y , and ω, where Q_x and Q_y are the coordinates of the wave vector transfer in the scattering plane. The resolution in Q_z, normal to the scattering plane, is uncorrelated with the resolution in the other variables. Matching this correlated resolution with the dispersion surfaces (focussing) is generally necessary in order to obtain optimum resolution and intensity (e.g., see Collins, 1963), although detailed knowledge of the resolution function is generally not needed in order to arrange reasonably good focussing conditions. However, the ability to calculate the resolution width within about 15 percent (using computer programs written by Mr. A. Larose and others) was very helpful in extracting the values for natural widths in the experiments described in Chapters II and III on Cu(Au) and Ni-Pd alloys, especially in the case of the latter.

D. THEORY OF THE DYNAMICS OF IMPERFECT CRYSTALS

In this section, a brief historical survey of the theory of vibrations in disordered crystals is presented, followed by an account of some basic equations for imperfect crystals. Brief descriptions of the theories directly used in the analysis of the experiments of the thesis are then given. Since the literature on the vibrations of disordered systems is now very extensive and diversified, the historical survey makes no attempt at completeness, but does mention most of the work of direct relevance to the thesis topic. Authoritative and comprehensive reviews of this field have been given by Maradudin (1966a, 1966b). A discussion of experimental techniques available for studying imperfect crystals, emphasizing neutron scattering methods, will be given at the beginning of Chapter II.

(i) Historical Survey

In the harmonic approximation, a classical normal mode analysis of the vibrations of a perfect crystal is adequate to describe many of the essential features of the dynamics. This holds true when defects are introduced, and it is not surprising that a few of the origins of the subject of impurity vibrations are very old, going at least as far back as some considerations by Lord Rayleigh in The Theory of Sound (Dover edition, 1945, original edition, 1877), which showed

that the introduction of a single subtitutional defect into a system of spring-coupled particles perturbed a particular normal-mode frequency by at most the spacing to the next unperturbed frequency. Thus only at the top or bottom of an unperturbed band can special (localized) modes be formed whose characteristics differ fundamentally from the modes of the perfect lattice.

The earliest work in more recent times was carried out in the Soviet Union by Lifshitz and his collaborators, starting about 1943. These studies, summarized in a review article by Lifshitz (1956), were the first to apply matrix Green's functions to the problem. They deal primarily with ioslated defects. The basic equations for the local mode frequency of a light defect, and the scattering of band modes by defects, were derived, as well as many other fundamental results. These studies, which appeared originally in untranslated Russian journals, went practically unnoticed in the West until the publication of the above-mentioned review article in English. However, parallel independent studies by Montroll and Potts (1955, 1956) contained some of the same results, with a slightly different emphasis. The latter were primarily concerned with the effect of isolated impurities on the additive functions of the normal mode frequencies, specifically the thermodynamic functions and the frequency distribution.

The existence of localized modes is in fact a rather obvious property of light defects and was predicted from the earliest considerations of defect vibrations. That heavy defects have analogous special modes is less obvious. Such 'resonance modes' were predicted independently by several authors (Brout and Visscher, 1962; Kagan and Iosilevskii, 1962; Takeno, 1963). It was indicated that the modes would have a finite lifetime because of their ability to decay into the continuum of band modes, and that the modes would be well defined if the mass of the impurity atom were much larger than that of a host atom. Large force constant changes to the defect can also produce special modes. Any atom that is sufficiently strongly bound will have a localized mode, and one that is very weakly bound will have a resonance mode. The vibrational amplitudes of the atoms participating in a localized mode die away from the defect site in an approximately exponential fashion. For resonance modes the amplitudes of the atoms are sharply peaked at the defect site, but do not go to zero at large distances from the impurity.

A number of studies on the frequency spectra of one-dimensional disordered systems have been reported. These range from purely formal theoretical solutions (Dyson, 1953; Englman, 1958; Schmidt, 1957) to theory with some calculated spectra (Langer, 1961; Davies and Langer, 1963) to partially numerical (Domb et. al., 1959; Agacy, 1964) and purely numerical methods (Dean, 1959, 1960, 1961; Dean and Martin, 1960;

Martin, 1961). The purely numerical methods, more accurately described as computer experiments rather than theory, have the advantage of greater reliability. The show how the frequency spectra actually behave as functions of concentration and mass and force constant differences. Thus they serve the function of experiment to the 'real' theories. Perhaps the most prominent feature of the more reliable frequency spectra is the appearance of 'spiky' structure around the local mode frequency, above the main band, for moderate concentrations of light defects. Such structure corresponds to the vibration frequencies of impurity complexes.

In extensions to higher dimensions, the theories necessarily become either more approximate or more limited in character, and the computer experiments become more involved and time-consuming. The computer experiments of Dean and Bacon (1965) in two dimensions and of Payton and Visscher (1967a) in two and three dimensions show that the 'spiky' structure around the local mode becomes less pronounced in higher dimensions because of the larger number of possible configurations of impurity complexes. Subsequent work by Payton and Visscher (1967b) also shows how the eigenvectors in particular normal modes vary about the location of light and heavy atoms in specific disordered arrays. It should be noted that the spectra obtained in this type of study are those of specific arrays of coupled atoms and are not ensemble

averages. The spectra of ternary mixtures and disordered systems with masses and force constants chosen from continuous random distributions (Payton and Visscher, 1968) have also been computed. A review of numerical studies of the vibrations of disordered systems has recently been given by Dean (1972).

The results on frequency spectra, although conceptually very important, cannot as yet be said to have stimulated a great deal of experimental work. However, there has been an extensive interplay of theory and experiment in other areas, notably optical properties, thermal conductivity, superconducting tunneling, and neutron scattering.

Particularly useful theoretical studies, which clearly point out where theory and experiment might meet, have been carried out by Elliott and his co-workers at Oxford. Following Lifshitz, Dawber and Elliott (1963) used classical Green's functions to calculate expressions for the amplitude of oscillation of a mass defect in localized modes and band modes as a function of frequency, as well as the mean-square amplitude and velocity of the defect. The latter two quantities are in principle accessible by the Mössbauer effect through measurements of the recoil-free fraction and second order Doppler shift. Specific calculations by Dawber and Elliott, assuming a Debye model,are particularly useful for estimating the host-impurity mass ratio needed to produce a well-defined in-band resonance. Elliott and Maradudin (1965)

calculated the one-phonon cross-sections for neutron scattering. Elliott and Taylor (1967) generalized mass defect theory to finite, but still small, defect concentrations and calculated frequency distributions, thermal energies and optical absorption. They also carried out a more detailed analysis of the neutron scattering cross-sections. The last two papers mentioned above use the Green's function methods of Zubarev (1960), which direcly give thermodynamically averaged observable quantities.

Lakatos and Krumhansl (1968, 1969) carried out detailed calculations of the effect of force-constant changes in F.C.C. and B.C.C. crystals containing substitutional impurities, formulating their treatment in terms of coherent and incoherent neutron scattering experiments. They did specific calculations for several types of heavy impurities in Al. Other treatments of force constant changes had appeared prior to this, but Lakatos and Krumhansl's treatment is more general. Bruno and Taylor (1971) independently carried out similar calculations for Cu(Au) alloys, since the then existing neutron measurements (Svensson, Brockhouse and Rowe, 1965; Svensson and Brockhouse 1967; Svensson and Kamitakahara, 1971) indicated that force constant changes were almost certainly important in this case. The effects of short range order (Hartmann, 1968) and self-consistency (Taylor, 1967) have also been considered. Aiyer, Elliott, Krumhansl and Leath (1969) have attempted to include the scattering of the lattice waves

from pairs of defects.

Taylor (1967) considered the case of very high defect concentrations, with mass changes only in a monatomic cubic crystal. He compared his results with the computer experiments of Payton and Visscher (1967a) with considerable success. Taylor's theory is similar in principle to the coherent-potential approximation (Soven, 1967) for the electronic structure of alloys. Taylor calculates expressions for the one-phonon neutron scattering cross sections. We give these expressions in a later section of this chapter, and use them in the analysis of the Ni-Pd experiment in Chapter III. Displacement correlation functions in mass-disordered lattices have also been considered in detail by Leath and Goodman (1966, 1968). These authors have also given an 'interpolation formula' (Leath and Goodman, 1969) for the frequency spectra of high-concentration imperfect crystals. The 'formula' requires somewhat less computation than Taylor's theory but the amount of computing required for the latter is in any case not excessive.

Before continuing on, it should perhaps be mentioned that there are many areas of research which are closely related in principle to the vibrations of imperfect crystals. Elliott (1969) has commented on the similarity of the theories for different types of excitations (excitons, electrons, magnons, and phonons) in random alloys. The dynamics of glasses and of crystal surfaces and interfaces also represent

related problems which have been actively pursued in recent years.

Some basic theory for imperfect crystals will now be presented. The accounts that follow are essentially those of Dawber and Elliott (1963), Elliott and Taylor (1967), and Elliott (1966).

(ii) Basic Equations for the Imperfect Crystal

In the harmonic approximation, the equations of motion for the Heisenberg operators $\underline{u}(\ell,t)$ representing the nuclear displacements are

$$M'_\alpha(\ell)\frac{d^2}{dt^2}u_\alpha(\ell,t) + \sum_{\beta\ell'}\Phi'_{\alpha\beta}(\ell,\ell')u_\beta(\ell',t) = 0 \qquad \text{(I-22)}$$

The index ℓ labels the unit cell (ℓ=1,2,...N); α labels the positions of the n atoms within the unit cell as well as the Cartesian components of $\underline{u}$ (α=1,2,...3n). The primes on the masses and force constants are to indicate the values that they take on in the imperfect crystal. Assumption of a time dependence exp(iωt) for $u_\alpha(\ell,t)$ gives

$$-\omega^2 M'_\alpha(\ell)u_\alpha(\ell,t) + \sum_{\beta\ell'}\Phi'_{\alpha\beta}(\ell,\ell')u_\beta(\ell,t) = 0 \qquad \text{(I-23)}$$

For a perfect crystal, the mass M does not depend on α and the force constants depend on the positional difference $(\underline{R}_\ell-\underline{R}_{\ell'})$ and not on ℓ and ℓ' separately. The difference from the imperfect crystal can be characterized by the mass defect parameter

$$\varepsilon_\alpha(\ell) = \frac{M_\alpha - M'_\alpha(\ell)}{M_\alpha} \qquad \text{(I-24)}$$

and by the defect matrix

$$C_{\alpha\beta}(\ell,\ell') = \Phi'_{\alpha\beta}(\ell,\ell') - \Phi_{\alpha\beta}(\ell,\ell') + \epsilon_\alpha(\ell) M_\alpha \omega^2 \delta_{\alpha\beta}\delta(\ell,\ell') \tag{I-25}$$

Eq. I-23 then becomes

$$-\omega^2 M_\alpha u_\alpha(\ell,t) + \sum_{\beta\ell'} \Phi_{\alpha\beta}(\ell,\ell') u_\beta(\ell',t) = -\sum_{\beta\ell'} C_{\alpha\beta}(\ell,\ell') u_\beta(\ell',t) \tag{I-26}$$

For a perfect crystal, the right hand side of this equation is zero, and the problem is formally solved by imposing periodic boundary conditions and introducing the dynamical matrix, which can be written

$$D_{\alpha\beta}(\underline{q}) = \sum_{\ell'} \Phi_{\alpha\beta}(\ell,\ell') \exp\{i\, \underline{q}.(\underline{R}_\ell - \underline{R}_{\ell'})\} \frac{1}{(M_\alpha M_\beta)^{1/2}} \tag{I-27}$$

The dynamical matrix is independent of ℓ since the force constants depend only on $(\underline{R}_\ell - \underline{R}_{\ell'})$. The transformation to normal coordinates is then

$$d_j(\underline{q},t) = N^{-1/2} \sum_{\alpha\ell} \xi_\alpha^j(\underline{q}) \exp(i\, \underline{q}.\underline{R}_\ell) M_\alpha^{1/2}\, u_\alpha(\ell,t) \tag{I-28}$$

where ξ_α^j are the components of the eigenvectors of the matrix $\underline{\underline{D}}$. The squared frequencies, $\omega_j^2(\underline{q})$, of the normal modes are the eigenvalues of $\underline{\underline{D}}$. The transformation inverse to I-28 is

$$u_\alpha(\ell) = N^{-1/2} \sum_{j\underline{q}} \xi_\alpha^{j*}(\underline{q}) \exp(-i\, \underline{q}.\underline{R}_\ell) M_\alpha^{-1/2}\, d_j(\underline{q}), \tag{I-29}$$

where the time dependence exp(iωt) has been dropped. The solutions to Eq. I-26 for the imperfect crystal can be expressed in terms of a matrix Green's function defined by

$$-\omega^2 M_\alpha \, g_{\alpha\gamma}(\ell,\ell',\omega) + \sum_{\beta\ell''} \Phi_{\alpha\beta}(\ell,\ell'') \; g_{\beta\gamma}(\ell'',\ell',\omega) = -\delta_{\alpha\gamma}\delta(\ell,\ell') \tag{I-30}$$

In matrix notation, this equation becomes

$$(-\omega^2 \underline{\underline{M}} + \underline{\underline{\Phi}})\,\underline{\underline{g}} = -\underline{\underline{I}} \tag{I-31}$$

or

$$\underline{\underline{g}} = (\omega^2 \underline{\underline{M}} - \underline{\underline{\Phi}})^{-1} \tag{I-32}$$

and Eq. I-23 itself becomes

$$(\omega^2 \underline{\underline{M}} - \underline{\underline{\Phi}})\;\underline{u} = \underline{\underline{C}}\;\underline{u}\;, \tag{I-33}$$

where the vector $\underline{u}$ has 3nN components. Also, the transformation of Eq. I-28 can be represented by

$$\underline{u} = \underline{\underline{X}}\;\underline{d}\;. \tag{I-34}$$

The elements of the Green's function matrix can be found by considering that it is the transformation $\underline{\underline{X}}$ that diagonalizes $(\omega^2 \underline{\underline{M}} - \underline{\underline{\Phi}})$, i.e., that gives $\underline{\underline{X}}(\omega^2 \underline{\underline{M}} - \underline{\underline{\Phi}})\underline{\underline{X}}^{\dagger}$ as a diagonal matrix. The elements of $\underline{\underline{X}}$ and $\underline{\underline{X}}^{-1}$ have been given explicitly in Eqs. I-28 and I-29. For the sake of convenience, they are rewritten

here, together with their Hermitian conjugates**.

$$(\underline{\underline{X}})_{j\underline{q},\alpha\ell} = N^{-1/2} M_\alpha^{-1/2} \xi_\alpha^{j*}(\underline{q}) \exp(-i\underline{q}.\underline{R}_\ell) \qquad \text{(I-35a)}$$

$$(\underline{\underline{X}}^{-1})_{\alpha\ell,j\underline{q}} = N^{-1/2} M_\alpha^{1/2} \xi_\alpha^{j}(\underline{q}) \exp(i\underline{q}.\underline{R}_\ell) \qquad \text{(I-35b)}$$

$$(\underline{\underline{X}}^{\dagger})_{\alpha\ell,j\underline{q}} = N^{-1/2} M_\alpha^{-1/2} \xi_\alpha^{j}(\underline{q}) \exp(i\underline{q}.\underline{R}_\ell) \qquad \text{(I-35c)}$$

$$(\underline{\underline{X}}^{\dagger})^{-1}_{j\underline{q},\alpha\ell} = N^{-1/2} M_\alpha^{1/2} \xi_\alpha^{j*}(\underline{q}) \exp(-i\underline{q}.\underline{R}_\ell) \qquad \text{(I-35d)}$$

$$= (\underline{\underline{X}}^{-1})^{\dagger}_{j\underline{q},\alpha\ell}$$

The elements of $\underline{\underline{X}}(\omega^2\underline{\underline{M}}-\underline{\underline{\Phi}})\underline{\underline{X}}^{\dagger}$ must be given by

$$\delta_{jj'}\delta(\underline{q},\underline{q}')(\omega^2-\omega_j^2(\underline{q})) \quad . \qquad \text{(I-36)}$$

Hence the elements of the inverse matrix
$\underline{g}' = (\underline{\underline{X}}^{\dagger})^{-1}(\omega^2\underline{\underline{M}}-\underline{\underline{\Phi}})^{-1}\underline{\underline{X}}^{-1}$ must be

$$\delta_{jj'}\delta(\underline{q},\underline{q}')(\omega^2-\omega_j^2(\underline{q}))^{-1} \equiv g'_{j\underline{q},j\underline{q}'}(\omega) \quad . \qquad \text{(I-37)}$$

** The transformation defined in this way is not quite unitary; $(\underline{\underline{X}}^{-1})_{\alpha\ell,j\underline{q}}$ and $(\underline{\underline{X}}^{\dagger})_{\alpha\ell,j\underline{q}}$ differ by a factor M_α.

Now since $\underline{\underline{g}} = \underline{\underline{X}}^{\dagger}\underline{\underline{g}}'\underline{\underline{X}}$, one gets

$$g_{\alpha\beta}(\ell,\ell',\omega) = \sum_{j\underline{q}} \sum_{j'\underline{q}'} N^{-1}(M_\alpha M_\beta)^{-1/2}\, \xi_\alpha^j(\underline{q})\xi_\beta^{j'*}(\underline{q}') \times \exp[i\underline{q}\cdot\underline{R}_\ell - i\underline{q}'\cdot\underline{R}_{\ell'}]\, \frac{\delta_{jj'}\,\delta(\underline{q},\underline{q}')}{\omega^2-\omega_j^2(\underline{q})} \tag{I-38}$$

And finally, the explicit form of the Green's function in the (α,ℓ) representation is obtained:

$$g_{\alpha\beta}(\ell,\ell',\omega)=N^{-1}(M_\alpha M_\beta)^{-1/2} \sum_{j\underline{q}} \frac{\xi_\alpha^j(\underline{q})\xi_\beta^{j*}(\underline{q})}{\omega^2 - \omega_j^2(\underline{q})} \exp[i\underline{q}\cdot(\underline{R}_\ell-\underline{R}_{\ell'})] \tag{I-39}$$

Eq. I-33 can be multiplied on the left by $\underline{\underline{g}}$ to give

$$\underline{u} = \underline{\underline{g}}\,\underline{\underline{C}}\,\underline{u} \tag{I-40}$$

In the case of the perfect crystal, this last step throws away all the information contained in the equations of motion. For the imperfect crystal, it separates out those equations that pertain to the impurity sites and the sites connected to them by force-constant changes. If there are exact normal modes which are solutions of this smaller set of equations, and the impurities are well separated, it is natural to expect that these will be modes which are localized about the impurity sites. Thus the equation that must be

satisfied by the frequencies of localized impurity modes is

$$\det|\underline{\underline{I}} - \underline{g}\,\underline{\underline{C}}| = 0 \qquad \text{(I-41)}$$

In order to derive useful equations for the local mode frequency in simple cases, the solutions of Eq. I-41 for an isolated mass defect at the origin will now be considered. The next few equations are labelled with an S to distinguish them from more general results. Now the matrix $\underline{\underline{C}}$ has only three non-zero elements along the diagonal, which are given by

$$C_{\alpha\beta}(\ell,\ell') = \varepsilon_\alpha M_\alpha \omega^2 \delta_{\alpha\beta}\delta(\ell,0)\delta(\ell',0) \qquad \text{(I-42S)}$$

where it is understood that $C_{\alpha\beta}(\ell,\ell')=0$ unless α,β are labels which belong to the defect atom within the unit cell.

With this substitution for $\underline{\underline{C}}$, the eigenvalue equation becomes

$$\det\Big|\delta_{\alpha\beta}\delta(\ell,\ell') - \sum_{\gamma\ell''}\sum_{j\underline{q}} \frac{\xi_\alpha^j(\underline{q})\xi_\gamma^{j*}(\underline{q})}{\omega^2 - \omega_j^2(\underline{q})} \exp[i\underline{q}\cdot(\underline{R}_\ell - \underline{R}_{\ell''})]$$

$$\times \frac{1}{N(M_\alpha M_\gamma)^{1/2}} \varepsilon_\gamma M_\gamma \omega^2 \delta_{\gamma\beta}\delta(\ell'',0)\delta(\ell',0)\Big| = 0 \qquad \text{(I-43S)}$$

or

$$\det\Big|\delta_{\alpha\beta}\delta(\ell,\ell') - \frac{\varepsilon_\beta\omega^2}{N}\sum_{j\underline{q}} \frac{\xi_\alpha^j(\underline{q})\xi_\beta^{j*}(\underline{q})}{\omega^2 - \omega_j^2(\underline{q})}\Big| = 0 \qquad \text{(I-44S)}$$

If the defect is in a site of cubic, tetragonal, or orthorhombic symmetry, then each of the coordinate axes x_1, x_2, x_3 can be chosen to lie in a mirror plane. Then an eigenvector component $\xi^j_{x_1}(\underline{q})$ has a cancelling component $\xi^j_{-x_1}(\underline{q}) = -\xi^j_{x_1}(\underline{q})$ associated with it through a reflection in the (x_2,x_3) plane. The values of $\xi^j_{x_2}(\underline{q})$, $\xi^j_{x_3}(\underline{q})$ and $\omega_j(\underline{q})$ however remain unchanged. Hence the sum in Eq. I-44 vanishes unless $\alpha = \beta$. Thus the off-diagonal terms of $(\underline{\underline{I}}-g\underline{\underline{C}})$ are all zero, and the diagonal elements are all unity except for three. These three elements are identical if the x_1,x_2, and x_3 axes are equivalent (cubic case), and two are the same if x_1 and x_2 are equivalent (tetragonal case). For the cubic case, the solutions of the equations are therefore triply degenerate and are given by

$$1 - \frac{\varepsilon_\alpha \omega^2}{N} \sum_{j\underline{q}} \frac{|\xi^j_\alpha(\underline{q})|^2}{\omega^2 - \omega_j^2(\underline{q})} = 0 \quad . \qquad \text{(I-45S)}$$

For a cubic crystal in which each atom has the same mass and an equivalent site, $|\xi^j_\alpha(\underline{q})|^2 = \frac{1}{3n}$, where n is the number of atoms per unit cell, and the preceding equation simplifies to

$$1 - \frac{\varepsilon\omega^2}{3nN} \sum_{j\underline{q}} \frac{1}{\omega^2 - \omega_j^2(\underline{q})} = 0 \quad . \qquad \text{(I-46S)}$$

This equation is valid for the simple cubic, face-centred cubic, body-centred cubic, and diamond structures.

If there is a new mode produced out of the band by the

impurity, then the denominator will always be large, and the sum can be replaced by an integral. This gives

$$1 - \varepsilon\omega_\ell^2 \int \frac{f(\omega_o)\,d\omega_o}{\omega_\ell^2 - \omega_o^2} = 0 \quad , \tag{I-47S}$$

where $f(\omega)$ is the host frequency distribution normalized to unity, and ω_ℓ is the local mode frequency.

If a new mode is produced within the band, then a few terms of the sum in Eq. I-46S will dominate, and one must proceed more cautiously. In reality, no truly localized mode can be produced within the band. However, as Brout and Visscher (1962) pointed out, Eq. I-47S can still be used when the impurity mass is much larger than the host mass (i.e., $\varepsilon<<0$) if the principal value of the integral is taken. The solution obtained is then the frequency ω_r of a resonance mode, which has a finite width, approximately given by $\frac{\pi}{2}|\varepsilon|\omega_r^2 g(\omega_r)$, since it can decay into the continuum of band modes.

In order to conveniently discuss the theories of Elliott and Taylor (1967) and Taylor (1967), we now introduce advanced (G_a) and retarded (G_r) double-time thermal Green's functions (Zubarev, 1960). These are defined by the equations

$$G_r(t,t') \equiv \langle\langle A(t);B(t')\rangle\rangle_r = i\theta(t-t')\langle[A(t),B(t')]\rangle \tag{I-48a}$$

$$G_a(t,t') \equiv \langle\langle A(t);B(t')\rangle\rangle_a = -i\theta(t'-t)\langle[A(t),B(t')]\rangle \tag{I-48b}$$

where the square brackets [ ] denote a commutator between the Heisenberg operators A and B, and the angular brackets < > denote a thermal average. The function θ is defined by

$$\theta(t-t') = 1 \quad (t>t') \quad , \qquad = 0 \quad (t<t') \quad . \tag{I-49}$$

Both Green's functions obey the equation of motion

$$i\hbar \frac{dG}{dt} = \hbar\delta(t)\langle[A(t),B(0)]\rangle + \langle\langle[A(t),\mathcal{H}(t)];B(0)\rangle\rangle \quad , \tag{I-50}$$

where $\mathcal{H}$ is the Hamiltonian of the system. For our purposes, the Fourier transform of G is a very useful and significant quantity.

$$G(\omega) = \frac{1}{2\pi}\int_{-\infty}^{\infty} G(t)\exp(i\omega t)dt \tag{I-51a}$$

$$G(t) = \int_{\infty}^{\infty} G(\omega)\exp(-i\omega t)dt \tag{I-51b}$$

For ω in the upper half of the complex plane, the Fourier transform of $G_r(t)$ is taken to obtain $G(\omega)$. In the lower half plane, the Fourier transform of $G_a(t)$ is taken.

The functions of physical interest are correlation functions like $F_{AB}(t-t') = \langle A(t)B(t')\rangle$ and their Fourier transforms. The Fourier transform of F_{AB} is

$$J(\omega) = \frac{1}{2\pi}\int_{-\infty}^{\infty} F_{AB}(t-t')\exp[i\omega(t-t')]d\omega \quad . \tag{I-52}$$

The neutron scattering cross section is proportional to $J(\omega)$

when F_{AB} is the displacement-displacement correlation function. $J(\omega)$ is related to the Green's function by

$$\lim_{\phi \to 0} [G(\omega+i\phi)-G(\omega-i\phi)]=-i[\exp(\beta\omega)-1]J(\omega) \quad , \qquad \text{(I-53)}$$

This quantity turns out to be independent of temperature since $J(\omega)$ contains a Bose-Einstein factor $[\exp(\beta\omega) - 1]^{-1}$, where $\beta = \hbar/k_B T$.

For the displacement-displacement Green's function defined by

$$G_{\alpha\beta}(\ell,\ell',t) = \frac{2\pi}{\hbar} << u_\alpha(\ell,t);\ u_\beta(\ell',0)>> \quad , \qquad \text{(I-54)}$$

the equation of motion can be shown to become

$$-M_\alpha\ \omega^2 G_{\alpha\beta}(\ell,\ell',\omega) + \sum_{\gamma\ell''} \Phi_{\alpha\gamma}(\ell,\ell'')G_{\gamma\beta}(\ell'',\ell',\omega) \qquad \text{(I-55)}$$

$$+ \delta_{\alpha\beta}\delta(\ell,\ell') = -\sum_{\gamma\ell''} C_{\alpha\gamma}(\ell,\ell''\omega)G_{\gamma\beta}(\ell'',\ell',\omega)$$

For $C_{\alpha\gamma} = 0$, this is the same equation as Eq. I-30. Thus the perfect lattice Green's function (call it P) for displacement-displacement correlation can be identified with the classical Green's function g of Eq. I-30.

When Eq. I-55 is expressed in matrix form, it follows easily that

$$\underline{\underline{G}} = \underline{\underline{P}} + \underline{\underline{P}}\ \underline{\underline{C}}\ \underline{\underline{G}} \qquad \text{(I-56a)}$$

$$= (\underline{\underline{I}} - \underline{\underline{P}}\ \underline{\underline{C}})^{-1}\ \underline{\underline{P}} \quad . \qquad \text{(I-56b)}$$

(iii) Results for Low Impurity Concentrations

In neutron scattering experiments, impurity concentrations must be typically a few atomic percent in order to produce an observable effect on the scattering cross sections. The theory with which we compare our experiment must therefore be one that is applicable to a finite, but low, impurity concentration. Such a theory has been worked out by Taylor (1965) and Elliott and Taylor (1967). The neutron scattering cross sections derived from this theory were first given by Elliott and Maradudin (1965). Earlier calculations of the neutron scattering from crystals containing defects had been carried out in the Soviet Union (e.g., Kagan and Ioselevskii, 1963), but not in such a useful form. The equations which we describe briefly below are those of Elliott and Taylor.

Iteration of Eq. I-56 gives

$$\underline{\underline{G}} = \underline{\underline{P}} + \underline{\underline{P}}\,\underline{\underline{C}}\,\underline{\underline{P}} + \underline{\underline{P}}\,\underline{\underline{C}}\,\underline{\underline{P}}\,\underline{\underline{C}}\,\underline{\underline{P}} + \ldots \qquad \text{(I-57)}$$

If the defects are few enough in number so that there is little probability that a site directly affected, through mass and force constant changes, by the presence of one impurity will also be affected by another impurity, then one can write

$$\underline{\underline{C}} = \sum_i \underline{\underline{C}}_i \qquad \text{(I-58)}$$

where $(\underline{\underline{C}}_i)_{\alpha\ell,\beta\ell'}$ is non-zero only when the labels $\alpha,\ell;\beta,\ell'$ all refer to sites affected by the impurity at site i. For mass

defects, this is valid for all concentrations, since only the impurity site itself is affected.

By examining Eq. I-57, one can pick out all the terms which contain only one i. This gives $\underline{\underline{G}}$ correct to first order in the impurity concentration. The result can be expressed as

$$\underline{\underline{G}} = \underline{\underline{P}} + \sum_i \underline{\underline{P}}\, \underline{\underline{X}}_i\, \underline{\underline{G}} \qquad \text{(I-59)}$$

where $\underline{\underline{X}}_i = \underline{\underline{C}}_i (\underline{\underline{I}} - \underline{\underline{P}}_i\, \underline{\underline{C}}_i)^{-1}$. The summation in Eq. I-59 is only over the impurity sites. $\underline{\underline{P}}_i$ has non-zero elements in the same block as does $\underline{\underline{C}}_i$.

An average over all possible configurations of the randomly-placed impurities gives

$$\underline{\underline{G}} = \underline{\underline{P}} + c \sum_i \underline{\underline{P}}\, \underline{\underline{X}}_i\, \underline{\underline{G}} \qquad \text{(I-60)}$$

where the sum now extends over <u>all</u> lattice sites.

Taylor (1965) and Elliott and Taylor (1967) show that making the substitution

$$\underline{\underline{X}}_i = \underline{\underline{C}}_i (\underline{\underline{I}} - (1-c)\underline{\underline{P}}_i \underline{\underline{C}}_i)^{-1} \qquad \text{(I-61)}$$

includes some terms to higher orders in the concentration, but not those that describe scattering from impurity pairs and impurity complexes. This equation differs from the expression previously given for $\underline{\underline{X}}_i$ only in the factor (1-c).

The configuration average has restored the translational symmetry, and the averaged Green's function has its simplest

form in the $(\underline{q},j)$ representation where it is diagonal on $\underline{q}$. For mass defects in a cubic Bravais lattice, or in the diamond structure, it is also diagonal on j, and the diagonal elements of the Green's function $G(\omega+i\delta)$, where δ is a very small positive number, are given by

$$G_j(\underline{q},\omega) = \frac{1}{\omega^2-\omega_j^2(\underline{q})-cV(\omega)} \tag{I-62}$$

where

$$V(\omega) = \frac{\varepsilon\omega^2}{1-(1-c)\varepsilon\omega^2 P(\omega)} \tag{I-63}$$

and

$$P(\omega) = \text{p.p.} \int \frac{f(\omega_o)}{\omega^2-\omega_o^2} + i\,\frac{\pi}{2}\,\frac{f(\omega)}{\omega} \tag{I-64}$$

The function $f(\omega)$ is the host frequency distribution normalized to unity, and p.p. indicates the principal part of the integral.

The cross section for coherent neutron scattering from the band modes is then given by (Elliott and Maradudin, 1965; Elliott and Taylor, 1967)

$$S_{coh}^{(1)}(\underline{Q},\omega) = [n(\omega)+1]\,\mathrm{Im}\{[B_h + \frac{c(B_d-B_h)}{1-(1-c)\varepsilon\omega^2 P(\omega)}]^2 \times \frac{1}{M_h}\sum_j (\underline{Q}\cdot\underline{\xi}^j(\underline{q}))^2 G_j(\underline{q},\omega)\} \tag{I-65}$$

B_h and B_d are the scattering lengths of host and defect atoms, combined with their respective Debye-Waller factors. ($B_h = b_h \exp(-W_h)$.) Some further results for the application of Eqs. I-62-65 to a neutron scattering experiment are given in Chapter II, section A(iii) .

(iv) Results for High Impurity Concentrations

Taylor (1967) has worked out the most satisfactory treatment to date for imperfect crystals in which the impurity concentration is very large. Since the formulation of the theory involves some very complicated equations, only a brief schematic description is given here. The theory employs the multiple scattering theory of Lax (1951) to calculate a function $\tilde{\epsilon}(\omega)$ which is related to a refractive index for the lattice waves, assumed to be complex in order to describe the damping of the waves. Only mass defects are considered.

In the low concentration theory described in the previous section, Eq. I-60 for the configurationally averaged Green's function can be written

$$\underline{\underline{\bar{G}}} = \underline{\underline{P}} + \underline{\underline{P}}(c\underline{\underline{X}})\underline{\underline{\bar{G}}} \qquad \text{(I-66)}$$

where $c\underline{\underline{X}}$ is called the self-energy. The bar on $\underline{\underline{\bar{G}}}$ denotes the configuration average. In this approximate equation, the immediate environment of an impurity is regarded to be the

perfect crystal, but the lattice waves are allowed to scatter from the single impurities any number of times.

Taylor's approximation for the high concentration case regards the environment of a 'defect' atom to be an average of the imperfect crystal, so that the P of Eq. I-66 is replaced by

$$\underline{\underline{G}}^{o} = \underline{\underline{P}} + \underline{\underline{P}}\ \underline{\underline{E}}\ \underline{\underline{G}}^{o} \tag{I-67}$$

where $\underline{\underline{E}}$ is an approximation to the self-energy in the disordered crystal. An equation analogous to Eq. I-66 is then derived, which can be written as

$$\overline{\underline{\underline{G}}} = \underline{\underline{G}}^{o} + \underline{\underline{G}}^{o}(c_A\ \underline{\underline{T}}_A + c_B\ \underline{\underline{T}}_B)\overline{\underline{\underline{G}}} \tag{I-68}$$

The subscripts A and B refer to 'host' and 'defect' type atoms. The matrices $\underline{\underline{T}}$ describe the scattering that is left after making the approximation of Eq. I-67. The average of this scattering is set equal to zero, i.e.,

$$c_A\ \underline{\underline{T}}_A + c_B\ \underline{\underline{T}}_B = 0 \tag{I-69}$$

so that $\overline{\underline{\underline{G}}} = \underline{\underline{G}}^{o}$, and $\underline{\underline{E}}$ is the final approximation to the self-energy.

The approximation leads to a pair of equations that can be solved by iteration:

$$\tilde{\varepsilon}(\omega) - c\varepsilon = \tilde{\varepsilon}(\omega)\,[\varepsilon - \tilde{\varepsilon}(\omega)]\,\omega^2 G^{o}(\omega) \tag{I-70}$$

$$G^{o}(\omega) = \int \frac{f(\omega_o)\ d\omega_o}{\omega^2 - \omega_o^2 - \omega^2\ \tilde{\varepsilon}(\omega)} \tag{I-71}$$

where $f(\omega)$ is the 'host' frequency distribution, and $\varepsilon=1-M_B/M_A$. The function $\tilde{\varepsilon}(\omega)$ gives the diagonal equal elements of $\underline{\underline{E}}$ in the (q,j) representation and $G^o(\omega)$ gives the diagonal equal elements of $\underline{\underline{G}}$ in the (α,ℓ) representation.

In the $(\underline{q},j)$ representation, the averaged Green's function is diagonal, with elements

$$G_j(\underline{q},\omega) = \frac{1}{\omega^2-\omega_j^2(\underline{q})-\omega^2\tilde{\varepsilon}(\omega)} \qquad \text{(I-72)}$$

Here, $\omega_j(\underline{q})$ is the dispersion relation for a lattice with all 'host' type atoms. The one-phonon coherent cross section for neutron scattering is related to the Green's function by

$$S_{coh}^{(1)}(\underline{Q},\omega)=<B(\omega)>^2[n(\omega)+1]\sum_j(\underline{Q}\cdot\underline{\xi}^j(\underline{q}))^2 \mathrm{Im}G_j(\underline{q},\omega) \qquad \text{(I-73)}$$

where

$$<B(\omega)> = [1-\frac{\tilde{\varepsilon}(\omega)}{\varepsilon}]<B_h> + \frac{\tilde{\varepsilon}(\omega)}{\varepsilon}<B_d> \qquad \text{(I-74)}$$

$$= B \quad \text{when} \quad B_h = B_d$$

Since the effects of the local environment on the dynamics of any particular atom have been neglected in this theory, the approximation is most suitable for very high impurity concentrations in three dimensions, where it can be argued that the local environment of an atom really does resemble the imperfect crystal.

The theory treats 'host' and 'defect' type atoms on an equivalent basis, an essential property for a high concentration theory. Davies and Langer (1963) have given a self-consistent theory of the dynamics of a disordered chain, generalizable to three dimensions, but according to Taylor, this theory is not symmetric with respect to A and B type atoms and gives an unphysical result for the behaviour of the impurity band for moderately low concentrations of light atoms. Leath (1968) has analysed the theories of Taylor and of Davies and Langer in terms of diagrams of the type introduced by Langer (1961). An extension to the self-consistent theory that includes pair scattering has been worked out by Aiyer, Elliott, Krumhansl, and Leath (1969). An error in this paper has been noted and corrected by Leath (1972).

CHAPTER II

LATTICE VIBRATIONS AND RESONANT MODES IN CU(AU) ALLOYS

A. INTRODUCTION

(i) Techniques for the Spectroscopy of Impurity Vibrations

Many experimental techniques are now available to study the vibrational properties of crystals containing impurity atoms. Maradudin (1966a, 1966b) has reviewed some of the experiments to mid-1965 and has indicated the types of information to be obtained from different methods. These are roughly divisible into two categories: (1) those that study bulk properties which are determined by an average over all the vibrational modes and (2) those that permit direct spectroscopy of the lattice vibrations. Into the first category fall measurements of the electrical resistivity, the thermal conductivity and the specific heat. These are particularly influenced by the presence of low frequency resonance modes. In the second category, apart from a few special cases, there are only four real possibilities: (1) optical methods, especially infrared absorption, (2) superconducting tunnelling, (3) the Mössbauer effect, and (4) inelastic neutron scattering.

Localized modes and resonance modes were first observed in infrared absorption experiments (Schaefer, 1960; Sievers, 1964) and to date perhaps the most detailed

information about impurity vibrations has come from measurements which employ this technique. Many interesting phenomena associated with defect modes in ionic crystals have been observed, including isotope shifts, the effects of uniaxial stress, and anharmonic effects. The sidebands of local mode absorption lines can give valuable information about the lattice dynamics of the host crystal. The vibrational properties of many types of defects have been investigated in detail, among them U centers (an H^+ impurity at a cation site), and a variety of other types associated with atomic or molecular impurities or with adjacent impurities and vacancies. Particularly interesting is the Li^+ impurity in KBr and KCl, which has a low frequency resonance despite its small mass because of very weak binding to its neighbours. In KCl, in which the resonance mode has been exhaustively studied by almost every applicable method except neutron scattering (Clayman and Sievers, 1968, Narayanamurthi and Pohl, 1970), the Li impurity is known to have its equilibrium position somewhat off the cation site, performing a tunnelling motion in a shallow double well. Several other examples of 'off-centre' impurities are known. Besides resonance modes and high frequency local modes, each of which are exhibited by a number of types of impurities, there are some cases in which a localized mode can be formed with a frequency in the band gap of the host (e.g., Nolt et. al., 1967).

In an infrared absorption experiment, the impurity-induced absorption is approximately proportional to the defect concentration, and very low defect concentrations are required for an observable effect. The method is thus a very sensitive one, but suffers somewhat from the rather complicated nature of the basic interaction between the probe and the absorber, and from its fairly limited applicability (viz., defects in ionic crystals and, sometimes, in semiconductors). The method is not well suited for investigations of the very high impurity concentrations that we consider in this thesis. Other optical methods that have been employed in the study of impurity vibrations are infrared reflectance measurements, Raman scattering, and the spectroscopy of the sidebands of electronic or molecular vibrational transitions associated with impurity centers.

The current-voltage characteristics of superconducting tunnelling junctions (metal-insulator-superconductor) at low temperatures contain structure that reflects the details of the phonon spectrum of the superconductor. The data can be inverted (McMillan and Rowell, 1965) to give a quantity $\alpha^2(\omega)g(\omega)$, where $g(\omega)$ is the phonon frequency distribution, and $\alpha(\omega)$ is a slowly varying function of frequency related to the strength of the electron-phonon interaction. When impurities are introduced, extra peaks may appear in $g(\omega)$. The experiments of Rowell et. al. (1965) and Adler et. al. (1966) clearly show localized modes. For this method to be

easily applicable, the host material must be a superconductor.

The Mössbauer effect can in principle be used to study defect vibrations (Visscher, 1962; Maleev, 1961), since either the γ-emitter or absorber, or both, can be impurity nuclei. It has not, however, been extensively used to date (1972), apparently because of technical difficulties. In addition to the sharp no-phonon line in the Mössbauer spectrum, there should be structure at slightly higher and lower γ-ray energies corresponding to one- and multi-phonon transitions. The observation of these sidebands would be a direct type of spectroscopy roughly equivalent to superconducting tunnelling or incoherent inelastic neutron scattering, but with much better resolution. Only the no-phonon line in the Mössbauer spectrum is accessible by present techniques. From measurements of the recoil-free fraction and second-order Doppler shift, the mean-square displacement and mean-square velocity of the impurity can be obtained. (For example, see Dawber and Elliott, 1963, Maradudin; 1966a, for the relevant theory.) These are properties averaged over all the modes, rather than of individual modes.

Many of the bulk properties of crystals are also strongly influenced by defects, notably the electrical resistivity, thermal conductivity and specific heat. Although measurements of these quantities do not represent direct spectroscopy of the impurity vibrations, the properties

themselves are obviously very important physical characteristics for any material. Thermal conductivity measurements in insulators, electrical resistivity in metals, and specific heat in both, all have been used to study resonance modes, with results often complementary to infrared or neutron experiments. References to experimental and theoretical papers on these methods may be found in the review articles of Pohl (1968) and Maradudin (1966a).

(ii) Neutron Scattering Experiments on Impurity Vibrations

As mentioned in Chapter I, the neutron scattering method has the inherent advantage that the interaction between the probe and the nuclei of the specimen is known precisely, either from tabulated information or, much more rarely, by means of an auxiliary experiment. However, in a defect experiment, the way in which the scattering lengths enter into the theory is slightly more complicated than is the case for perfect crystals. The situation has been considered in detail by Elliott and Taylor (1967) and Taylor (1965) for low concentrations of mass defects.

For a perfect cubic Bravais crystal, the incoherent inelastic scattering (equation I-7) from one-phonon processes is proportional to the frequency distribution $g(\omega)$. For a crystal containing impurities, this is only approximately true. The extra peaks contributed to $g(\omega)$ by resonance modes or local modes can be enhanced or diminished by the

scattering properties of the host and defect atoms. Both local modes and resonance modes have been observed by incoherent neutron scattering. The first experiments were carried out by Mozer et. al. (1962), who observed the local modes associated with 5 and 10 at.% Ni in Pd, and by Chernoplekov and Zemlyanov (1966), who observed the resonance mode of heavy Pb impurities in an alloy of Mg-2.8 at.% Pb. In both cases, the results were in good agreement with the predictions of mass defect theory. It should be noted that the incoherence in these cases arises from the difference in the coherent scattering lengths of host and defect atoms as well as from the incoherent scattering cross-sections of the host and defect atoms separately. For Mg(Pb), the incoherence must be solely of this nature, since the incoherent scattering cross-sections of pure Mg and pure Pb are negligible. This is probably why the resonance mode shows up so strongly - the incoherence that is present reflects the self-correlation, i.e. the large individual motion, of the defect atoms, and not the host atoms, in the impurity mode. Similarly, in Pd(Ni), the fairly large incoherent cross-section and large coherent scattering length of Ni must enhance the scattering from the local mode. In these experiments, the possibility of spurious structure arising from the coherent background casts doubt on the nature of the results, although that spurious peaks should so precisely simulate peaks from impurity modes seems rather unlikely.

In order to remove this objection, Mozer (1968; see also Mozer et. al., 1966) has reported further measurements on alloys of vanadium containing a few atomic percent of Be, Ni, Ta, W, and Pt. These alloys should be almost purely incoherent scatterers. Local modes were observed for Be (a light impurity) but no resonance modes were seen for W, Ta, or Pt (heavy impurities). The latter fact was attributed by Mozer to correlation between pairs of defects and perhaps anharmonic effects. Zemlyanov et. al. (1968) have carried out similar measurements in vanadium based alloys but report positive observation of resonance modes in V(W) and V(Ta). Chernoplekov et. al. (1967) have made measurements on an alloy of Ti(5%U); the scattering from the resonance mode does not show up very strongly in this case. Natkaniec et. al. (1967, 1968) have reported experiments on local modes in Mg(Li), Cu(Be), Cu(Mg), Pb(Na), and Pb(Mg) alloys. These authors attribute the local mode intensity entirely to incoherent scattering, but it is possible that some contribution from coherent scattering is present. The conclusions which they draw would not be modified even if this is the case. The deviations of the measured local mode frequencies from mass defect theory were used by Natkaniec et. al. to estimate force constant changes. Incoherent scattering has also been used to study the local modes of interstitial hydrogen defects in vanadium (Rubin et. al., 1965). The importance of incoherent neutron scattering

lies in the fact that it provides a relatively simple way of looking at defect modes in normal metals. This cannot be done by infrared absorption or tunneling measurements. A single crystal is not needed, and only a few scattered neutron distributions must be measured. However, in the experiments that have been carried out to date, the only quantitative pieces of information that have been obtained in a convincing manner are the frequencies of the impurity modes. In principle, the method should reveal the width and shape of the impurity mode as a function of concentration and local environment. Possibly such information will be obtained if the incoherent scattering technique is used in conjunction with crystal spectrometry or at reactors with intense neutron beam facilities.

On the basis of the few experiments carried out to date, coherent inelastic neutron scattering shows much more promise as an effective means of investigating the dynamics of imperfect crystals. The method allows the experimenter to measure the dispersion curves and phonon widths in any crystal that does not absorb neutrons too strongly. (Only a few elements such as B, Cd, Gd, Sm, and Eu are strong enough absorbers in their natural isotopic composition to make an experiment essentially undoable for this reason.) By using coherent scattering, one should therefore be able to determine the frequencies and lifetimes of the modes in the imperfect system for a wide variety of materials. Thus it is potentially

the most powerful and universally applicable of all methods of studying defect vibrations and the dynamics of disordered systems,particularly in those cases where optical methods are not applicable. Experiments by coherent neutron scattering can be carried out on materials with moderate or large impurity concentrations, provided suitable specimen crystals are available. Concentration dependent effects are of major interest in this type of measurement. In common with incoherent scattering, most of the experiments to date have been on cubic monatomic metals containing impurity concentrations of a few atomic percent or more. There is thus not much overlap of those aspects of impurity dynamics examined so far by optical and neutron methods. However, as we have just emphasized, there is no restriction in principle of neutron scattering to metals, and studies complementary to optical experiments may turn out to be useful. The main obstacles to further progress in the application of coherent neutron scattering are the availability of suitable single crystal specimens, the limited intensity and resolution available with present neutron sources and spectrometers, and the relative complexity and cost of a neutron experiment.

In coherent scattering, localized modes can be observed directly, just as in infrared absorption, tunnelling, or incoherent scattering measurements, but in addition to the ability to measure the frequency position of the local mode, one is also able to study its dispersion and spatial

variation. The latter is done by measuring the intensity of the scattering from the local mode as a function of the wave vector transfer Q. This is analogous to determining the lifetime of a mode by measuring its energy width; here the localization in real space is determined by measuring the width in reciprocal space.

Three experiments on local modes have already been reported. Nicklow et. al. (1968a, 1968b) have determined the spatial extent as well as the frequency of local modes in Cu(Al) alloys containing 4 and 10 at.% Al. They find good agreement with mass defect theory for both the frequency and extent of the local mode vibration, but not for the perturbation of the band modes, also measured in their experiment. It was found to be possible to adjust the latter into agreement if allowance was made for the expansion of the lattice upon alloying by means of an average Grüneisen parameter obtained from thermodynamic data. In a similar experiment on Ta-12 at.% Nb, Als-Nielsen (1968) was unable to resolve the local-mode peak from the band modes, but showed that the shapes of the observed neutron groups were indicative of the presence of a local mode. Very recently, Wakabayashi et. al. (1971) have made measurements on the local mode in Ge-9.2 at.% Si. They observe an appreciable amount of dispersion for the local mode, indicating that in this alloy, the impurity concentration is too high for an isolated defect theory to apply. The amount of dispersion was found to be in

remarkably good agreement with the finite concentration theory of Elliott and Taylor (1967). Again, it was found to be necessary to allow for the expansion of the host lattice, but once this had been done, good agreement with mass defect theory was obtained for the frequency shifts of the band modes.

In contrast to the case of local modes, resonance modes cannot be observed directly by coherent scattering. One observes instead a characteristic resonant perturbation of the dispersion curves. The introduction of impurities that are sufficiently heavy or weakly bound causes the normal modes to acquire widths and frequency shifts which show a complementary resonant behaviour for phonons having frequencies near the frequency of the impurity mode.

The first studies of the effects of impurities on lattice vibrations using coherent neutron scattering were concerned with resonance modes rather than local modes. Bjerrum Møller and Mackintosh (1965) carried out measurements of the impurity-induced shifts in the $[\zeta\zeta 0]T_2$ branch in Cr-3 at.% W, while Svensson, Brockhouse and Rowe (1965) carried out similar measurements on the $[00\zeta]T$ branch in Cu-9 at.% Au, measuring impurity-induced widths as well. Resonant perturbation was observed in both cases, but with results in only qualitative agreement with mass defect theory. In Cu(Au), the amplitudes of the impurity-induced effects were

accurately predicted by calculations based on the mass defect theory of Elliott and Maradudin (1965), but the resonance was much broader and occurred at a higher frequency than was indicated in the calculations. The line shapes of the calculated and observed neutron groups were also found to be in serious disagreement. (Detailed computations carried out by Svensson (1967) for Cu-9% Au are shown in figure II-8, reproduced from Svensson and Kamitakahara (1971).) In Cr(W), the resonance was sharply defined, but occurred at a higher frequency and with a larger amplitude than in mass defect calculations by Svensson (1967).

Force constant changes, concentration effects, lack of self-consistency, and the possible existence and influence of short range order were all considered as the source of non-correspondence of experiment and theory in these original measurements on Cu(Au) and Cr(W). The first two appeared to be the most probable causes. For Cr-3 at.% W, the alloy should be sufficiently dilute for a low concentration theory to apply, and force constant changes are the obvious thing to consider. It nevertheless seems rather strange that the resonance should be both larger in amplitude and higher in frequency than predicted, since one would expect a resonance enhanced by weaker force constants to the impurity to be lowered in frequency. In Cu-9 at.% Au, the smearing out of the resonance suggested a concentration effect, and an experiment on Cu-3 at.% Au was undertaken to determine if this was in fact the case.

The impurity-induced shifts and widths were measured for phonons in the $[\zeta\zeta 0]T_1$ branch up to $\zeta = 0.45$. Quantitative agreement with mass defect theory was observed (Svensson and Brockhouse, 1967). However, since it was a different branch - $[00\zeta]T$ - that had been measured in Cu-9 at.% Au, the concentration dependence had still not been conclusively demonstrated. In further measurements on Cr-3 at.% W by Mackintosh and Bjerrum Møller (1968), the impurity-induced widths and shifts in the $[00\zeta]T$ and $[\zeta\zeta 0]T_2$ branches showed a strong dependence on the branch, not being simply functions of the unperturbed (host lattice) frequencies as predicted by mass defect theory. The resonance in the [110] direction has a slightly higher frequency and a substantially larger amplitude than in the [001] direction. The disagreement has been shown to persist to very low W concentrations by Cunningham et. al. (1970), who have measured the frequency shifts in the same branches for alloys of Cr-0.3, 0.8, and 1.6 at.% W. The shifts do not appear to be simply proportional to the impurity concentration but it is difficult to know if this is not an instrumental effect. In our own results for Cu-1 at.% Au, shown in Fig. II-6, the resonances also look smeared out. Considering the trend of the data in these two branches for Cu-3 and 9 at.% Au, a resolution effect, or simply a statistical effect arising from the large random errors on the points, seems most probable.

Further results on Cu(Au) alloys have been reported (Svensson and Kamitakahara, 1971); these measurements,

supplemented by more recent data, are presented and discussed in the remainder of this chapter. The measurements have been made for three alloy concentrations - 1,3, and 9 atomic percent Au - and several different branches - [00ζ]L, [00ζ]T, [ζζ0]T_1, and [ζζζ]T in Cu-9% Au, [00ζ]T, [ζζ0]T_1 and [ζζζ]T in Cu-3% Au, and [00ζ]T and [ζζ0]T_1 in Cu-1% Au. The results, which clearly show that the resonance mode has a strong branch dependence as well as a concentration dependence, are compared with detailed calculations based on low concentration mass defect theory. Theoretical work pertaining to the way in which force constant changes and other factors might be included in the theory are discussed, and some suggestions for the direction of future work are given.

(iii) Choice of the Cu(Au) System

The Cu(Au) system is a particularly favourable candidate for an impurity mode experiment from several points of view. The mass ratio of Au to Cu is large (3.1) and well developed resonance modes should occur. Other favourable properties of the system are the following:

(1) Physical, chemical, and alloying properties

It is well known that gold and copper have similar electronic structure. Also, the lattice constants differ by only about 11% (Pearson, 1958, 1967).

$$a_{Cu} = 3.6147 \text{ Å at } 20^{\circ}C$$

$$a_{Au} = 4.0785 \text{ Å at } 23^{\circ}C$$

The melting temperatures are also very close.

$$T_m \text{ (Cu)} = 1083^{\circ}C$$

$$T_m \text{ (Au)} = 1063^{\circ}C$$

Copper and gold are chemically similar. They are, respectively, the noble metals with one 4s and 6s valence electron per atom. Hence it was anticipated that a gold atom in copper would simulate, as well as possible, a substitutional impurity which differs from an atom of its host only through its much larger mass.

The phase diagram (Hansen, 1958, p. 198) shows that alloys of Au and Cu are solid solutions with no long range order for gold concentrations of less than 18 at.%. Large single crystals are available commercially; these are essential for a neutron scattering experiment in which extensive measurements are to be made with good resolution.

(2) Lattice dynamical properties

The crystal dynamics of copper have been very thoroughly investigated by several workers. The most accurate measurements of the phonon dispersion curves are by triple-axis spectrometry, carried out by Svensson, Brockhouse and Rowe (1967) at 296°K, by Nicklow et. al. (1967) at 49 and 298°K, and by Miiller and Brockhouse (1971) at 296, 473, and 673°K. Further measurements are presently being made at McMaster University at temperatures up to 1050°C, 30° below the melting temperature, in order to study anharmonic properties (A. Larose,

private discussion). The dispersion curves at room temperature are devoid of unusual features; they are dominated by strong nearest-neighbour force constants that almost satisfy the conditions of central forces. Observation of the Kohn effect in copper has been reported (Nilsson, 1968), but it is a very small effect. This is in contrast to the case of chromium where large anomalies related to the electronic structure have been shown to occur (Muhlestein et. al., 1972.)

The dispersion curves of gold have not yet been measured, although the experiment is probably not very difficult. Those of silver (Kamitakahara and Brockhouse, 1969, and Appendix I of this thesis) show a great similarity to copper, apart from a scaling factor. There is some indication from specific heat measurements (Martin, 1966) that the lattice vibrations in Au may exhibit some anomalous behaviour, but this is far from certain, and, we feel, rather unlikely, if the dispersion curves of other F.C.C. noble and transition metals serve as any indication. The force constants that determine the lattice vibrations in pure Au do not, of course, bear a direct relationship to those of a gold impurity in copper, but they would be a valuable indication. Some measurements are now being made at Laurentian University, Sudbury, Ontario (E.D. Hallman, private discussion) on a crystal of Cu_3Au in both the ordered and disordered states. If Cu-Cu, Au-Au, and Au-Cu force constants can be extracted from these,

hopefully one should be able to estimate what they are in the Cu(Au) alloys that are the subject of the investigations described in this chapter.

The initial slopes of the dispersion curves for different branches, ν/q, are proportional to $(ac_i/M)^{1/2}$, where c_i is the appropriate linear combination of elastic constants, a is the lattice parameter, and q is the phonon wave vector in units of $2\pi/a$ (reduced wave vector). The elastic constants of Cu (Overton and Gaffney, 1955), Au (Neighbours and Alers, 1958), Cu_3Au (Flinn, McManus and Rayne, 1971), and of Cu(Au) alloys containing 0.23, 2.8, and 10.0 atomic percent Au (O'Hara and Marshall, 1971) have been measured. An estimate of the elastic constant changes from pure Cu to Cu (3% Au) was made by plotting the available values of the elastic constants as functions of the Au concentration and drawing a smooth line through the points. The fractional frequency shift arising from force constant changes, in the long wavelength limit, is then given by

$$\frac{\Delta\nu}{\nu} = \frac{1}{2}\frac{\Delta(ac_i)}{ac_i} = \frac{1}{2}\frac{\Delta a}{a} + \frac{1}{2}\frac{\Delta c_i}{c_i}$$

Similarly, the fractional frequency shift arising from the mass change, in the long wavelength limit, is $-\frac{1}{2}\frac{\Delta M}{M}$, where ΔM is the change in the mean mass. The magnitude of the shift from force constant changes was found to be less than 10% of

of the shift from the mass change for the three transverse branches [ζζζ]T, [00ζ]T, and [ζζ0]T_1, and about 20% for the [00ζ]L branch. However, this does not necessarily mean that the effects of force constant changes are small for higher frequencies, particularly in the resonance region. It is the average force constant changes that one is estimating through the elastic constants. The changes in the Au-Cu force constants can still be large if they are compensated by changes of opposite sign in the average Cu-Cu force constants. In the resonance region, the effects of these force changes could be large and are difficult to estimate in a simple way.

(3) Neutron properties

The tabulated thermal neutron cross sections (Hughes and Schwartz, 1958; Goldberg et. al., 1966), listed below, show that, apart from the fairly high absorption cross section of gold, the neutron properties of the Cu(Au) system are very favourable for an experiment by coherent scattering.

	Copper	Gold
σ_{coh}(barns)	7.25 ± 0.4	7.3 ± 0.1
σ_{abs}	3.77 ± 0.03	98.8 ± 0.3
σ_{inc}	0.7	-

The incoherent cross sections are small, and the coherent cross sections are identical within errors. The latter fact

means that equation I-65 for the one-phonon coherent cross section in low concentration mass defect theory becomes somewhat simpler. The second term inside the square brackets on the right hand side of the equation drops out, and we have, neglecting the difference between host and impurity Debye-Waller factors,

$$S_{coh}^{(1)}(\underline{Q},\omega) = [n(\omega)+1]\frac{b^2}{M_h}\exp(-2W)\sum_j (\underline{Q}\cdot\underline{\xi}^j(\underline{q}))^2 \text{ Im } G_j(\underline{q},\omega) \tag{II-1}$$

Thus in this case we are able to look directly at the Fourier transform of the displacement-displacement pair correlation function, averaged over all configurations of the impurities.

From Eq. I-62, writing $V(\omega) = V_1(\omega) + iV_2(\omega)$, where V_1 and V_2 are real functions of ω, we obtain

$$\text{Im } G_j(\underline{q},\omega) = \frac{cV_2(\omega)}{[\omega^2 - \omega_j^2(\underline{q}) - cV_1(\omega)]^2 + [cV_2(\omega)]^2} \tag{II-2}$$

This is a quasi-Lorentzian form in ω^2, and therefore in ω for ω sufficiently large compared with the width of the peak in Im $G_j(\underline{q},\omega)$. The peak is shifted away from $\omega = \omega_j(\underline{q})$ by an amount approximately given by

$$\Delta(\omega) = \frac{cV_1(\omega)}{2\omega} \tag{II-3a}$$

and acquires a width

$$\Gamma(\omega) = \frac{cV_2(\omega)}{\omega} \tag{II-3b}$$

Eqs. II-3 assume that V_1 and V_2 are slowly varying functions of ω, not changing appreciably in a region of breadth Γ centred about $\omega = \omega_j(\underline{q}) + \Delta$. Hence, the approximation of these equations is better for small concentrations and frequencies away from the resonance, i.e., when the widths are small. 'Better' values of the shift and width, not involving this approximation, can be obtained directly from calculations of the line shapes themselves by means of Eq. II-2.

In the limit of zero concentration, the line shape reduces to

$$\text{Im } G_j(\underline{q},\omega) = \frac{\pi}{2\omega} [\delta(\omega - \omega_j(\underline{q})) - \delta(\omega + \omega_j(\underline{q}))] \qquad \text{(II-4)}$$

As one can see from Eq. II-2, the line shape in this (mass defect) theory depends on $\underline{q}$ only through the mode frequency of the host $\omega_j(\underline{q})$. Hence one can calculate a set of line shapes $L(\omega,\omega_o)$ valid for all branches of the phonon spectrum by replacing $\omega_j(\underline{q})$ by ω_o on the right hand side of equation II-2. We need only have knowledge of the frequency distribution $f(\omega)$ of the host lattice in order to calculate the functions V_1 and V_2 through Eqs. I-63 and I-64. For copper, because of the simplicity of the dispersion relation, a very accurate $f(\omega)$ can be obtained from a force constant model fitted to neutron scattering measurements of the dispersion curves. Calculations of V_1, V_2 and the line shapes $L(\omega,\omega_o)$ from an $f(\omega)$ obtained from a 6th neighbour model fitted to

the neutron measurements of Svensson et. al. (1967) have been carried out by Svensson (1967, Svensson and Kamitakahara, 1971). The calculated line shapes for Cu(3% Au) and Cu(9.3% Au) are shown in Fig. II-8. For these calculations and for all the experimental measurements in the thesis, the angular frequency has been replaced by the frequency $\nu = \omega/2\pi$. The unit of frequency conventionally used is THz, or 10^{12} cycles per second.

B. EXPERIMENT

(i) The Specimen Crystals**

The Cu and Cu(9.3 % Au) crystals used in the first measurements on Cu(Au) alloys (Svensson et. al. 1965) were approximate spheres of about 1" diameter which had been machined from 1" diameter cylindrical crystals. The composition (9.3 % Au) of the alloy crystal was determined by chemical analysis by a commercial analytical laboratory. (In this thesis, % means atomic percent when specifying an alloy composition.) This alloy crystal was of rather poor quality (mosaic spread about 1.2^{o}FWHM), and subsequently a much better crystal (mosaic spread about 0.5^{o}FWHM) of nominal composition

---

** The following two subsections, II B(i) and II B(ii), are taken, with some modifications, from Svensson and Kamitakahara (1971). This excerpted portion of the paper was written primarily by W.A.K.

Cu(9.3 % Au)was obtained . This crystal and all of the other specimen crystals used for the measurements reported in this thesis were cylindrical. Some of the characteristics of these crystals are summarized in Table II-1. The second Cu(9.3 % Au) crystal was cut into 2 pieces of about equal length which were mounted parallel to each other.

TABLE II-1

Characteristics of copper and copper-gold crystals

specimen	diameter (inches)	angle between [100] and cylinder axis	approximate mosaic spread	lattice constant (A)
Cu(9 % Au)	1/2	5^{o}	0.5^{o}	3.666_{6}
Cu(3 % Au)	5/8	2^{o}	0.5^{o}	3.634_{1}
Cu(1 % Au)	1/2	30^{o}	0.5^{o}	3.621_{5}
Cu(crystal#1)	1	0^{o}	0.5^{o}	3.6147
Cu(crystal#2)	3/4	0^{o}	0.3^{o}	3.6147

The lattice constants in Table II-1 were obtained by neutron diffraction following the method of Ng et. al. (1967). At each of a set of equally incremented values of the scattering angle ϕ around the Bragg angle, the specimen is rocked through the Bragg position. The peak intensity of each rocking curve is plotted against the scale reading of ϕ, yielding a peak similar to a power diffraction peak. The procedure is then repeated with a reference crystal (usually an element

with an accurately known lattice constant) which has a Bragg peak near the same value of ϕ as the recorded peak position for the primary specimen. The peaks obtained for the (220) Bragg reflections of Cu and two Cu(Au) alloys are shown in Fig. II-1. When both incident and diffracted beams are highly collimated, and only neutrons of a very narrow energy range are accepted (by using a rather perfect monochromator crystal or analyser crystal), one can then calculate an accurate value of the lattice constant of the primary specimen with respect to that of the reference crystal. Neglecting extinction effects, the average lattice constant obtained in this way should be precisely the value which applies to actual phonon measurements. If one takes the width (FWHM) of the peak for the reference crystal as the instrumental resolution, then the width of the peak for an alloy specimen gives a measure of its inhomogeneity. As shown in Fig. II-1, appreciable inhomogeneity is present in the Cu(3% Au) and Cu(9% Au) specimens. For Cu(9% Au), the width (FWHM) indicates a spread of about 2 at.% in the impurity concentration over the volume of the crystal. No significant broadening was observed for the Cu(1% Au) specimen which is omitted from Fig. II-1 because it was characterized using slightly different experimental conditions. Although the cylindrical crystals were not subjected to chemical analysis in order to determine their composition, the lattice constant measurements show that the nominal and actual compositions are quite close.

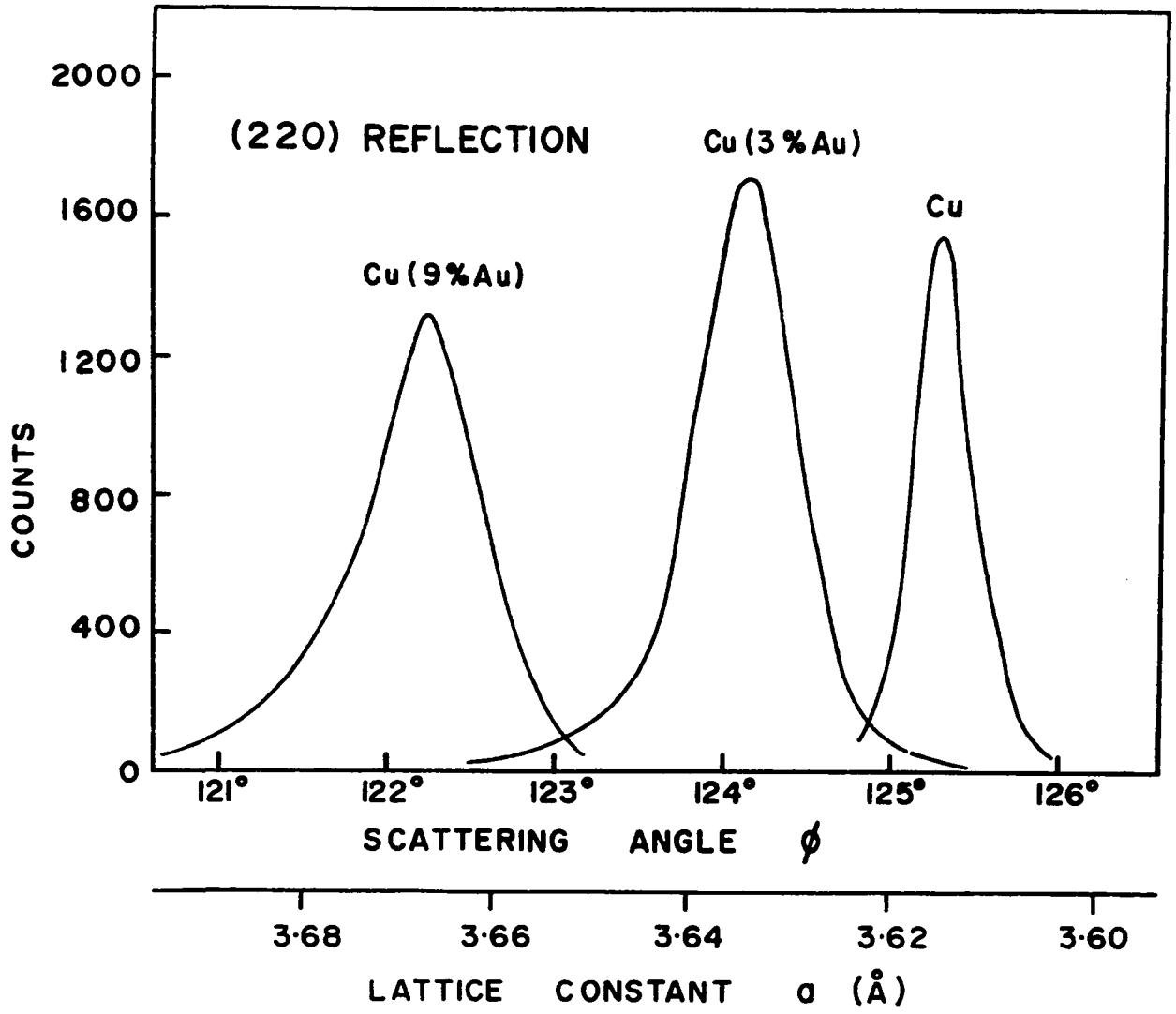

Fig. II-1. Characterization of Cu(Au) and Cu single crystals by neutron diffraction as described in the text. The peaks are comparable with powder diffraction peaks; the positions and widths of the copper-gold peaks, relative to the position and width of the copper reference peak, accurately indicate the lattice constants and inhomogeneities of the alloy specimens.

The lattice constants indicate that for nominal compositions of 9.3, 3, and 1 at.% Au, the actual compositions are 8.8±1.0, 3.1±0.4 and 1.17±0.15 at.% Au, respectively. The accuracy here is limited by the lack of accurately measured lattice constants as a function of composition for Cu(Au) alloys (Pearson 1958). Henceforth the alloy crystals will be labelled as having compositions of 1, 3, and 9 at.% Au. Except for the Cu(1 % Au) crystal, which was supplied by Materials Research Corporation, Orangeburg, New York, all specimens were obtained from Research Crystals Incorporated, Richmond, Virginia.

(ii) Neutron Scattering Measurements

The measurements were carried out using three different triple-axis spectrometers. The [00ζ]L and [00ζ]T branches in Cu(9% Au) were studied using the spectrometer (Brockhouse, 1961) at the C5 facility of the NRU reactor, Chalk River. The earlier measurements (Svensson and Brockhouse, 1967) on the $[\zeta\zeta 0]T_1$ branch in Cu(3% Au) were carried out using the triple-axis spectrometer (Brockhouse et. al., 1968) at the McMaster University Nuclear Reactor. All other measurements were carried out using the McMaster University spectrometer (Brockhouse et. al., 1968), described in Chapter I, located at the E2 facility of the NRU reactor, Chalk River. The C5 spectrometer normally operates with fixed scattered-neutron energy (fixed-E'). During the course of most of the

measurements reported in this chapter, both of the McMaster spectrometers used fixed incident-neutron energy (fixed-E_o). The E2 spectrometer has recently been modified so that it now is normally operated using the fixed-E' mode of operation, which has several important advantages over fixed-E_o in an experiment in which large widths are to be measured and consecutive measurements over a wide range of phonon frequencies are desirable. The measurements on the [ζζζ]T branch in Cu(3% Au) and Cu(9% Au), which have not been previously reported, were taken using fixed-E'.

More difficulty was encountered in the measurements with the E2 spectrometer than with the other two spectrometers. Because of an oversight in the design of the double-crystal monochromator, the beam reaching the specimen table was not, until recently, purely monochromatic. It contained a contaminant component which was of higher energy than the main component of the beam and which comprised about 15% of the total intensity. The number of processes that could give rise to spurious peaks in the scattered-neutron distributions was thereby increased. Spurious peaks caused by the contaminant component were encountered in the measurements of the [00ζ]T branch for Cu(3% Au) and Cu(1% Au), and consequently there are gaps in the data in these cases (see Figs. II-4, II-5, and II-6). We were unable to completely eliminate these spurious peaks, but by using different incident-neutron

energies, E_o, they could be shifted to different regions of the [00ζ]T branch. The gap(s) occurring for a particular E_o could therefore be filled in with results obtained with a different E_o (see Figs. II-4, II-5, and II-6). New monochromator crystals were recently installed to eliminate the contaminant and the beam is now very clean. Because the second order reflectivity for most crystal reflections used in neutron monochromatization is usually much less than the first order reflectivity, a double monochromator gives intrinsically less second order contamination since two reflections are involved.

All of the measurements were carried out using the constant-momentum-transfer (constant-$\underline{Q}$) technique (Brockhouse, 1961) described in Chapter I. For each alloy and each branch studied, constant-$\underline{Q}$ scans were carried out consecutively at adjacent (and usually equally incremented) wave vectors along the branch. For comparison, corresponding scans (same values of $a\underline{Q}/2\pi$ where a is the lattice constant) were carried out for pure copper under identical experimental conditions. An important advantage of this procedure is that any systematic errors in the measurements have an almost negligible effect on the impurity-induced widths and on the relative frequency shifts along any particular branch. Systematic errors, such as might arise from specimen misalignment, calibration errors, or the effects of finite collimation of the neutron beams, can of course lead to an approximately constant error in the

frequency shifts for any particular branch. Systematic errors could therefore cause a vertical displacement (possibly different for each branch) of the frequency shifts shown in Figs. II-3 to II-6, but they could not significantly alter the general 'shapes' of the results. Systematic errors are relatively much more important at low impurity concentrations where the absolute frequency shifts are small. For Cu(1% Au), we estimate that the contribution of possible systematic errors to the frequency shifts is about 0.02 THz which is 25% (40%) of the maximum observed shift for the $[00\zeta]T$ ($[\zeta\zeta 0]T_1$) branch (see Fig. II-6). The errors assigned to the frequency shifts in Figs. II-3 and II-4 allow, at least partially, for possible systematic errors, and hence, in general, the scatter of the experimental results is considerably less than would be expected from the errors shown.

(iii) Results for Cu(9% Au)

The impurity-induced widths and frequency shifts for four branches in Cu (9% Au) are shown in Figs. II-2 and II-3 respectively. The results are plotted against the frequency of the corresponding mode (i.e., the mode of the same reduced wave vector) in pure copper. The reason for the arrangement of the data for different branches in these figures is to permit an easy comparison with the results on Ni(55%)Pd(45%) described in the next chapter. The earlier results of Svensson et. al. (1965) for the $[00\zeta]T$ branch in Cu(9.3% Au), which

Fig. II-2. Impurity-induced widths for Cu(9% Au) plotted against the frequency of the corresponding mode in pure copper. The solid and dotted lines are derived from low concentration mass defect theory and represent Eq. II-3b and the FWHM's of the calculated line shapes respectively.

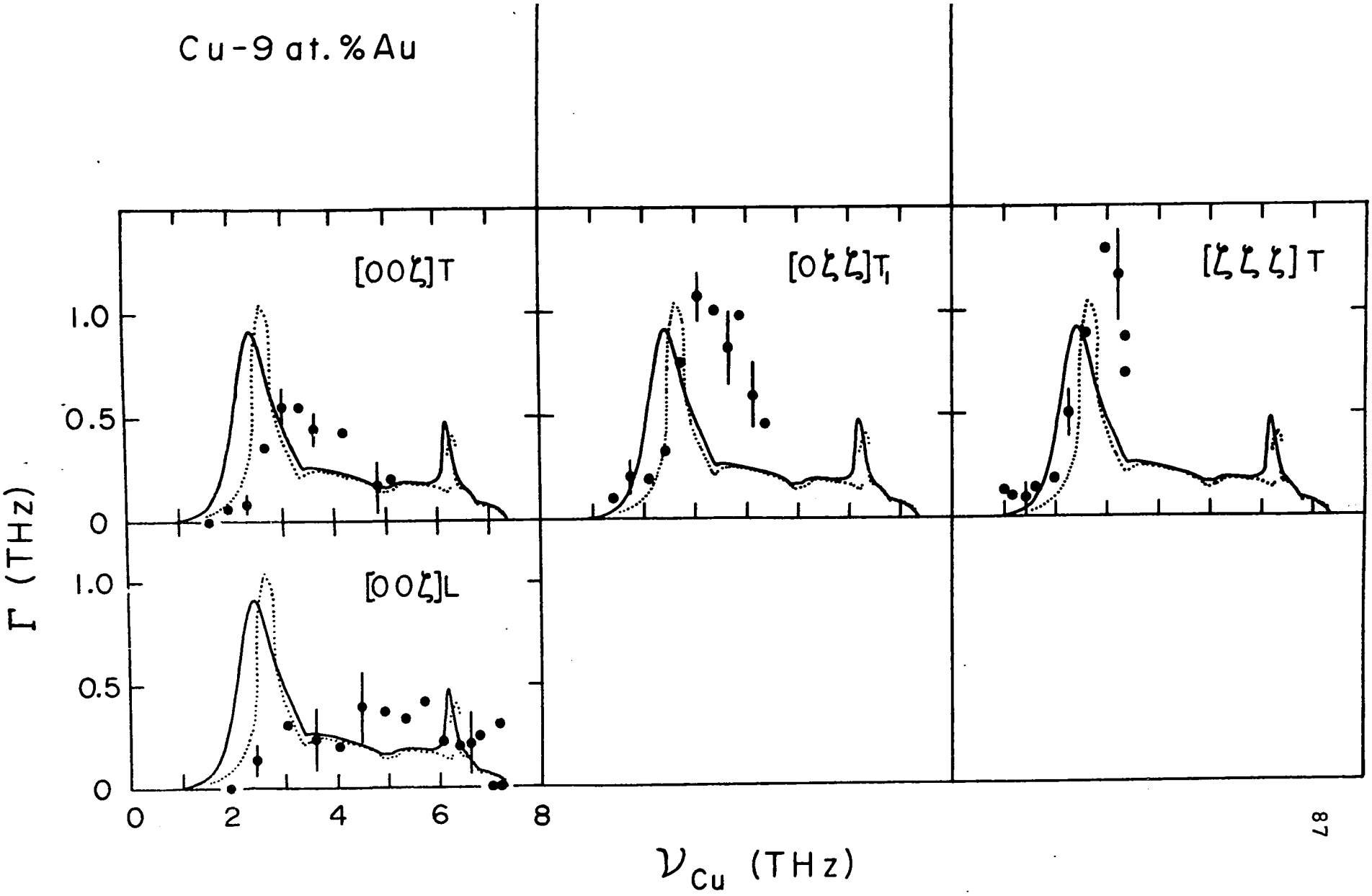
Cu-9 at.% Au
[00ζ]T
[0ζζ]T1
[ζζζ]T
[00ζ]L
Γ (THz)
1.0
0.5
0
0
2
4
6
8
νCu (THz)

Fig. II-3. Impurity-induced frequency shifts for Cu(9% Au). The lines are from low concentration mass defect theory. The solid, dashed, and dotted lines respectively represent Eq. II-3a, and the peak and centre positions of the calculated line shapes.

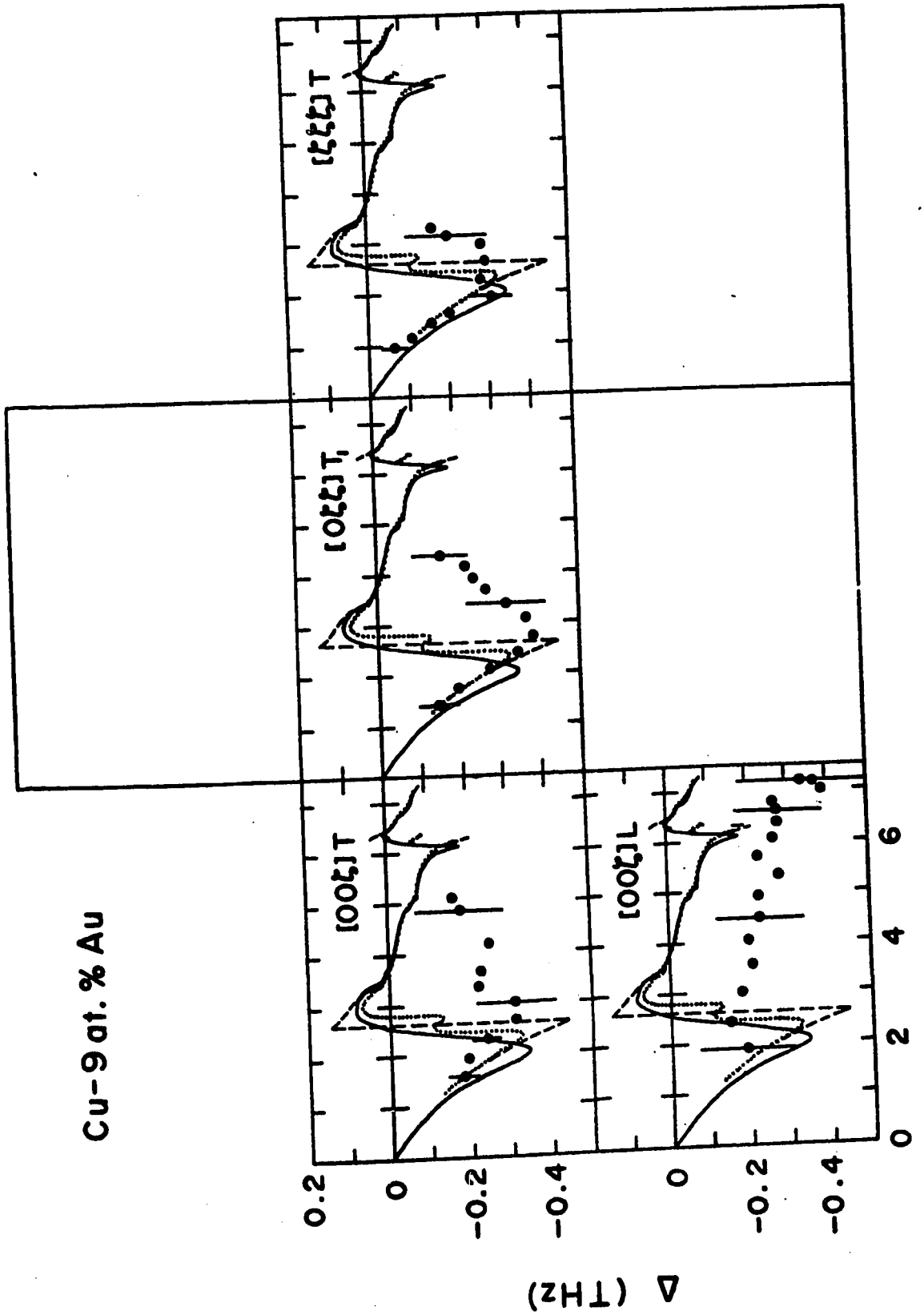
Cu-9 at. % Au
[ξξ0]T
[0ξ0]T
[00ξ]T
[00ξ]L
0.2
0
-0.2
-0.4
0
2
4
6
Δ (THz)
ν_{Cu} (THz)

were made on a different specimen crystal, are not shown. They agree within experimental error with the data for the same branch shown in Figs. II-2 and II-3. The measured impurity-induced widths and shifts for this branch were systematically slightly larger in the earlier experiment, but this may simply reflect a slightly higher Au concentration (determined by chemical analysis to be 9.3 at.% for the crystal used by Svensson et. al., and estimated from neutron diffraction measurements to be 8.8±1.0 at.% for the crystal used in the present experiment.)

Resolution extraction procedure for widths

In order to obtain the data points of Fig. II-2, which are natural widths, the resolution of the spectrometer had to be subtracted off. This was done by assuming that the observed line shapes could be adequately represented by a convolution of the Gaussian spectrometer resolution function with the natural line shapes, assumed to be Lorentzian. The validity of this assumption was tested for Ni(55%)Pd(45%) by using the quasi-Lorentzian line shapes produced by low concentration mass defect theory and was found to be quite adequate in that case (see Fig. III-3). Since the theoretical line shapes for Cu(9.3% Au) are qualitatively similar to those for Ni(55%)Pd(45%) (compare Figs. II-8 and III-11), showing double peaks in the resonance regions, but less radically non-Lorentzian, the resolution extraction procedure is undoubtedly also quite

adequate for Cu(9% Au). In fact, the experimental neutron groups did not show the radical structure predicted by mass defect theory, although pronounced asymmetries were observed, so that the procedure should work even better than indicated by Fig. III-3. The line shapes will be discussed in detail later in this chapter.

For most of the measurements on Cu(9% Au), the resolution was taken to be the width of the corresponding mode in pure copper. At room temperature, the observed widths contain a small contribution from anharmonicity which is detectable in well-focussed neutron groups corresponding to tranverse modes (Nicklow et. al., 1967). However, this contribution should be about the same for both the Cu and Cu(Au) specimens. The adequacy of this procedure may be questioned in view of the fact that the theoretical dispersion curves, obtained by adding the mass defect theory frequency shifts to the Cu dispersion curves, show 'kinks' (i.e. rapid changes in slope) in each branch near the resonance frequency. Since focussing effects (see Chapter I) in a crystal spectrometer make the resolution width fairly sensitive to the slope of the dispersion curve, the resolution for Cu and Cu(Au) are not necessarily the same. However, in the experiment, no real 'kinks' were observed, the resonances being generally broader than anticipated. Also, in the low wave vector region where there is no appreciable impurity broadening, the Cu and Cu(Au) experimental widths were very nearly the same,

in spite of the fact that the dispersion curves start out with somewhat different slopes. Finally, for the results on the $[\zeta\zeta\zeta]T$ branch**, the resolution widths were calculated (Cooper and Nathans, 1967) and checked against widths measured for pure copper at five equally spaced points along the branch out to the zone boundary. There is generally good agreement between the calculated and measured widths, within about 15 or 20%.

Typical resolution widths for Cu(9% Au) were about 0.3 THz for transverse phonons, and 0.6 THz for longitudinal modes. In comparison, the amplitude of the resonance in the natural width is about 0.6 THz for $[00\zeta]T$, 1.05 THz for $[\zeta\zeta 0]T_1$ and 1.3 THz for $[\zeta\zeta\zeta]T$. It should be noted that the absolute correction to be applied for resolution, using the Gaussian-Lorentzian width subtraction procedure, becomes smaller as the observed width increases. For a resolution width of 0.3 THz the corrections are about 0.16, 0.07, and 0.06 THz respectively for observed widths of 0.6, 1.0, and 1.4 THz. Under the conditions of this experiment, one would not expect

---

** The non-planar nature of the constant-frequency surfaces in the neighbourhood of this branch makes a small contribution to the resolution width, not included in these calculations. This point is considered further in the discussion of resolution calculations for Ni(55%)Pd(45%) in Chapter III.

a change in focussing conditions near the resonance to affect the resolution width by more than about 30% at most. Hence the uncertainty in the resolution cannot possibly account for any significant difference in the widths in the region of a resonance peak for Cu(9% Au). The errors assigned to the impurity-induced widths, shown in Fig. II-2, were estimated from the counting statistics and shapes of the individual neutron groups. They are possibly conservative estimates, but serve as a useful guide.

The frequency shifts were determined by direct subtraction. Errors for these, with the exception of the points for the [ζζζ]T branch, were also determined by examining each neutron group, adding the squares of the errors for the copper and alloy groups, and then taking the square root to obtain the error in the shift. In the case of [ζζζ]T, where a Cu group was not measured for each alloy group, the error reflects the uncertainty in the Cu(Au) group, combined with the estimated uncertainty in the calculation. As mentioned earlier, the errors for the shift allow at least partially for the possibility of systematic errors in the measurement.

Description of results for Cu(9% Au)

The natural widths for Cu(9% Au) exhibit definite resonance behaviour for each of the three transverse branches investigated, but there is clearly a strong dependence of

the amplitude and sharpness of the resonance on the branch. The resonance is strongest and of the lowest frequency in the $[\zeta\zeta\zeta]T$ branch, slightly weaker and higher in frequency in the $[\zeta\zeta 0]T_1$ branch, and considerably weaker and higher in frequency in $[00\zeta]T$. In the $[00\zeta]L$ branch, it cannot be said that there is a definite resonance, although the impurity-induced width does show a low broad peak. The resolution for L phonons is about twice as large as for T modes, while the natural widths appear to be fairly small, and it is possible that a resonance may have been missed or 'washed-out' because of this combination. However, it is much more reasonable to assume that the results for this branch show at least the correct general behaviour.

A detailed comparison of the resonances in the shift and width for different branches will be left to section C of this chapter, so that the results may be compared simultaneously with the data for Cu(3% Au) and Cu(1% Au).

The solid and broken curves in Figs. II-2 and II-3 represent various ways of treating the predictions of mass defect theory. The solid curves are obtained from equations II-3a and II-3b: that is to say, they assume that the theoretical line shapes have a nearly Lorentzian form. As shown in Fig. II-8, this is not really true, especially in the resonance region. The broken lines in Figs. II-2 and II-3 are derived directly from calculations of the line shapes from equation II-2. The dotted and dashed lines in Fig. II-3

represent the frequency shifts obtained from the centre (of a line drawn at half-maximum) and peak positions, respectively, of the calculated line shapes.

(iv) Results for Cu(3% Au)

The widths and frequency shifts for three transverse branches in Cu(3% Au) are shown in Fig. II-4. Again, the points are plotted against the frequency of the corresponding mode in pure copper.

Treatment of resolution and errors

In the case of Cu(3% Au), the resolution widths (typically 0.22 THz) are of the same order of magnitude as the impurity-induced widths. (The maximum natural width predicted by mass defect theory is less than 0.4 THz). When the observed width is only slightly larger than the resolution width, the error in the natural width is magnified by the Gaussian-Lorentzian subtraction procedure (by a factor of two over the error in the observed width, in the limit $\Gamma(\text{obs}) \rightarrow \Gamma(\text{res})$). The procedure can still be used, since in the resonance region the observed widths are substantially larger than the resolution, but the possibility of systematic error being introduced into the data by the treatment of resolution is a more worrisome consideration than for Cu(9% Au). Because of this, the widths for the $[00\zeta]T$ and $[\zeta\zeta 0]T_1$ branches in Cu(3% Au), as shown in Fig. II-4, are displayed in a manner somewhat different from that used for

Fig. II-4. Widths Γ, and frequency shifts Δ, for three transverse branches in Cu(3%)Au). For $[\zeta\zeta 0]T_1$ and $[00\zeta]T$, the widths shown are observed widths and are to be compared with the dashed lines, which represent theory with resolution. The other lines have the same meaning as in Figs. II-2 and II-3; the dash-dotted lines for the shift correspond to the dashed lines in Fig. II-3. For $[\zeta\zeta\zeta]T$, resolution has been extracted to give impurity-induced widths.

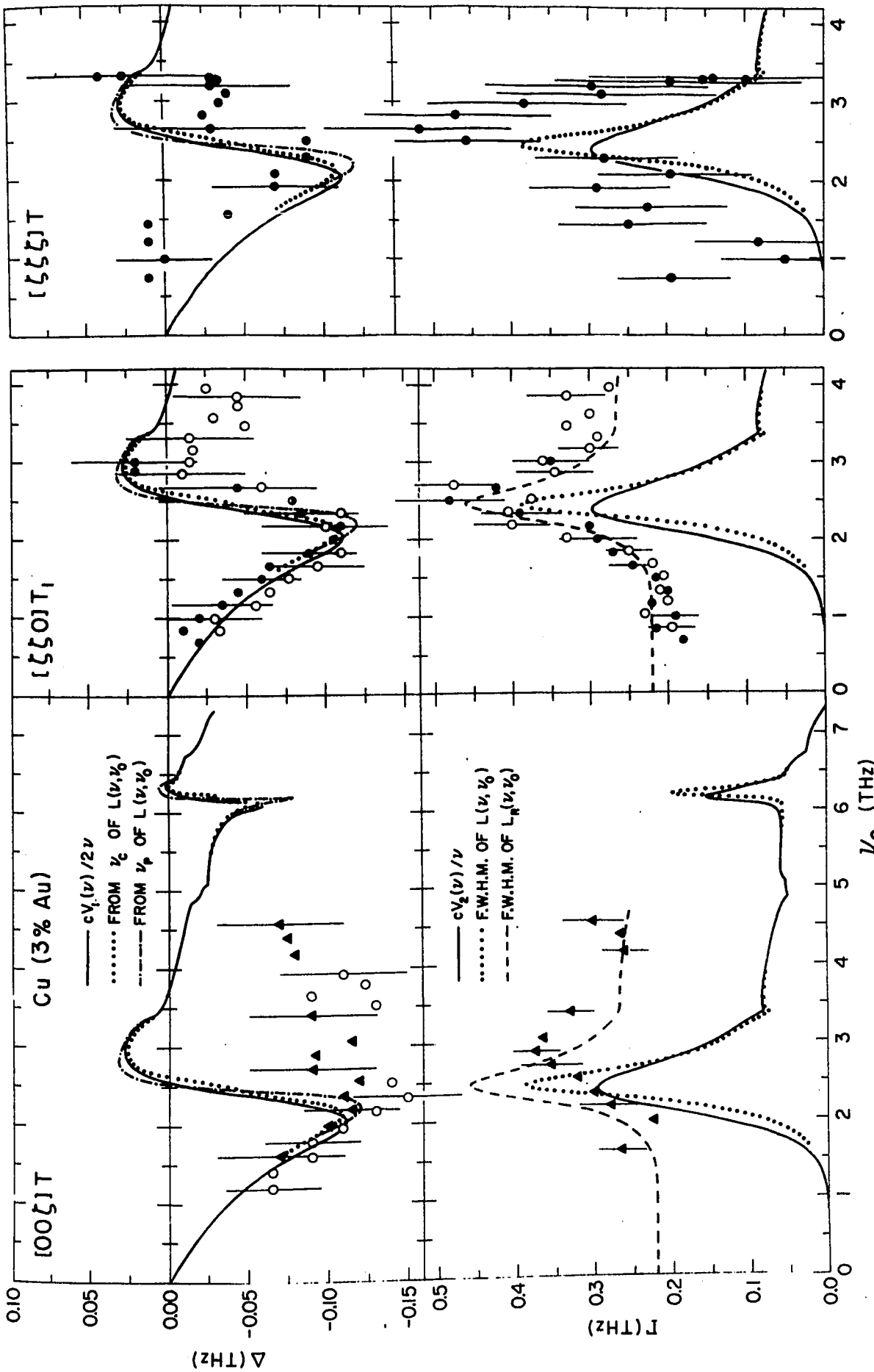
[ζζζ]T
[ζζ0]T₁
[00ζ]T
Cu (3% Au)
cV₁(ν)/2ν
..... FROM ν_ε OF L(ν,ν₀)
— — FROM ν_p OF L(ν,ν₀)
cV₂(ν)/ν
..... F.W.H.M. OF L(ν,ν₀)
— — F.W.H.M. OF L_R(ν,ν₀)
Δ (THz)
Γ (THz)
ν_Cu (THz)

Cu(9% Au). The widths shown at bottom left and bottom centre of this figure are the actually observed widths. Comparison with mass defect theory was made by putting resolution into the theory. A Gaussian profile of width 0.22 THz, representing the resolution, was folded into the line shapes calculated from mass defect theory, and the FWHMs of the resultant line shapes were then taken to produce the dashed curves of Fig. II-4. The resolution widths (i.e., copper) for both the $[00\zeta]T$ branch and the $[\zeta\zeta 0]T_1$ branch were approximately constant at about 0.2 THz in the range of the measurements. In these two branches, measurements were taken to only about 0.6 of the way to the zone boundary.

For the $[\zeta\zeta\zeta]T$ branch, the resolution was not put into the theory, since the resonance occurs quite close to the zone boundary where the resolution width is increasing fairly quickly with increasing phonon frequency. Therefore, for the data for this branch, the resolution widths (obtained from resolution calculations and checked against the widths of a few copper groups) were subtracted off by the same Gaussian-Lorentzian procedure used for the widths in Cu(9% Au). The fluctuations that are produced when the resolution width is nearly as large as the observed width are evident in the low frequency portion (low ν_{cu}) of Fig. II-4,bottom right. The non-zero 'shoulder' in this region is probably not real, in all likelihood arising from a small systematic discrepancy between the calculated and actual resolution. As mentioned

above in the section on the Cu(9% Au) results, resolution calculations for this branch using the planar approximation are somewhat less reliable than for other branches.

In Fig. II-5, the results of the Gaussian-Lorentzian width subtraction procedure for the [00ζ]T and [ζζ0]T_1 branches are shown. For [00ζ]T, the widths corresponding to the open circles for the shift (Fig. II-4, top left) have been included, since now the two sets of data for the widths in this branch are directly comparable. In order to reduce the fluctuations produced by the uncertainty in the resolution (copper) widths, the resolution widths for these data were taken from a smooth line hand-drawn through the widths of the Cu reference groups plotted as a function of phonon frequency. Different lines were, of course, used for different sets of data. The procedure gives very reasonable-looking widths for both branches. Displayed in this manner, several features of the data are emphasized, perhaps too strongly. First, the widths for the [00ζ]T branch bear a closer resemblance to the results for the same branch in Cu(9% Au) than is apparent from Fig. II-4, bottom left. Secondly, the widths for the [ζζ0]T_1 branch appear to be systematically higher than mass defect theory for phonons with frequencies above the resonance frequency. Thirdly, the resonance for [ζζ0]T_1 appears to be broadened over mass defect theory. (Compare the points for this branch with the dotted line, which is obtained from the calculated line

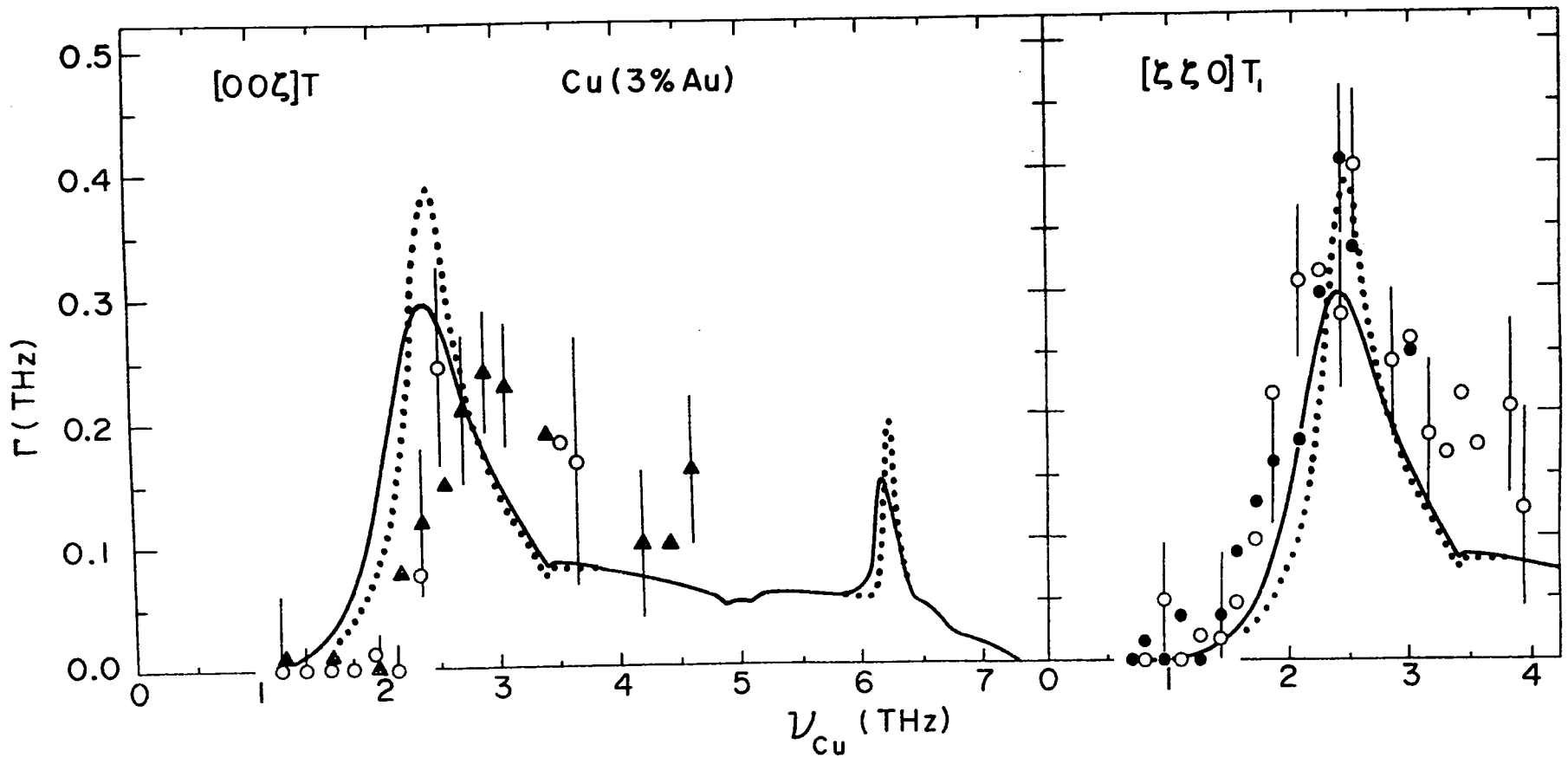

Fig. II-5. Impurity-induced widths for the $[00\zeta]T$ and $[\zeta\zeta 0]T_1$ branches in Cu(3% Au). Resolution was extracted from the observed widths by the procedure described in the text.

shapes.) However, the third tendency in particular could just be a resolution effect arising from the finite resolution of the spectrometer, especially from the resolution in wave vector, although it is equally as likely to be real. The first two tendencies are more likely to be real than the third. It should, however, be borne in mind that the actual uncertainty in the natural widths shown in Fig. II-5 is larger than the scatter of the points.

The frequency shifts were again determined by direct subtraction, as was done for Cu(9% Au), with errors being assigned in much the same fashion. The assignment of the 'best' frequency to a neutron group was made in all cases by strongly weighting the peak frequency, whenever the counting statistics were adequate to do this. A simple argument can be given that this is the best procedure to follow when the resolution in both wave vector and frequency is comparable in extent with a 'kink' in the dispersion curve.

The solid and open circles for the shift and width in the $[\zeta\zeta 0]T_1$ branch (top and bottom centre, Fig. II-4, and right, Fig. II-5) respectively represent the measurements of Svensson and Brockhouse (1967), and those of the present experiment. The two sets of data are in good agreement, although the newer data, which extend to higher phonon frequencies, do not show the nominally positive frequency shifts at about 3 THz exhibited by the earlier results.

The open circles and closed triangles for the $[00\zeta]T$

branch (top and bottom left, Fig. II-4, and left, Fig. II-5) represent two sets of data taken in the present experiment with different incident neutron energies and, consequently, different experimental resolution. Only closed triangles are shown for the widths in Fig. II-4 since the observed widths corresponding to open circles have a resolution which is somewhat larger than 0.22 THz, and therefore are not directly comparable with the other set of data or with the dashed theoretical curve.

A small systematic discrepancy is evident between the two sets of data for the shift, in both the $[\zeta\zeta 0]T_1$ branch and the $[00\zeta]T$ branch. As we have mentioned above, systematic errors of this size (about 0.02 THz) are difficult to eliminate, and we have allowed for their presence in estimating the errors on the shifts. Closer attention should be given to the 'shape' of the frequency shift as a function of the unperturbed (copper) frequency, within each set of data points, rather than to the magnitude of the shift itself, although the latter is also important.

The solid, dotted, and dashed-dotted curves in Figs. II-4 and II-5 were obtained from mass defect theory in the same manner as the lines in Figs. II-2 and II-3 for Cu(9% Au); their meaning has been described above. The curves are now in much closer agreement with each other because the calculated line shapes are much closer to being Lorentzian.

(v) Results for Cu(1% Au)

When the impurity concentration is decreased to 1% Au, the impurity-induced effects become much more difficult to measure. Only the shifts are shown in Fig. II-6, because in this case, although the widths for the alloy are measurably larger than for pure copper, the fluctuations of the points obscure any structure that may be present. Two branches were measured for Cu(1% Au), $[\zeta\zeta 0]T_1$ and $[00\zeta]T$, with two sets of data being taken for the latter.

The errors on the points in Fig. II-6 are about ± 0.03 to 0.04 THz, including the possibility of a systematic error of up to 0.02 THz. Error bars are not shown, since they would tend to mask the systematic and, we believe, real, trends in the measurements. In spite of the large errors, there are still certain conclusions that can be drawn from the data of Fig. II-6. The resonances are still there and in about the same positions. There still appears to be a general downward trend to the impurity-induced shifts, in contrast with mass defect theory, which predicts that the trend of the data at higher frequencies should be to fairly small positive and negative shifts. The solid curve in the figure is the mass defect theory prediction for a gold concentration of 1.17 at.% (the concentration indicated by neutron diffraction measurements of the lattice parameter). The shift for $[00\zeta]T$ is nominally larger than for $[\zeta\zeta 0]T_1$, although this is not certain because of the possibility that systematic error may be

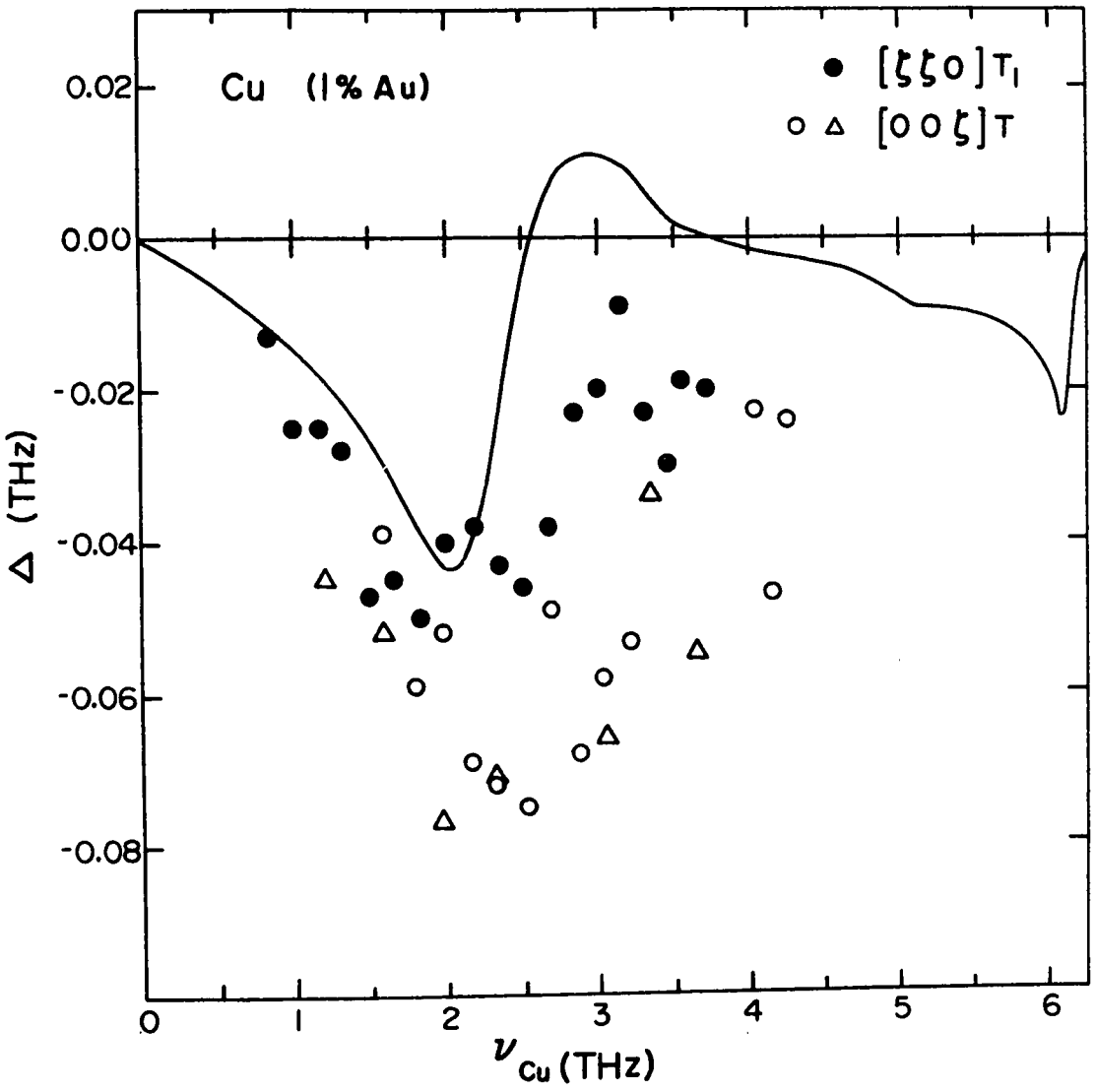

Fig. II-6. Impurity-induced frequency shifts for two transverse branches in Cu(1% Au). The solid line represents mass defect theory (Eq. II-3a) with c=.0117. Circles (triangles) indicate measurements carried out with an incident-neutron energy of 7.43 (8.62) THz. Typical estimated errors are ±(0.03 - 0.04) THz.

present. However, in view of the excellent agreement between the two sets of data for [00ζ]T, one may tend to think that this is a real effect. The resonance in $[\zeta\zeta 0]T_1$ appears to be more 'washed-out' than in the case of Cu(3%Au), but probably this is an effect arising from the small size of the resonant perturbation in comparison with the resolution. As we have mentioned near the end of subsection II-A(ii), the results of Cunningham et. al. (1970) for very small concentrations of W in Cr also appear to show this effect.

C. DISCUSSION

(i) Important Features of the Experimental Results

The two most important characteristics of the data on the impurity - induced widths and shifts are first, the branch dependence of the resonance and secondly, its concentration dependence. The general downward trend of the frequency shifts shown in Figs. II-3, II-4, and II-6 is also an obvious and significant feature. Low concentration mass defect theory is clearly inadequate to explain the perturbation of phonons in all three alloys. There is a gratifying overall consistency with respect to the behaviour of the resonances at different concentrations and a complementarity in the behaviour of the width and shift for each individual branch. The actual line shapes of the neutron groups, in cases where the widths are large, show asymmetries that are also consistent with, and complementary to, the information contained in the results for the shift and the width. We now turn to discussing these basic features of the experimental findings in detail.

Branch dependence

Beyond the observation that one generally sees resonant behaviour in each branch and at all concentrations (1, 3, and 9 at.% Au), the most obvious feature of the data shown in Figs. II-2 to II-6 is that the frequency, the amplitude, and the sharpness of the resonant perturbation of the dispersion

curves depend on the particular branch studied and not just on the mode frequency in the host crystal. Even for Cu(1% Au), the $[\zeta\zeta 0]T_1$ branch appears to show a sharper resonance than $[00\zeta]T$.

In Cu(9% Au), the resonant perturbation shows decreasing sharpness and a decreasing amplitude as one goes from the $[\zeta\zeta\zeta]T$ branch to $[\zeta\zeta 0]T_1$, to $[00\zeta]T$, and finally to $[00\zeta]L$, where there is no well-defined resonance. The 'centre' (of a line drawn at half-maximum) of the resonance peak in the width (see Fig. II-2) shifts to higher frequencies as the amplitude and sharpness of the resonance decrease, as one might expect it would. For $[\zeta\zeta\zeta]T$, $[\zeta\zeta 0]T_1$, and $[00\zeta]T$, the 'centre' frequencies are about 2.95, 3.35, and 3.55 THz respectively, while the 'width' of the resonance in the width goes from 1.0 THz to 1.6 THz to about 2.0 THz,and the amplitude of the resonance in the width goes from 1.3 THz to 1.1 THz to 0.55 THz. The 'peak' position, i.e., the frequency where the width attains its maximum value in a particular branch, does not show as clearly defined a systematic increase in value as the 'centre' frequency as the strength of the resonance increases. The 'peak' occurs at about 3.0 THz for $[\zeta\zeta\zeta]T$, at 3.3 THz for $[\zeta\zeta 0]T_1$ and 3.2 THz for $[00\zeta]T$.

The impurity-induced frequency shifts in each branch in Cu(9% Au) show behaviour complimentary to the behaviour of the widths for that branch. For $[\zeta\zeta\zeta]T$, the frequency shifts start

to turn sharply upward at about 2.8 THz, a frequency slightly lower than the 'peak' position of the resonance in the width. In the $[\zeta\zeta 0]T_1$ and $[00\zeta]T$ branches, the shift also starts to turn upward at a frequency slightly below the 'peak' frequency, but the upward slope of the rise decreases as the strength of the resonance decreases. For $[00\zeta]L$, where there is only a single broad peak in the impurity-induced width as a function of frequency, there is no upward turn visible at all in the shift, which shows a continuous decrease with increasing mode frequency.

In Cu(3% Au), no measurements were taken for $[00\zeta]L$. The $[\zeta\zeta 0]T_1$ resonance has shifted to a lower frequency and narrowed up, but otherwise exactly the same remarks apply as for Cu(9% Au). The overall pattern of the resonances in the different branches remains unchanged. From Figs. II-4 and II-5, it is apparent that the resonance shows decreasing amplitude, increasing centre frequency, and increasing width in the order $[\zeta\zeta\zeta]T$, $[\zeta\zeta 0]T_1$, $[00\zeta]T$. There is complementarity in the behaviour of the width and shift for each branch, the upward rise in the frequency shifts starting at a frequency just below the 'peak' frequency of the resonance in each case. This is especially evident for $[\zeta\zeta 0]T_1$, where the results for both the shift and the width show substantial agreement with the predictions of mass defect theory.

For Cu(1% Au), the results are restricted to shifts for the $[\zeta\zeta 0]T_1$ and $[00\zeta]T$ branches, and the errors on these

data are large. However, it still appears that the resonance is sharper in $[\zeta\zeta 0]T_1$. The maximum downward shift is nominally larger for $[00\zeta]T$ than for $[\zeta\zeta 0]T_1$ in Cu(1% Au), whereas it was about the same in Cu(3% Au), and smaller in Cu(9% Au). It is tempting to regard this as a real systematic trend indicative of a concentration-dependent change in the mean crystal force constants, although in view of the errors involved for the Cu(3% Au) and the Cu(1% Au) measurements, this is by no means a certain observation.

All of the data for the frequency shifts would be brought into substantially better agreement with theory if it is assumed that the disorder-induced shifts are superimposed on a smooth, continuously decreasing function of frequency that goes to zero at the origin. A different function may be required for each branch at each concentration since the downward trend of the frequency shifts appears to be more pronounced in some cases than in others. The overall downward trend of the frequency shifts is an indication that the appropriate reference lattice seen by a defect atom is not pure copper, but a lattice with somewhat weaker force constants.

By far the most probable explanation for the pronounced branch dependence of the resonance and its persistence to low Au concentrations (3% and 1%) is that there are important force constant changes to the defect which need to be included in low concentration theory in order to explain our results.

This, of course, is quite apart from the changes in the average force constants alluded to in the preceding paragraph. What we mean here is that the Au-Cu force constants are different from Cu-Cu force constants. Both Au-Cu and Cu-Cu force constants could conceivably depend on the local configuration of impurity atoms about the two atoms which are connected by the force constants. For Cu(9% Au), one would probably have to consider Au-Au force constants as well, since at this concentration, each Au atom has, on the average, another Au atom as one of its nearest neighbours.

Besides force constant changes, other possibilities that could produce a branch dependence in the resonance are the presence of short range order, and the scattering of the lattice waves by defect pairs and larger complexes of impurities. However, one would expect these factors to diminish greatly in importance on going from Cu(9% Au) to Cu(3% Au), but, as we have been, the overall pattern of the resonances actually remains unchanged. Theoretical work bearing on these other possibilities, and on the inclusion of force constant changes in low concentration theory, is discussed below, in II-C(ii) and II-C(iii).

Concentration dependence

For the sake of convenient comparison, the impurity-induced widths for the three transverse branches measured in both Cu(3% Au) and Cu(9% Au) are shown superimposed in Fig. II-7.

Fig. II-7. Concentration dependence of resonances from Cu(3% Au) to Cu(9% Au). The impurity-induced widths have been divided by c = 0.088 and c = 0.031 in order to make a direct comparison. The lines are simply guides to the eye. In the top part of the figure, the widths are plotted against the frequency of the corresponding mode in pure copper. In the bottom part, they are plotted against the frequency of the mode in the alloy.

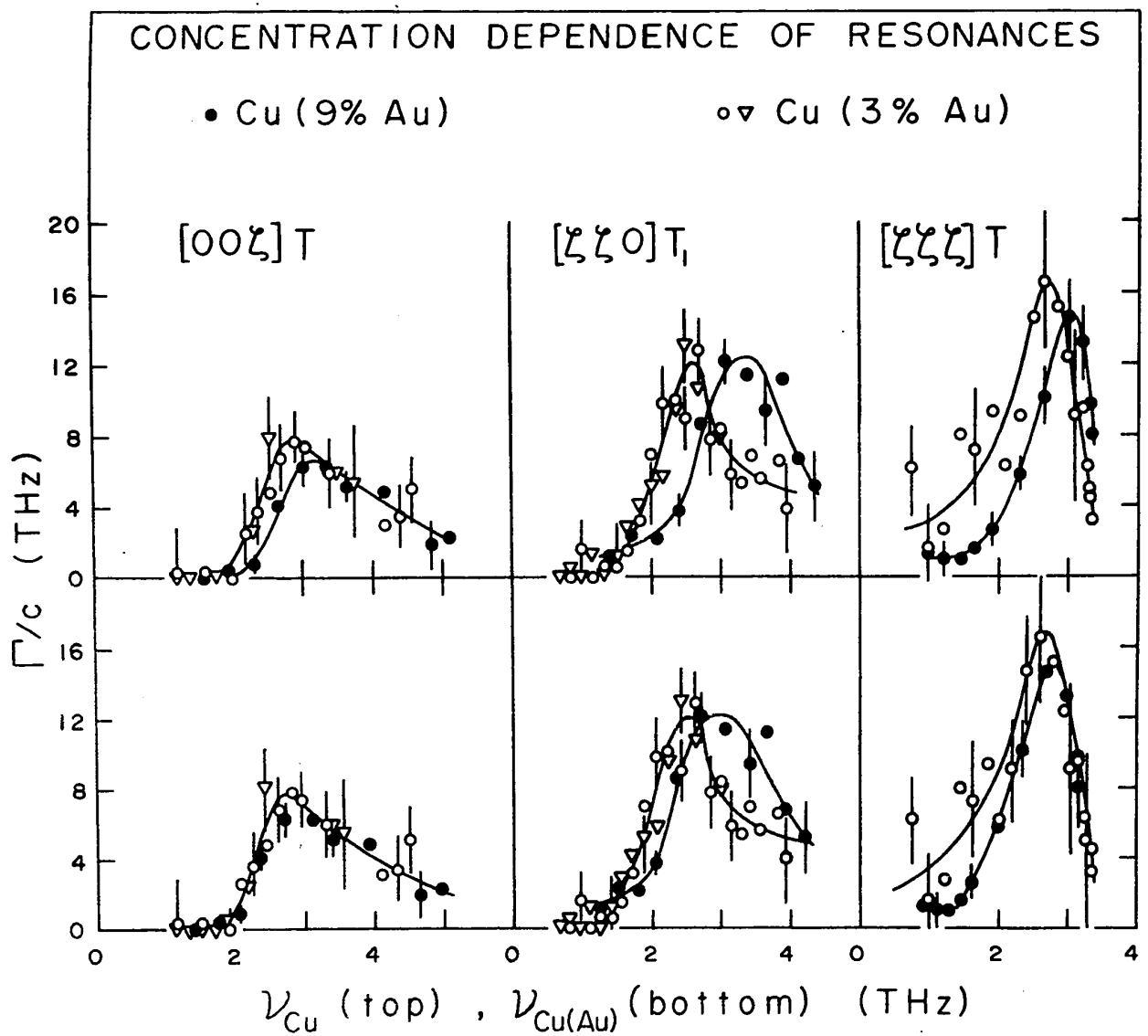
CONCENTRATION DEPENDENCE OF RESONANCES
• Cu (9% Au)
∘▽ Cu (3% Au)
[00ζ] T
[ζζ0] T1
[ζζζ] T
Γ/c (THz)
0
4
8
12
16
20
0
2
4
νCu (top) , νCu(Au) (bottom) (THz)

The results for Cu(3% Au) are shown as open symbols, and those for Cu(9% Au) are shown as filled circles. The widths have been divided by the concentration (c = 0.031, 0.088) to afford a direct comparison of the amplitudes of the resonances at the two concentrations. The lines are merely a guide to the eye.

When the results are plotted against the frequency of the corresponding mode in pure copper (top, Fig. II-7), the resonance in each branch appears to show a shift to higher frequency on going from 3% to 9% Au, by a small amount for $[\zeta\zeta\zeta]T$ and $[00\zeta]T$, but by a substantial amount for $[\zeta\zeta 0]T_1$. The amplitudes of the resonances are unchanged, well within errors, for each branch.

Bearing in mind the overall downward trend of the frequency shifts, which we interpreted as arising from a change in the appropriate reference lattice, the results have also been plotted as a function of the actual mean frequency of the mode in the alloy. This shows that the actual frequencies at which the resonances occur in $[\zeta\zeta\zeta]T$ and $[00\zeta]T$ are very nearly the same for Cu(3% Au) and Cu(9% Au). The 'shapes' of the resonances in the width as functions of frequency are also very nearly concentration-independent in these two branches. (As mentioned earlier, we do not believe the low frequency 'shoulder' on the widths for the $[\zeta\zeta\zeta]T$ branch in Cu(3% Au) to be real.) However, it must be said that if there is a concentration dependence, the resonances in

Cu(9% Au) occur at a higher frequency than in Cu(3% Au), and not vice versa.

For the $[\zeta\zeta 0]T_1$ branch, the resonance shows a pronounced concentration dependence in both methods of plotting the data. The resonance increases in width and in frequency on going from 3% Au to 9% Au, although the amplitude (divided by the concentration) remains about the same. The concentration dependence that we observe for this branch does not necessarily imply that scattering by pairs and higher order corrections to the theory need to be applied. The force constant changes may depend on the impurity concentration, and in fact it is quite reasonable that they should. Au-Au force constants are probably coming into play for Cu(9% Au), and one would expect these to be different from Au-Cu force constants. Theoretical calculations carried out to date on concentration-dependent effects, discussed in the next section, make concentration-dependent force constant changes seem a rather more attractive possibility than higher order concentration corrections. Hopefully, reasonable force constant changes can be chosen for each concentration to match the experimental results, and a sensible connection made between the changes for different concentrations.

Line shapes

The mass defect calculations of Svensson (1967; Svensson and Kamitakahara, 1971) predict that in the neighbourhood of the resonances, the natural line shapes should not be

Lorentzian, but should show marked asymmetries. Fig. II-8 (top) shows the calculated line shapes for Cu(9.3% Au), which exhibit pronounced double peaks around the resonances at about 2.5 and 6.2 THz. For Cu(3% Au), the calculated line shapes (Fig. II-8, bottom) no longer have double peaks, but asymmetries are still apparent.

In Cu(9% Au), the observed neutron groups show no definite double peaks. Since resolution will smear out the structure of the line shapes and the resonances in this alloy are generally broader than predicted by mass defect theory, this is not surprising. Some of the observed neutron groups do, however, show definite asymmetries; these were particularly pronounced in the [ζζζ]T branch, for which the resonance is fairly sharp. Fig. II-9 shows some of the neutron groups measured for this branch, for wave vectors ranging from $\zeta = 0.15$, where there is essentially no impurity broadening, to the zone boundary at $\zeta = 0.5$. The horizontal bars in the figure represent the calculated resolution widths (FWHM). The resonance peak in this branch occurs at about $\zeta = 0.37$. Asymmetric tails to the left are apparent for $\zeta = 0.4$, 0.45 and 0.5, and one to the right occurs for $\zeta = 0.3$. There could possibly be a double peak or a shoulder on some of the groups, especially $\zeta = 0.35$ and $\zeta = 0.4$, but this is uncertain within counting statistics. Comparing the neutron groups of Fig. II-9 with the calculated line shapes of Fig. II-8, we can see that the calculations do in fact predict

Fig. II-8. The calculations of Svensson (1967) for the line shapes in Cu(3% Au) and Cu(9% Au) from mass defect theory (Eq. II-2). The arrows indicate the values of the unperturbed frequencies ν_o.

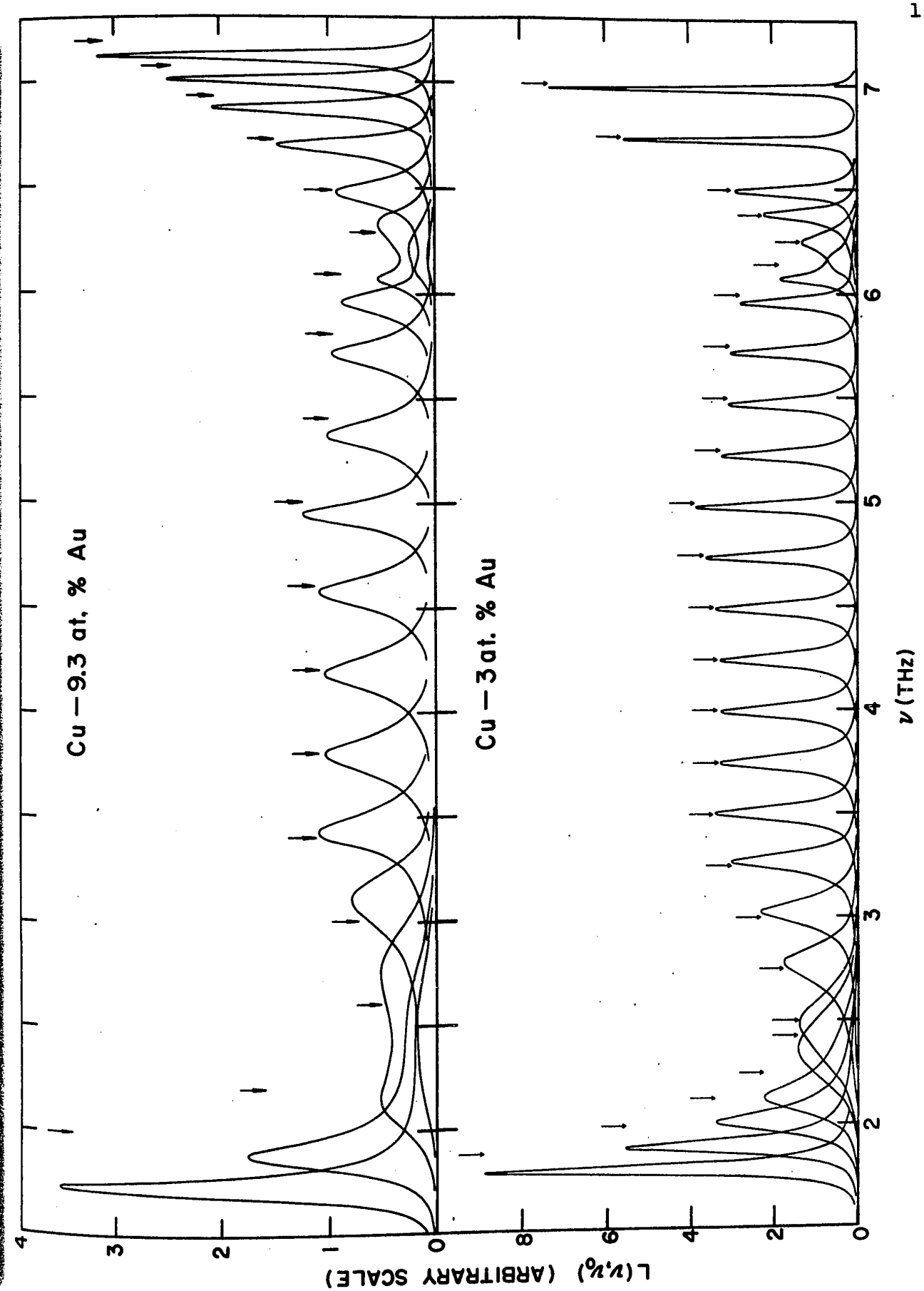
Cu – 9.3 at. % Au
Cu – 3 at. % Au
L(ν,ν₀) (ARBITRARY SCALE)
ν (THz)
0
1
2
3
4
0
2
4
6
8
2
3
4
5
6
7

Fig. II-9. Neutron groups for the [ζζζ]T branch in Cu(9% Au). The horizontal bars represent the calculated resolution widths. The groups were measured with reduced wave vector transfers $(a\underline{Q}/2\pi) = (2-\zeta, 2-\zeta, 2+\zeta)$.

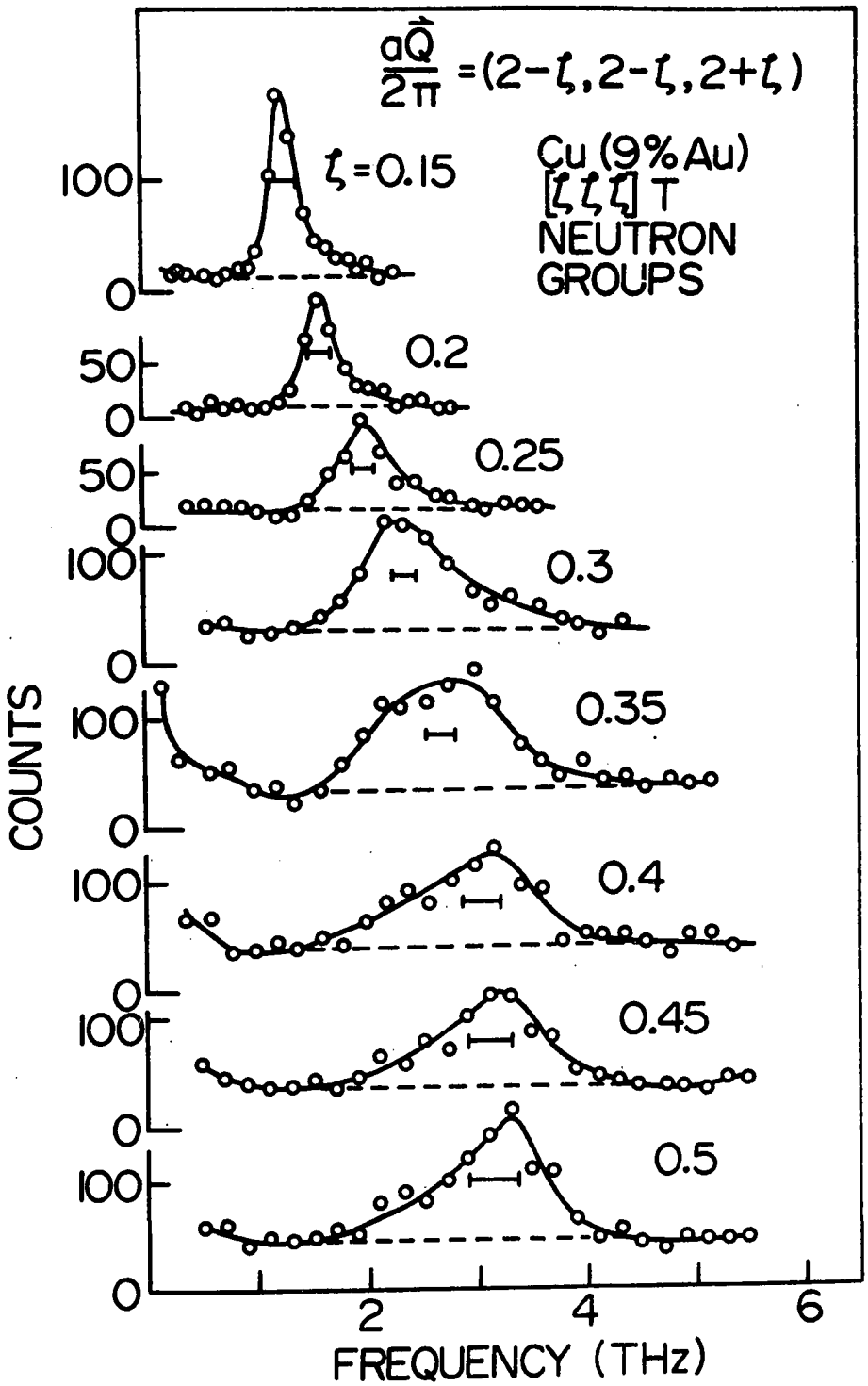
$\frac{a\vec{Q}}{2\pi} = (2-\zeta, 2-\zeta, 2+\zeta)$
Cu (9% Au)
[ζ,ζ,ζ] T
NEUTRON
GROUPS
ζ = 0.15
0.2
0.25
0.3
0.35
0.4
0.45
0.5
100
50
0
COUNTS
2
4
6
FREQUENCY (THz)

asymmetric tails to the left for phonons slightly above the resonance and to the right for phonons with frequencies slightly below the resonance, just as we observe.

Similar asymmetries were observed for the [00ζ]T branch of Cu(9.3% Au) in the early (1965) experiment of Svensson, Brockhouse and Rowe. The zone boundary mode of the [ζζζ]T branch (ζ = 0.5), was also measured in the 1965 experiment, which, it should be noted, was carried out using a different specimen crystal and a different spectrometer. The width, shift, and line shape are in very good agreement with the neutron group, shown at the bottom of Fig. II-9, for the same mode measured in the present experiment. In the 1967 experiment of Svensson and Brockhouse, in which the shift and width for the $[\zeta\zeta 0]T_1$ branch of Cu(3% Au) were found to be in agreement with mass defect theory, the line shapes were also found to agree with calculations similar to those shown in Fig. II-8 (bottom). Asymmetries to the left and right, less pronounced than those discussed above for Cu(9% Au), were observed.

The measurements on the same branch, $[\zeta\zeta 0]T_1$, carried out by the author using a different spectrometer, also show these asymmetries. Neutron groups for ζ = 0.225, well below the resonance, with no impurity broadening, and for ζ = 0.425, just above the resonance, with an asymmetric tail to the left, are shown in Fig. II-10 (centre). No real asymmetries were seen for the [00ζ]T branch, where the resonance is weak. The

Fig. II-10. Representative neutron groups for the $[\zeta\zeta 0]T_1$ branch in Cu-3% and 9% Au, and for the $[00\zeta]T$ branch in Cu(3% Au). The horizontal bars represent the width of the corresponding neutron group in pure copper.

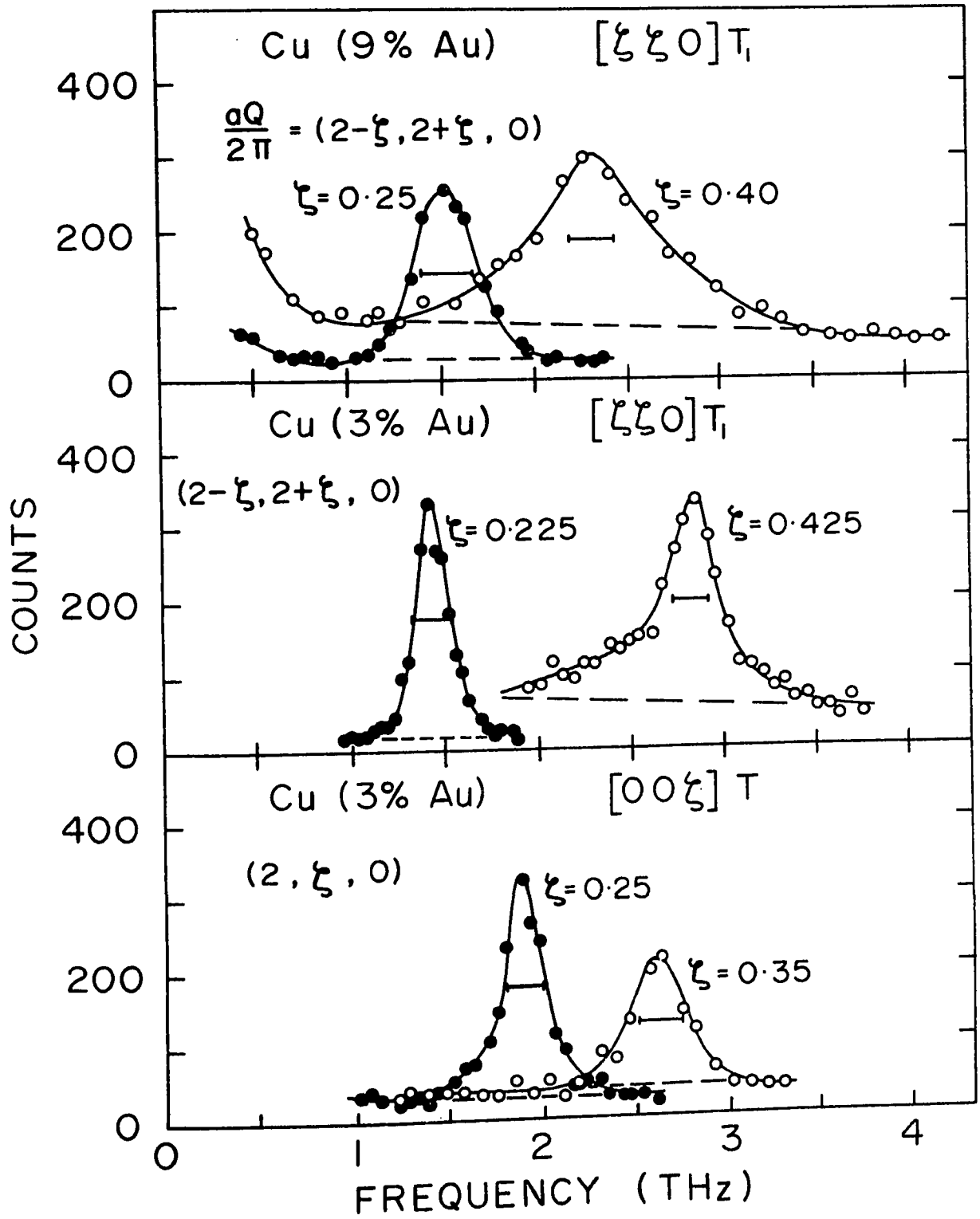
Cu (9% Au) [ζζ0] T1
aQ/2π = (2-ζ, 2+ζ, 0)
ζ= 0·25
ζ= 0·40
Cu (3% Au) [ζζ0] T1
(2-ζ, 2+ζ, 0)
ζ= 0·225
ζ= 0·425
Cu (3% Au) [00ζ] T
(2, ζ, 0)
ζ= 0·25
ζ= 0·35
COUNTS
FREQUENCY (THz)
0
200
400
1
2
3
4

group for $\zeta = 0.35$ (Fig. II-10, bottom), just below the resonance peak, is broader than that for $\zeta = 0.25$, well below the resonance peak, but is not noticeably asymmetric. For the $[\zeta\zeta 0]T_1$ branch in Cu(9% Au), in view of the fact that the resonance here is fairly strong, the groups were surprisingly symmetric. Fig. II-10 (top) shows a group for $\zeta = 0.25$, well below the resonance, and one for $\zeta = 0.40$, just below the resonance peak. For each of the groups shown in Fig. II-10, the horizontal bar represents the width of the corresponding group in pure copper.

(ii) Inclusion of Force Constant Changes

To explain our results, the theory of Elliott and Taylor (1967) must be extended to include force constant changes to the defect. The problem has already been analysed in considerable detail by Lakatos and Krumhansl (1968, 1969), who have formulated their treatment of force constant changes in terms of coherent and incoherent neutron scattering experiments. Their calculations for a variety of different mass changes and force constant changes for impurities in an Al host, indicate that strong effects are produced by force constant changes of reasonable magnitude.

Bruno and Taylor (1971) have analysed our results for the $[00\zeta]T$ and $[\zeta\zeta 0]T_1$ branches in Cu(3% Au) by means of similar calculations. They attempt to approach the problem from a somewhat more fundamental point of view by introducing Cu-Cu

and Au-Cu force constants derived from Morse potentials fitted to independent experimental data (heats of vacancy formation and bulk moduli). They first calculate the force constant changes produced in the copper lattice by the volume change that occurs when the gold atoms are introduced. Next they add these changes to the experimental Cu force constants (Svensson et. al., 1967) to produce mode Grüneisen parameters (volume dependencies for each lattice frequency) to account for the general downward trend of the alloy frequencies that we have mentioned before. Assuming that there is negligible local relaxation of the copper atom positions upon the substitutional introduction of a gold atom (i.e., the atoms are constrained to be situated on the exact lattice sites of the expanded crystal), the force constant changes to the first and fourth nearest neighbours, estimated to be the only ones of importance, were then calculated from the Au-Cu Morse potential, and impurity-induced shifts and widths were calculated from these force constant changes. The results, after the volume-induced shift was added on to the impurity-induced shift, were found to be in serious disagreement with experiment for the shift and width in the $[\zeta\zeta 0]T_1$ branch, although the $[00\zeta]T$ branch measurements were reproduced reasonably well. Better results, in agreement with experiment for both branches within errors, are obtained by fitting the force constant changes to the experimental results.

The procedure of somehow taking into account the

volume dependence of the lattice frequencies seems to be necessary to produce any sort of reasonable match to the impurity-induced shifts in Cu(Au). This has also been found to be true for the perturbation of the band modes induced by light impurities in the experiments on Cu(4% Au), Cu(10% Al) (Nicklow et. al., 1968a, 1968b), and Ge(9.2% Si) (Wakabayashi et. al., 1971). In Cu(Al), the Al atoms produce a volume expansion of the lattice of about 1 and 2% for the concentrations considered, while in Ge(Si), the Si atoms produce a contraction of about 1.5%. The shifts in the Cu(Al) alloys show a downward trend, as do our results for Cu-1, 3, and 9% Au, (where the volume expansions are about 0.5, 1.5 and 4.3 % respectively), whereas those for Ge(Si) show an upward trend. The trend of the data in both Ge(Si) and Cu(Al) seems to be well reproduced by use of an average Grüneisen parameter obtained from thermodynamic properties. In Ge(Si), once the volume-induced shift is added on, the results show excellent agreement with mass defect theory, which predicts substantial positive shifts up to about 8 THz, with a sharp downward turn to a negative shift up to a maximum lattice frequency of about 9 THz. The downward turn, which may be interpreted as a depletion of the band mode by the local mode, or as a 'repulsion' by the local mode, is also predicted for Cu(Al), and there are indications that it may be present in the experimental data, although because of relatively large errors, it is not possible to make a definite

statement about this.

Turning back to the paper of Bruno and Taylor, although in principle the mode Grüneisen parameters calculated by them should be better than the average Grüneisen parameters used by Nicklow et. al. and Wakabayashi et. al., the former show several unsatisfactory features. One is that they do not agree with the experimental parameters for very small phonon wave vectors ($\underset{\sim}{q} \approx 0$), obtained from elastic constant measurements, for the $[\zeta\zeta 0]T_1$ branch. Also, in addition to the measurements we have been describing in detail, we have measured a few points on the dispersion curves for each branch in the symmetry directions of Cu(3% Au). The frequency shifts from pure copper calculated by Bruno and Taylor for the L branches do not agree with these later measurements. For the $[00\zeta]L$ branch, we find no shift less (i.e., more negative) than that given by a linear relationship between shift and phonon frequency $\Delta = -0.021\nu$, which means a shift of -0.15 THz at the zone boundary (phonon frequency of 7.1 THz), whereas Bruno and Taylor calculate shifts of about -0.3 THz at the zone boundary. Inclusion of impurity-induced effects, with or without force constant changes, does not appreciably improve the agreement. Bruno and Taylor comment that screening effects of the valence electrons, which are not explicitly taken into account in their calculations, are much larger for L branches than for T branches, and that the disagreement for L branches was therefore not completly unexpected. Thus, although these

authors have shown that force constant changes can be chosen to agree with the experimental results for Cu(3% Au), if the volume effect is taken into account, the microscopic origins of the changes in both the host lattice force constants and the impurity-host force constants are, apparently, considerably more difficult to understand.

(iii) Other Factors

Apart from force constant changes, there are several other possibilities that may conceivably influence the resonant perturbation in Cu(Au), although theoretical treatments, and the limited concentration dependence that we observe, decrease the likelihood of their being major factors.

Since the Cu-Au system forms ordered phases near 25 and 50 at.% Au, the possibility of short or long range order which affects the lattice dynamics cannot be neglected. Hartmann (1968) has extended the theory of Elliott and Taylor (1967) to partially allow for the presence of short range order. Performing explicit calculations for Cu(9.3% Au), he found only small effects producible at this concentration. The scattering of phonons by impurity pairs has been considered by Aiyer et. al. (1969). Calculations for Cu(9% Au) based on this formulation have been carried out by Bruno and Taylor (unpublished results); they indicate that the inclusion of pair scattering raises the resonance frequency slightly but otherwise has little effect. Self-consistent treatments of

the concentration dependence (Taylor, 1967; Leath, 1968), which replace the environment of an impurity by an average of the imperfect crystal, also fail to produce appreciable changes in the resonance at a gold concentration of 9 at.%. For Cu(3% Au), all of the theoretical formulations mentioned here would certainly differ very little in their predictions from low concentration mass defect theory with random order. However, in view of the fact that the theories are only approximate and thus serve only as indications, short range order and pair effects have not been shown to be completely negligible for Cu(9% Au).

(iv) Other Experiments on Phonons and Magnons in Disordered Alloys

Several experiments have been performed by neutron scattering on the crystal dynamics of disordered metallic alloys in which the component elements are neighbours or near neighbours in the periodic table. Bi-Pb-Tl (Ng and Brockhouse, 1968), Nb-Mo (Powell *et. al.*, 1968), Fe-Ni (Hallman and Brockhouse, 1969) and Cu-Ni alloys (Chapter IV of this thesis) have all been studied over wide ranges of composition. The mass disorder in these cases is much too small to produce effects observable by neutron scattering, but one might expect significant broadening from force constant disorder, particularly since the components in these alloys have very different electronic structure and are

present in large concentration. However, little or no broadening was noted in these alloys, with the exception of a Bi-Pb-Tl ternary alloy, which showed some appreciably broadened modes. It can be fairly stated that on the whole the effects from disorder in these alloys are surprisingly small.

An impurity spin can produce defect modes in the spectrum of excitations of an ordered magnetic system in a manner analogous to the production of defect vibrational modes by an impurity with changed mass or force constants. Both localized and resonant magnons have been observed by neutron scattering and by optical methods. The neutron measurements are very similar to those described in this chapter for phonons. An extended research program by neutron scattering, carried out at Chalk River, described in detail in review articles by Svensson et. al. (1972) and by Cowley and Buyers (1972), has shown that a low concentration Green's function theory generally gives a very good description of the spin dynamics in dilute alloys of antiferromagnetic transition metal fluorides. The theory is more complicated than most of the phonon theories, since there is no analogue of the mass defect for magnetic impurities; a changed spin implies a different exchange. However, the impurities in these alloys, which are mostly transition metal ions (Mn, Fe, Co, Ni) from the same row of the periodic table, produce almost no distortion of the lattice upon their introduction, so that the requirements of the theory are well satisfied in practice. For the case of Zn

impurities (which are non-magnetic) in MnF_2, a resonant perturbation occurs which is in excellent agreement with a Green's function calculation with no adjustable parameters. In other cases, the value of the impurity-host exchange is given fairly accurately by the geometric mean of the host-host and impurity-impurity exchange constants in the pure materials.

(v) Summary

Measurements of the inelastic neutron scattering from single crystal specimens of Cu-1, 3, and 9 at.% Au show that the resonant perturbation of phonons in these alloys cannot be adequately described by regarding the Au atoms as mass defects in a Cu host. The pronounced branch dependence of the resonances, and the negative trend of the frequency shifts, indicate that force constant changes to the impurities, and in the host lattice, need to be considered as well. A concentration dependence of the resonant perturbation was observed in at least one branch - $[\zeta\zeta 0]T_1$. Calculations based on complicated theories, involving phonon scattering from pairs and larger clusters of impurities, may thus be needed to explain the results for Cu(9% Au). However, it is not yet clear that it is necessary to perform such calculations. An attempt should first be made to find a set of force constant changes that give a good description of all branches in Cu(3% Au). Some calculations of this sort have already been reported,

but show several unsatisfactory features. It is hoped that the experiment on Cu(Au) will stimulate further experimental and theoretical work on impurity modes. Hopefully, this will lead to an understanding of concentration-dependent effects and, perhaps, of the microscopic origin of the force constant changes that accompany the introduction of an impurity atom.

CHAPTER III

DYNAMICS OF AN IMPERFECT CRYSTAL WITH HIGH IMPURITY CONCENTRATION: NI(55%)PD(45%)

A. INTRODUCTION

(i) General Remarks

In Chapters I and II, some theoretical and experimental aspects of vibrations in crystals containing fairly low impurity concentrations were reviewed. A few theoretical studies for high impurity concentrations were also mentioned, and the theory of D. W. Taylor (1967) was outlined. For high concentration imperfect crystals, neither experiment nor theory is as well developed as for cases of low impurity concentrations. The theories are complicated and involve questionable assumptions. Fewer experimental techniques seem to be applicable, and most of those which can still be applied give less detailed information.

A number of optical experiments, primarily on alkali halide and semiconductor mixed crystals, are relevant to this topic, but deal with an aspect of the disordered crystal problem that is rather different from the one we have chosen to study by neutron scattering. Optical methods give the frequencies of the optical phonons at $\underline{q}=0$, which can be measured as a function of concentration. (See Chang and Mitra, 1968, for a list of systems studied to that date.) It appears that

the mixed crystal systems that have been investigated are divisible into two classes, characterized by one-mode or two-mode behaviour. In one-mode behaviour, the frequency of an optical mode shifts more or less uniformly with composition, while in two-mode behaviour, two sets of excitations of concentration-dependent 'strength' and different frequencies are seen for intermediate concentrations, each of which can be associated with one of the constituents of the mixed crystal.

Information that is perhaps of a more fundamental kind is available from methods which essentially study the frequency distribution of the modes in the disordered system. These methods are superconducting tunneling, incoherent neutron scattering, and the numerical studies which were discussed in Chapter I, section D(i). The latter, which are really computer experiments rather than theory, have given by far the most detailed information of the three, but of course do not deal with real physical systems. Superconducting tunnelling has been applied to the Pb-In system (Chandrasekhar and Adler, 1968) with In concentrations of up to 40 at.%. At this concentration, the impurity band arising from the In has broadened and merged with the host band, while the peaks in the host band have become less pronounced. Results for the In-Tl system (Dynes, 1970; also see Taylor and Vashishta, 1972) have also been obtained.

Incoherent neutron scattering has not been extensively applied to high concentration disordered solids. The

measurement of the frequency distribution of any material by this method is in any case not easy, and has not been satisfactorily done even for pure vanadium, which is an almost purely incoherent scatterer. An additional difficulty arises because, if polycrystalline speciments are used, there are few cases of high concentration disordered solids in which the effects of coherent scattering can be neglected. Only relatively dilute concentrations of impurities can be introduced into vanadium before the effects of coherent scattering start to become important. Another possibility is to look at a system in which the coherent scattering lengths of the components average out to zero at a certain composition. This method was first employed by Stewart and Brockhouse (1958) on an alloy of Mn and Co, in which the components are chemically different, but have similar masses. Mozer, Otnes, and Palevsky (1965) and Chernoplekov et. al., (1963) have made measurements on Ti(67%)Zr(33%), which has a mass ratio Zr:Ti of about 1.9. The negative scattering length of Ti compensates the positive scattering length of Zr at about this composition. The frequency distributions derived from the measurements do not give detailed information but show broadened features. Experiments have also been carried out on polycrystalline metallic alloy specimens in which the scattering must be primarily coherent, but the meaning of the measurements is not easily interpreted. For high concentration imperfect crystals, the detailed structure of the

frequency distribution is important, and structure from coherent scattering, which must be taken into account in a complicated fashion, is very undesirable.

By coherent inelastic scattering, the frequencies and widths of individual modes of the system can be measured as a function of the wave vector. The information contained therein is much more detailed than frequency distributions, or the q=0 mode frequencies. It is therefore by far the most powerful method applicable to the study of disordered systems, particularly for the monatomic systems which will naturally constitute the most tractable theoretical cases. It thus appears that more extensive application of coherent scattering to disordered crystals is long overdue. Besides the work that is reported in this chapter, there has been to our knowledge only one other experiment by coherent scattering on a high concentration imperfect crystal, a study of some branches in KBr:RbBr mixed crystals containing 22 and 45 molar percent RbBr (Buyers and Cowley, 1968). On the whole, little evidence of the influence of the mass disorder on the frequencies or widths of the phonons was seen in this experiment. In the [111]LA branch, effects characteristic of a resonance mode of frequency approximately 2.1 THz were observed. The natural width of the phonon corresponding to the resonance peak was about 0.5 THz, and, oddly enough, about the same at the two concentrations. In the other branches that were measured,

[111]TA, [111]TO, and [110]TA, the shifts in frequency from pure KBr were essentially those to be expected from the change in the mean lattice, and no significant broadening above the resolution was observed. Buyers and Cowley compare their experiment with calculations from a model in which the K and Rb atoms are regarded as defects from the mean lattice. The resonance in the [111]LA branch is not predicted. The calculated shifts for the other branches are of the right order of magnitude, but these result largely from the change in mean lattice. As Cowley has mentioned (1968), the inadequacy of the model is not surprising, since it is basically a modification of low concentration theory with only an intuitive justification. The primary conclusion to be drawn from the experiment is that phonons remain a good description of crystal dynamics even in the presence of substantial mass disorder. It should be noted, however, that in a system like KBr:RbBr where there are two atoms per unit cell, even at a concentration of 45 molar percent RbBr, only 22.5 percent of the atoms are Rb, so that the amount of disorder in this case is not really very large, particularly since the nearest neighbours of a rubidium atom are always bromine atoms. The calculational difficulties associated with diatomic or polyatomic disordered crystals are also considerable. Even models for the host or reference lattice which give reliable frequency distributions and eigenvectors are much more difficult to produce than for simple monatomic crystals. Certainly it is

very desirable to study the vibrations in a high concentration imperfect crystal with a B.C.C. or F.C.C. structure, in order to maximize the amount of disorder, and, at the same time, to retain the possibility of adequately interpreting the results.

(ii) Choice of the Ni-Pd System

The mass ratio of Pd to Ni (M_{Pd}/M_{Ni} = 1.812) is certainly not small, but is not as large as that of Au to Cu (M_{Au}/M_{Cu} = 3.100). This may make a high concentration imperfect crystal of Ni and Pd a more approachable theoretical problem than a high concentration alloy with a very large mass ratio. Other properties of the Ni-Pd system make it a particularly favourable case for a neutron scattering experiment.

(1) Physical, chemical and alloying properties

Ni and Pd are chemically similar, coming from the same column of the periodic table; they are the transition metals that end the 3d and 4d series respectively. The similarity of their electronic structures, which are fairly complicated, is less well defined than for the noble metals.

Some properties of Ni and Pd relevant to our experiment are listed in TableIII-1. The lattice parameters differ by about 11% (compared with 10% for Cu and Au) and the melting temperatures differ by about 6% (compared with about 2% for Cu and Au).

TABLE III-1 Properties of Ni and Pd

	Ni	Pd
Atomic number	28	46
Atomic mass (amu)	58.71	106.4
Free atom ground state	$3d^8 4s^2$	$4d^{10}$
Lattice constant[a] (fcc) at room temperature	3.524 Å	3.8904 Å
Thermal neutron cross sections[b] (barns) :		
$\sigma_{coherent}$	13.2±0.2	5.0±0.3
$\sigma_{incoherent}$	4.8±0.3	—
$\sigma_{absorption}$	4.8±0.2	8.0±1.5
Elastic constants[c,d] at 296° K (10^{12} dynes/cm):		
C_{11}	2.46	2.270
C_{12}	1.50	1.759
C_{44}	1.22	0.717
Melting temperature (°C)	1455	1549.4

[a] Pearson (1958), p.127.

[b] Hughes and Schwartz (1958)

[c] Alers, Neighbours, and Sato (1960)

[d] Rayne (1960)

The alloying properties of Ni and Pd are particularly well suited to the purpose of our experiment. Solid solutions are formed at all concentrations, and no indications of long range order have been observed down to 0°C. At 45 at.% Pd, the phase diagram (Hansen, 1958) shows that the liquidus and solidus touch. At this concentration, very convenient for a study of a high concentration mass-disordered crystal, a homogeneous single crystal should be relatively easy to grow. Numerous other alloy systems exist which show similar points in their phase diagrams; the liquidus and solidus of a solid solution phase diagram always appear to touch at the minimum of the melting temperature as a function of composition. Hansen (p. 179) comments, "The occurence of a minimum melting point in a continuous series of solid solutions is often characteristic of a transformation in the solid state." The absence of any observed transformations in the Ni-Pd system is one of its most attractive features, and leads one to hope that the condition of complete random substitutional disorder is satisfied as well as is possible for a real system in which there is a large mass difference between the components. Most other phase diagrams that show a solid solution minimum melting temperature are more complicated than Ni-Pd in other respects. For example, at temperatures below about 400°C, Cu-Au alloys tend to form the ordered structures Cu_3Au and CuAu for compositions near 25 and 50 at.% Au. The minimum melting temperature for Cu-Au solid solutions

occurs at 56.5 at.% Au. Specimens of an ordered alloy can often be easily disordered by quenching, but the tendency to form an ordered structure at all leads one to expect that short range order will still be present. Alloys of the alkali metals K, Rb, and Cs show phase diagrams that are equally as simple as Ni-Pd, and have even simpler lattice dynamics for their constituents, but are more difficult experimental subjects from several technical points of view.

(2) Lattice dynamical properties

In common with other F.C.C. transition and noble metals, the dispersion curves of Ni (Birgeneau et. al,, 1964; de Wit and Brockhouse, 1968) and Pd (Miiller and Brockhouse, 1968, 1971) are dominated by large, almost central nearest neighbour forces. Palladium has been particularly thoroughly studied, partially in order to investigate a fairly strong temperature-dependent anomaly in the $[\zeta\zeta 0]T_1$ branch, now felt to be caused by the Kohn effect (Miiller and Brockhouse, to be published). The anomaly is only strong in this particular branch; the dispersion curves of Pd are otherwise very simple. Ni has no unusual features whatever in its dispersion curves, which are very similar to those of copper, scaled upwards by a factor of about 1.25. The force constants derived from the dispersion curve measurements are about 15% larger in Pd than in Ni, as shown in Table III-2.

The elastic constants of Pd and Ni are comparable in size, but certainly show significant differences. As one can

TABLE III-2

Force constants of Pd and Ni, in units of dyn/cm, as derived from neutron measurements at room temperature. Also shown are the force constants of the $Ni_{55}Pd_{45}$ mean crystal model used in the calculations discussed in the text. These were obtained by averaging appropriately between fifth-neighbour models of Ni and Pd.

Force Constant	Pd		Ni	$Ni_{55}Pd_{45}$
1xx	19159	± 236	17319	18221
1zz	-2781	414	-436	-1396
1xy	22405	440	19100	21085
2xx	1514	348	1044	1362
2yy	147	224	-780	-459
3xx	712	257	842	821
3yy	331	136	263	212
3yz	288	207	-109	272
3xz	489	101	424	606
4xx	-1115	118	402	-221
4zz	-117	175	-185	10
4xy	-849	393	660	-561
5xx	178	240	-85	21
5yy	-205	110	7	-55
5zz	-254	145	18	-65
5xy	144	130	-35	28
6xx	84	91		
6yz	-202	176		
7xx	-28	128		
7yy	96	134		
7zz	-7	51		
7yz	10	19		
7xz	14	28		
7xy	29	52		
8xx	97	146		
8yy	-49	129		

see from TableIII-1, c_{11} differs by about 10%, c_{12} by about 16%, and c_{44} by almost a factor of two. The elastic constant c_{44} determines the initial slope of two transverse symmetry branches, $[\zeta\zeta 0]T_2$ and $[00\zeta]T$. The elastic constants of Ni bear about the same relation to those of Pd as do those of Cu to Au (see Appendix I), except that c_{11} is slightly smaller for the heavy element in the case of Ni-Pd and slightly larger in the case of Cu-Au.

Overall, there is a good deal of resemblance between the systems of this and the preceding chapter with respect to the similarity of the constituents in each case, the Ni-Pd difference being perhaps slightly greater than the Cu-Au difference on the basis of the lattice constants, melting temperatures and lattice dynamical properties. Since force constant changes were important for Cu(Au), there is no reason to expect that they can be neglected for Ni-Pd.

(3) Neutron properties

These are reasonably favourable (see Table III-1); the absorption cross sections are not too large compared with the coherent cross sections. The fairly high incoherent cross section of nickel was at first thought to be a potentially serious disadvantage, but in practice, this did not turn out to be too much of a problem. The scattered neutron distributions are always dominated by the coherent scattering, even for high frequency modes with large widths. The substantial difference between the coherent scattering lengths

of Ni and Pd produces additional incoherent scattering (about 0.5 barns per atom in $Ni_{55}Pd_{45}$), but this is much smaller than the incoherence produced by the Ni itself (about 2.7 barns per atom in the alloy). However, the different coherent scattering lengths must be properly accounted for when experimental coherent inelastic cross sections are compared with theoretical calculations; i.e., one should use expressions like Eqs. 1-65 and 1-73 or their equivalents.

B. EXPERIMENT

(i) The Specimen Crystal

Our specimen of $Ni_{55}Pd_{45}$ was grown by the Czochralski method by Research Crystals Inc. of Richmond, Virginia. The crystal as grown was about 1.6 cm in diameter by 10 cm in length, and had a [100] axis about 20^{o} off the cylinder axis. The top 2 cm of the boule is a fairly good crystal, with a mosaic spread of about 0.5^{o} FWHM, but the mosaic progressively increases further down the crystal to about 3^{o}FWHM at the bottom end of the crystal. The mosaic distribution is anisotropic, and it was found that if the crystal was mounted with the cylinder axis approximately horizontal, all the observable rocking curves were in the range 0.8^{o} to 1.2^{o} FWHM. Since the collimation in a crystal spectrometer is typically 2^{o} or 3^{o} FWHM vertically and 1^{o} horizontally, it was felt that the effects of the mosaic of this crystal should not be too serious although not negligible. Some of the observations were made on the uncut boule, with the cylinder axis horizontal. During the course of the experiment, it was found that some modes had to be observed in a consistently bad geometry. Accordingly, two sections, 2.5 cm in length, were cut from the more perfect end of the boule and mounted one above the other, and the rest of the measurements were taken. Checks were made on previously measured groups as well, and the widths as well as the frequencies were found to be in good agreement. The crystal was characterized

with respect to its lattice constant (found to be 3.720±0.002 Å) and its homogeneity by neutron diffraction, following the method of Ng et. al. (1967), as described in Chapter II. The width of the characterization peak, which was 0.38° in the scattering angle ∅ at ∅ = 118°, was not significantly larger than the experimental resolution width, also 0.38°, as indicated by a reference measurement on a single crystal of pure copper. This fact indicates very good homogeneity (i.e., uniformity of composition throughout the crystal), as might have been expected from the phase diagram. The composition, as determined by an accurate density measurement, was found to be c_{Pd} = 45.16±0.10 atomic percent, in very good agreement with the nominal composition and with the measured lattice constant (Pearson, 1958, 1967).

(ii) Neutron Scattering Measurements

All of the measurements were taken on the McMaster University triple-axis spectrometer E2 at the NRU reactor, Chalk River. The constant-Q mode was used throughout, with the specimen at room temperature.

For some of the less-intense scattered-neutron distributions corresponding to L modes of higher frequency, a double-peak structure was observed, with one peak close to the expected frequency of the longitudinal mode, and a lower frequency peak near the frequency of a transverse mode of the same wave vector. Because the standard one-phonon cross-section

formula contains a factor $(\underline{Q}\cdot\underline{\xi})^2$, where $\underline{Q}$ is the wave-vector transfer to the crystal in the scattering, and $\underline{\xi}$ is the phonon polarization vector, the "transverse" peak should be absent in a crystal with no disorder if one chooses $\underline{Q}$ parallel to the phonon wave-vector $\underline{q}$. It is possible that such a peak could arise from a real dynamical effect caused by the disorder (effectively an uncertainty in the polarization vector). However, this feature has been investigated quite thoroughly because of its possible dynamical origin and has been demonstrated conclusively to be spurious. It is almost certainly caused by multiple scattering (e.g., see Dolling and Woods, 1965): Bragg reflection of the incident (scattered) beam prior (subsequent) to scattering from a phonon. The effect can be eliminated or almost eliminated by properly choosing the instrumental variables for the constant-$\underline{Q}$ scans.

In the case where the elastic process precedes the inelastic, the multiple scattering processes may be described by the following equations, in which $\underline{k}_o$ is the incident wave vector, $\underline{k}$ is the wave vector after the first (elastic) scattering, and $\underline{k}'$ is the wave vector after the second (inelastic) scattering. $\underline{G}_1$ and $\underline{G}_2$ are reciprocal lattice vectors and $\underline{q}$ is the phonon wave vector.

$$\underline{k}_o - \underline{k} = \underline{G}_1 \qquad \text{(elastic)} \qquad \text{(III-1)}$$

$$\underline{k} - \underline{k}' = \underline{G}_2 \pm \underline{q} \qquad \text{(inelastic)} \qquad \text{(III-2)}$$

The situation corresponding to these equations is illustrated in Fig.III-1. The programmed wave vector transfer is $(\underline{k}_o - \underline{k}') = \underline{G} + \underline{q}$, which has been chosen parallel to $\underline{q}$, in order to be sensitive only to longitudinal modes. The incident beam is partially scattered into $\underline{k} = \underline{k}_o + \underline{G}_1$, and the elastically scattered beam acts as a new incident beam. The analysing spectrometer thus looks at the wave vector transfer $\underline{k} - \underline{k}' = \underline{G}_2 + \underline{q}$ at the same time, and with the same energy transfer, as for the programmed scan. The wave vector transfer $\underline{G}_2 + \underline{q}$ is not parallel to $\underline{q}$; hence, if multiple scattering occurs, the spectrometer is sensitive to transverse modes of wave vector $\underline{q}$. By its nature, multiple scattering depends sensitively on the specimen mosaic width and on the exact spectrometer configuration, since the fairly restrictive conditions for Bragg scattering must be satisfied for one of the scattering processes.

In the Ni-Pd experiment, the relative intensity of a 'transverse' peak on a longitudinal scan was found to depend on the following factors:

(1) the specimen mosaic spread. (Specimens cut from different parts of the boule have different mosaic spreads.)

(2) whether the longitudinal scan was made with a wave vector transfer of $\underline{G} + \underline{q}$ or $2\underline{G} + \underline{q}$, where G is parallel to q.

(3) whether the constant-$\underline{Q}$ scan was made with fixed incident-neutron energy E_o or fixed scattered-neutron energy E'.

Fig. III-1. Reciprocal space diagram illustrating a double scattering process in which a Bragg reflection is followed by an inelastic process. See text for symbols and explanation.

Fig. III-2. A pair of neutron groups for Ni(55%)Pd(45%), showing the dependence of a spurious 'transverse' peak on the mode of spectrometer operation. The upper scan, which was made with fixed incident-neutron energy $h\nu_o$, shows a prominent 'T' peak at about 3.5 THz, whereas in the lower scan, made with fixed scattered-neutron energy $h\nu'$, the 'T' peak is entirely absent. Both of the constant-$\underline{Q}$ scans were programmed with $\underline{Q} = \frac{2\pi}{a}(2.3, 2.3, 2.3)$ in order to be sensitive only to the longitudinal mode with phonon wave vector $\underline{q} = \frac{2\pi}{a}(0.3, 0.3, 0.3)$. The rise at about 9.5 THz in the upper scan is caused by a contaminant energy in the incident neutron beam. Replacement of the monochromating crystals eliminated the contaminant prior to the running of the lower scan.

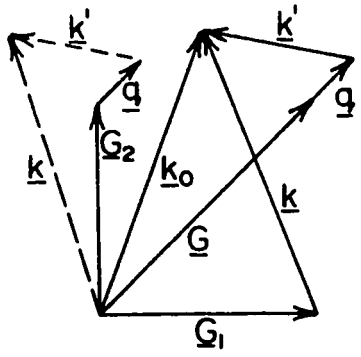

$$\underline{G} = \underline{G}_1 + \underline{G}_2$$

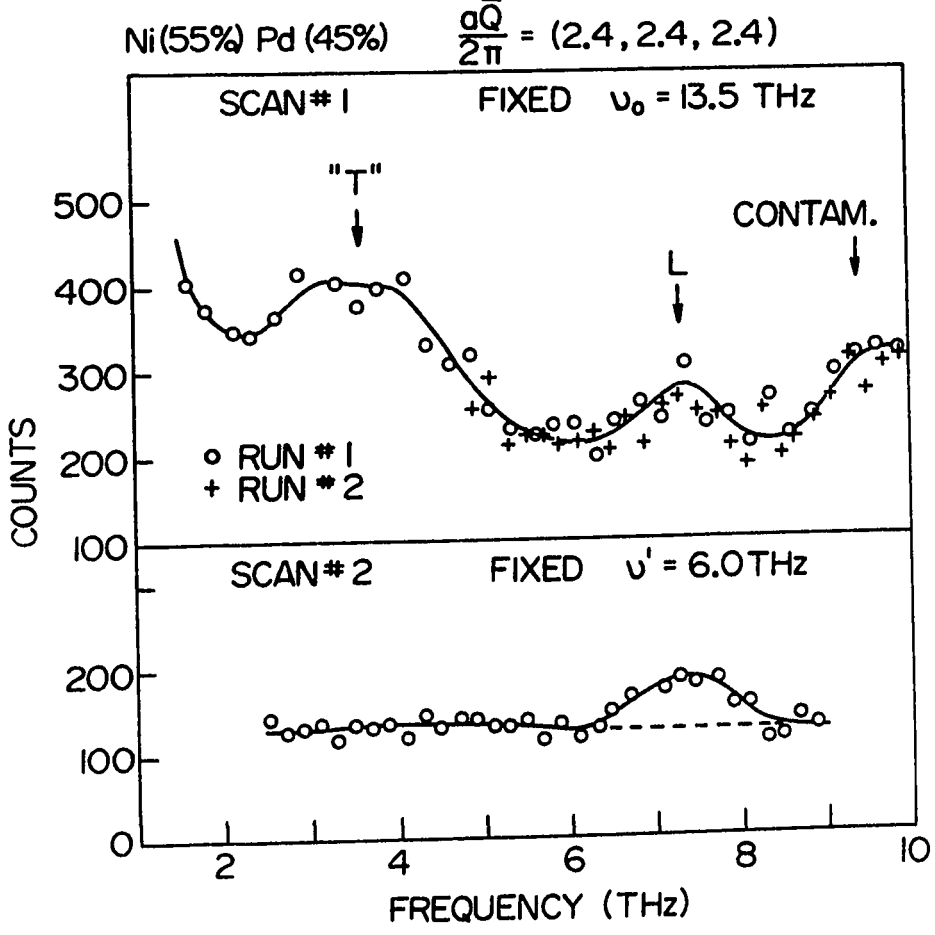

The last dependence is illustrated in Fig.III-2, which shows a pair of scans made at $a\underline{Q}/2\pi$ = (2.3, 2.3, 2.3) in order to observe the [ζζζ]L mode with ζ = 0.3. A broad, prominent peak is present in the upper (fixed-E_o) scan at approximately the transverse mode frequency. The 'transverse' peak is entirely absent in the lower (fixed-E') scan. When fixed-E' is used in a scan that covers a wide energy range, the incident wave vector is considerably shortened at low energy transfers, and multiple scattering can occur to a smaller number of reciprocal lattice vectors. Also, in fixed-E_o, the analysing spectrometer detection efficiency is variable across the scan, and higher at low energy transfers, whereas in fixed-E', it is constant across the scan.

The fixed-E' method also has other advantages in the type of experiment described in this chapter, apart from the lessened sensitivity to multiple scattering. The resolution in this method is better at low energy transfers than at high energy transfers, while the reverse is true for fixed-E_o. A series of consecutive neutron groups can thus be measured along a branch, with a resolution that is convenient for both high and low frequency modes. In fixed-E_o, the resolution is worse at low energy transfers than at high energy transfers, and different values of E_o must be used for low and high frequency modes. Integrated intensities of neutron groups are also easier to compare when fixed-E' is used, because the analyser detection efficiency is then held constant. Also,

the k'/k_o factor in the cross section can be eliminated by the use of a monitor counter with a 1/v efficiency to regulate the counting times, where v is the incident neutron velocity. Thus in an experiment like the present one, in which consecutive and easily comparable measurements are desirable, the fixed-E' method is much to be preferred. For the widths in Fig.III-4, which summarizes the results of the experiment, the open circles for the $[\zeta\zeta\zeta]L$, $[\zeta\zeta 0]L$, $[00\zeta]L$, and $[\zeta\zeta 0]T_2$ branches were done with fixed-E'. The rest of the measurements were taken with fixed-E_o, since our spectrometer was only recently converted to be operable with fixed-E'.

(iii) Treatment of Resolution

In order to extract the natural widths which are the primary results of this experiment, it was necessary to be able to reliably determine the experimental resolution widths. This was done mainly by means of resolution calculations based on the formulation of Cooper and Nathans (1967), which was mentioned in Chapter I. Several different computer programs were used to do this, two of which were written at McMaster University by Mr. A. Larose and Dr. J.R.D. Copley, and two others which originated from Brookhaven National Laboratory. Larose's program and one of the BNL programs assume a planar approximation for the dispersion of the frequencies inside the resolution ellipsoid. Almost all of the calculations were made with this approximation. The resolution calculations

were checked in selected cases by measuring, under experimental conditions very nearly the same as in the primary experiment, the widths of neutron groups in pure copper, which has dispersion curves very similar to those of $Ni_{55}Pd_{45}$. The calculated widths and copper widths were found to be in good agreement for all cases tested, generally within 15 or 20 percent, which is about the accuracy to which the copper widths were measured.

Special attention was given to the possibility of an extra contribution to the resolution width from the vertical mosaic of the crystal and also, for the $[\zeta\zeta\zeta]T$ branch, from the non-planar nature of the dispersion surface in the neighbourhood of that branch. Both of these turned out to be fairly small effects. The effect of the vertical mosaic was estimated by calculating the frequencies out of the planes of measurement (the (001) and $(1\bar{1}0)$ mirror planes of the reciprocal lattice) from a force constant model of the mean crystal. In fifteen selected cases, the frequency change corresponding to a deviation of 1^{o} from the plane was found to be less than 0.1 THz, and in most cases much less, except for a longitudinal mode, $[\zeta\zeta 0]L$, $\zeta=0.7$, measured at $(a\underline{Q}/2\pi)= (2.7, 2.7, 0)$. In the latter case, the somewhat larger deviation, about 0.21 THz, arises from the accidental degeneracy of the $[\zeta\zeta 0]L$ and $[\zeta\zeta 0]T_2$ branches at about $\zeta=0.66$. Near the degeneracy, the frequencies and eigenvectors are changing fairly rapidly as a function of wave vector, for wave vectors slightly out of the symmetry

planes. Within the range of our measurements, the only other points in the Brillouin zone for which the planar approximation is expected to be invalid occur at the zone centre, where all modes go to zero frequency, and along the [111] direction for transverse modes.

For the [ζζζ]T branch, the constant frequency surfaces are cones (Gilat, 1969). That is to say, the two transverse frequencies, which are the same along the [111] symmetry direction, split linearly away from the symmetry mode frequency for small deviations away from this direction. At the zone boundary, the gradient of the frequencies with respect to wave vector goes to zero, and the planar approximation is valid. The effect of the non-planar dispersion surfaces for this branch was estimated with the aid of programs that directly calculate the frequencies on a mesh inside the resolution ellipsoid from a force constant model. The effect was found to be a surprisingly small one. Corrections of the order of 10% to a planar approximation resolution of typically 0.3 THz were indicated.

The resolution widths were extracted from the experimentally observed widths by assuming that the observed line shape could be adequately approximated by the convolution of a Gaussian resolution function with a Lorentzian natural line shape. This assumption was tested by using the quasi-Lorentzian line shapes produced by low concentration mass defect theory for 45 at.% Pd in Ni. These line shapes, shown in Fig. III-11,

are markedly non-Lorentzian, showing pronounced double peaks in some frequency regions. The theoretical line shapes were folded with a Gaussian of width 0.7 THz (about the maximum value for the neutron groups which were used to determine natural widths), and the FWHM's of the resulting line shapes were then taken. A resolution width of 0.7 THz was then subtracted from these theoretical FWHM's by the same Gaussian-Lorentzian procedure that was employed for the experimentally observed widths. The resulting widths, which in this theory depend only on the frequency ν_{Ni} of the corresponding mode (same reduced wave vector) in pure nickel, are shown as the dotted line in Fig. III-3. The solid line represents the widths of the theoretical line shapes without resolution; the discontinuities are caused by the behaviour of the double peaks. The difference between the dotted and solid lines can be taken as an indication of the effect of resolution on the natural widths derived from the experiment. As one can see from Fig. III-3, resolution tends to smooth out the structure, but produces very little real distortion in the overall behaviour of the width as a function of frequency. Strictly speaking, the error in the width produced by the resolution extraction procedure is large on the side of a resonance peak, but the effect of the error, when the widths are plotted against frequency or wave vector, is just to produce a slight broadening of the resonances.

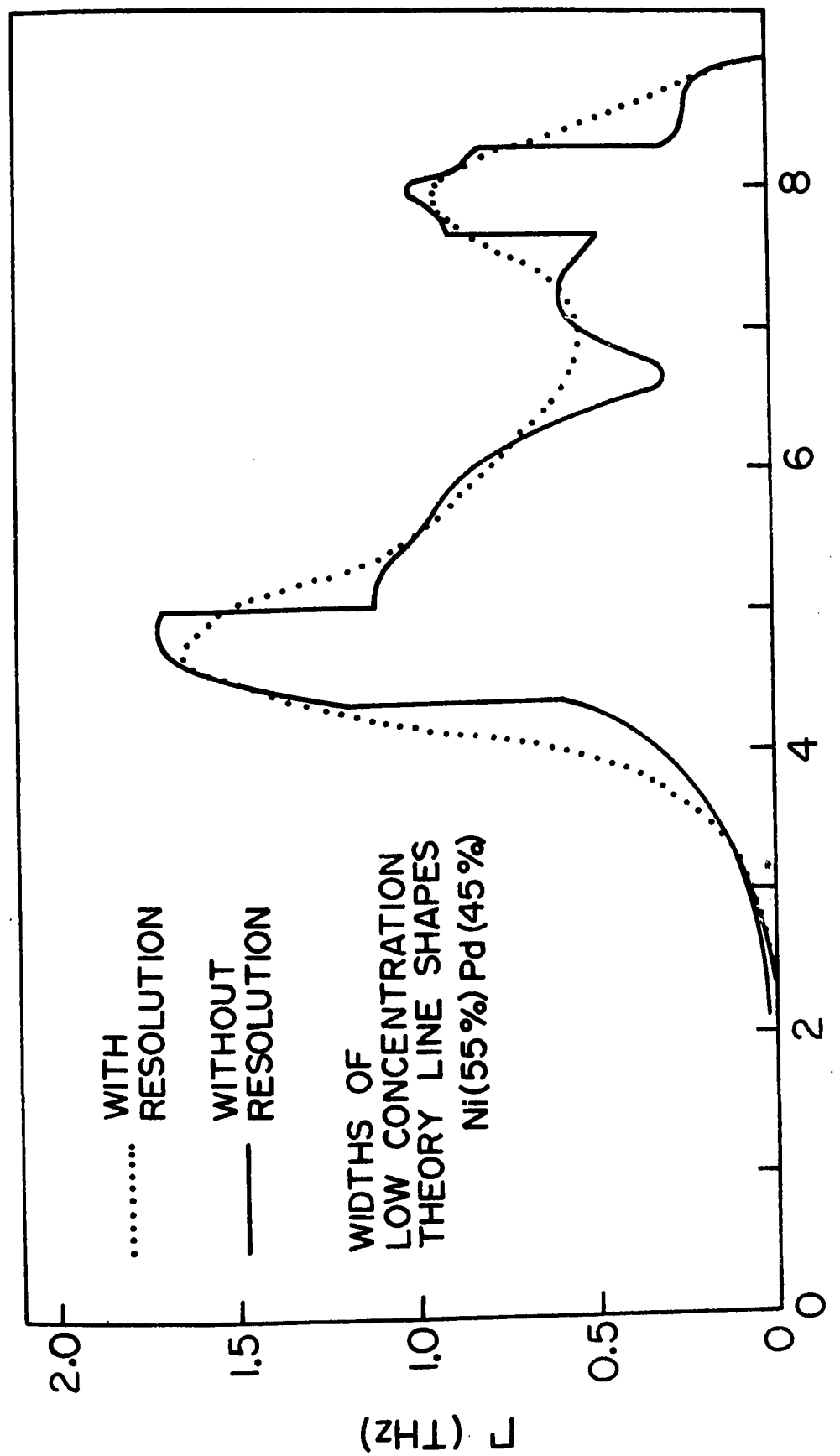

Fig. III-3. Effect of resolution extraction procedure on widths. The dotted line is almost, but not exactly, the same as the dashed line in Fig. III-7. The frequency distribution used here was that of pure nickel, and the difference in the scattering lengths of Ni and Pd was not taken into account.

C. RESULTS AND DISCUSSION

(i) General Description of Experimental Results

The neutron scattering measurements on $Ni_{55}Pd_{45}$ are summarized in Fig. III-4, which shows the disorder-induced widths (top) and the mean frequencies (bottom) of the modes, plotted against reduced wave vector. The widths, as we have indicated in detail in the previous section, are the natural widths obtained after extracting resolution from the experimental widths. Seven branches have been measured along the symmetry directions [001], [110], and [111].

In each branch, the modes show significant natural widths at larger wave vectors. In the low frequency regions, the widths are small but start to become significant when the phonon frequency reaches about 3 THz. Theories based on approximations that consider multiple scattering from single sites, such as the low concentration and self-consistent mass defect theories described in Chapter I, predict the width to be dependent only on the unperturbed phonon frequency. In the experiment, we do find that the widths start to increase at a particular phonon frequency, around 3 THz, rather than at a particular phonon wave vector. Thus in branches that slope steeply near the origin ([ζζζ]L and [ζζ0]L), the widths start to increase at smaller wave vectors. The widths of modes of higher wave vectors are generally quite large, allowing a substantially more complete and accurate determination of natural

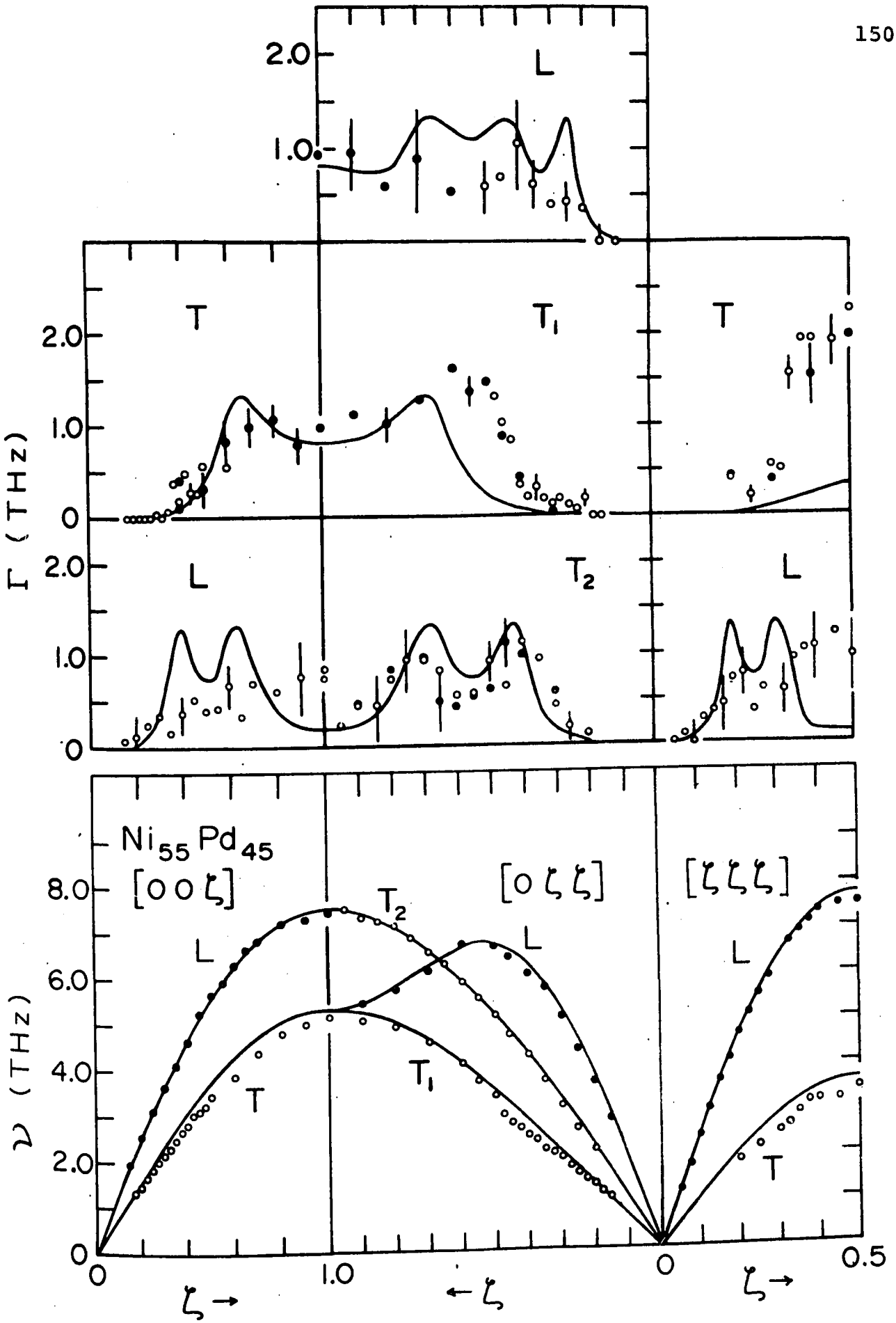
2.0
1.0
L
T
T1
T
2.0
1.0
0
Γ (THz)
L
T2
L
2.0
1.0
0
Ni55 Pd45
[0 0 ζ]
[0 ζ ζ]
[ζ ζ ζ]
8.0
6.0
4.0
2.0
0
ν (THz)
T2
L
L
L
T1
T
T
0
1.0
ζ →
← ζ
0
0.5
ζ →

Fig. III-4. Dispersion curves (bottom) and disorder-induced widths (top) observed along three symmetry directions in Ni(55%)Pd(45%). In the top figure, for a given branch, the open circles represent measurements with better resolution than the filled circles. The wave vector coordinates are in units of $2\pi/a$. The solid lines represent (top) widths predicted by the self-consistent theory of Taylor, and (bottom) a Born-von Kármán model of a mean crystal with force constants and mass averaged between Ni and Pd (55% to 45%).

widths than has been carried out in previous experiments.

In the transverse branches, the widths show behaviour characteristic of resonance modes, with the resonance frequency varying from about 3 THz to slightly more than 4 THz. The resonance is strongest and of lowest frequency (about 3 THz) in the $[\zeta\zeta\zeta]T$ branch, strong in the $[0\zeta\zeta]T_1$ branch (also at about 3 THz), and weaker, but still evident, in the $[0\zeta\zeta]T_2$ and $[00\zeta]T$ branches at a higher frequency (slightly more than 4 THz). In the $[0\zeta\zeta]T_2$ branch, there is also a strong indication of a second resonance of higher frequency (around 7 THz).

Note that in the $[\zeta\zeta\zeta]T$ branch, the width (FWHM) of the zone boundary phonon is about 0.8 of its mean frequency. The dramatic increase in width for phonons in this branch is shown in Fig. III-5. The mean frequencies and widths for the wider groups in this branch were corrected for the distortion caused by the temperature-dependent factor $(n(\nu) + 1)$ in the cross-section, where $n(\nu)$ is the Bose-Einstein population factor. In order to check that anharmonicity does not significantly affect the width, the $[\zeta\zeta\zeta]T$ zone boundary mode was also measured at a lower temperature (about 150°K). The width was little affected by the change in temperature. Fig. III-6 shows more neutron groups typical of those used in obtaining the data points of Fig. III-4. For each of the three branches $[0\zeta\zeta]T_1$, $[0\zeta\zeta]L$ and $[\zeta\zeta\zeta]L$, a pair of groups is shown, one group of low wave vector and the other of higher wave vector. For the latter, broadening is apparent in

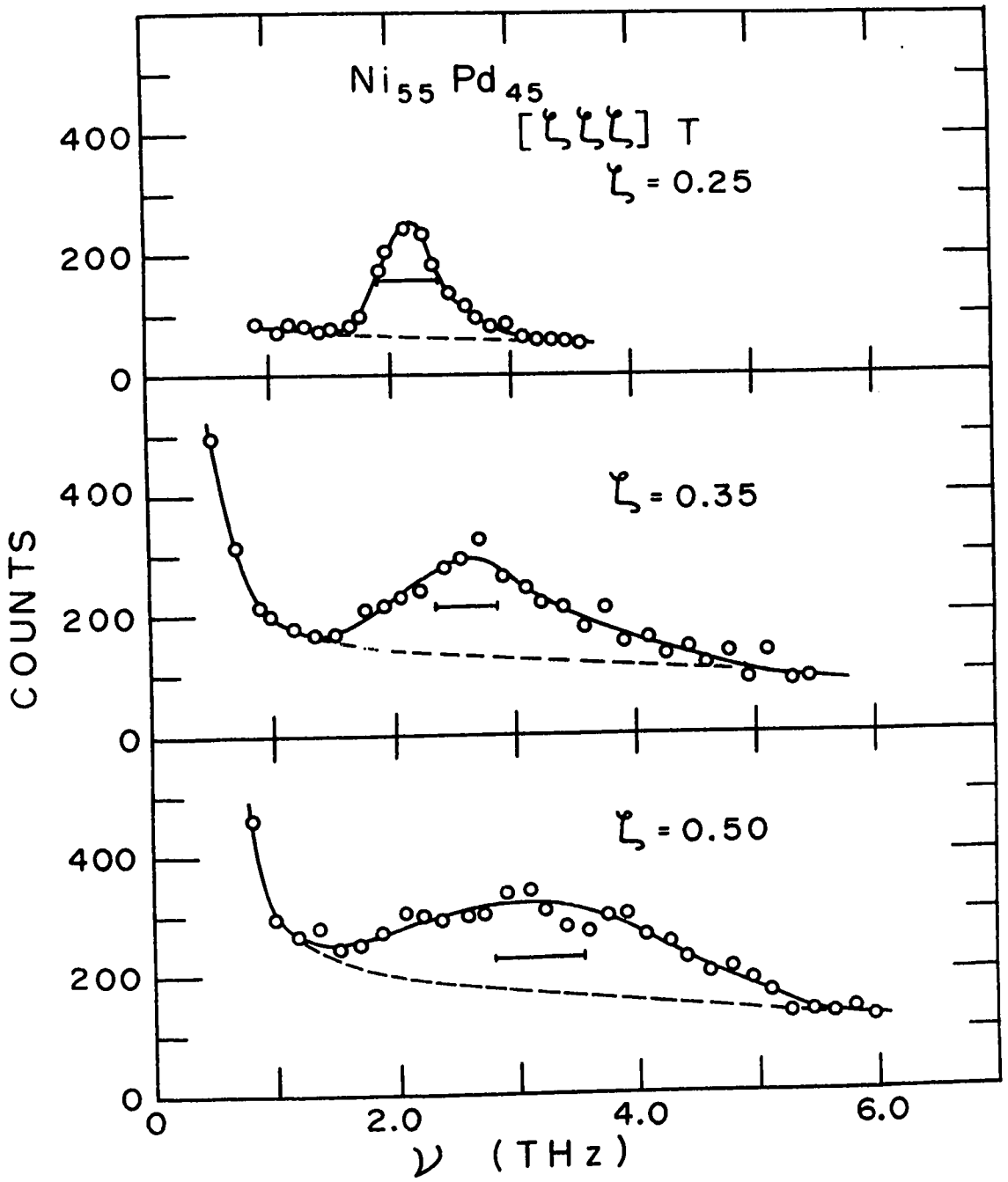

Fig. III-5. Observed neutron groups for the [ζζζ]T branch of Ni(55%)Pd(45%). The horizontal bars represent the calculated resolution widths (FWHM).

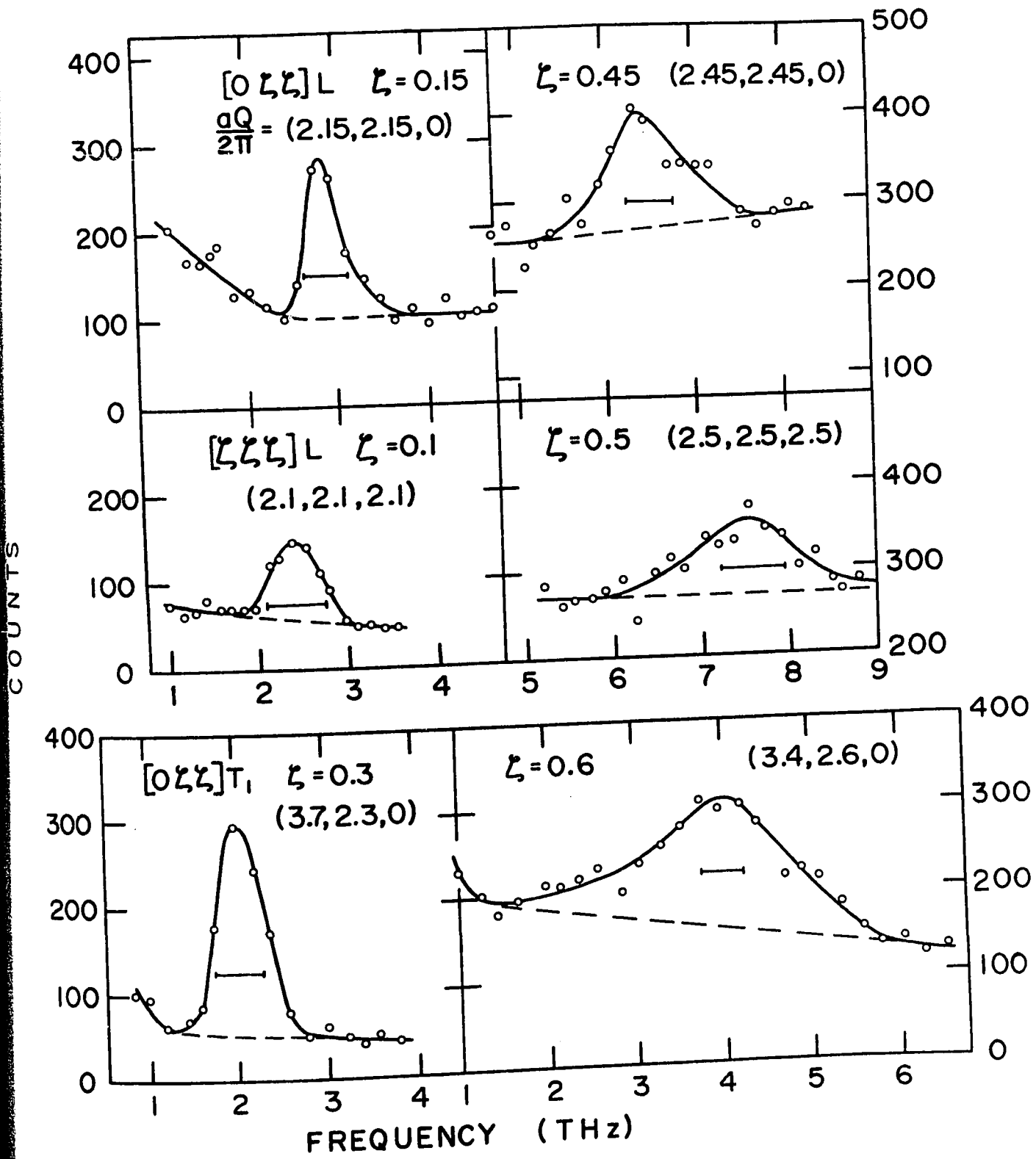

Fig. III-6. Typical neutron groups used in obtaining the data points of Fig. III-4, showing modes of low and higher wave vector in three different branches. In each case, the horizontal bar represents the calculated resolution width (FWHM).

each of the three branches, but is especially pronounced in $[0\zeta\zeta]T_1$.

There appears to be a qualitative difference between transverse and longitudinal modes with respect to the behaviour of the natural widths. The longitudinal widths are generally smaller and show little sign of the existence of resonant perturbation. There is some indication of the presence of two resonances in the $[\zeta\zeta\zeta]L$ branch (at about 4.5 and 7.5 THz) but within errors, the width could just increase monotonically from the origin to the zone boundary. In the $[00\zeta]L$ branch, there is no indication at all of resonances and the amplitude of the width is smaller than for the other branches.

Turning now to the dispersion curves themselves, we find the behaviour of the natural widths complemented in the behaviour of the frequencies. The solid lines of Fig. III-4 (bottom) represent a fifth-neighbour Born-von Kármán model of a mean crystal with force constants and mass averaged between those of Ni and Pd (55% to 45%). The force constants are listed in Table III-2. As one can see, there is very good overall agreement of the measured frequencies with this model. In fact, the regions in which there are significant deviations from the model are generally regions where a resonance is occurring and the natural widths are large. This is especially apparent in the $[0\zeta\zeta]T_1$ branch, where a prominent kink in the dispersion curve occurs at $\zeta = 0.5$. The

frequencies in the [ζζζ]T and [00ζ]T branches are also low at higher wave vectors where large natural widths occur. There are also less certain regions of lowered frequency in the low wave vector part of the $[0\zeta\zeta]T_2$ branch and near the zone boundary in the [ζζζ]L branch, both of which are also regions in which the natural widths are fairly large. In the [00ζ]L branch, where no resonances occur and the widths are small, the mean crystal model gives almost exact agreement with the measured frequencies. The behaviour of the frequencies thus seems to indicate that force constant changes from the pure substances to the mixed crystal must be quite small in an average sense, although there may be fairly large fluctuations of the force constants betwen individual atoms about the average values.

(ii) Important Features of the Experimental Results

Order of Magnitude of Natural Widths

Perhaps the most significant information contained in the measurements lies in the order of magnitude of the widths for the alloy. The measurements have shown that, in the presence of the substantial amount of mass disorder implied by a heavy atom concentration of 45 atomic percent and a mass ratio of 1.8, phonons can still be considered to exist, but often have large widths, ranging up to 80% of the mode frequency. The order of magnitude of the widths and their qualitative behaviour can be understood on the basis of fairly

simple models, but quantitative understanding is much more difficult.

Resonance Behaviour

When the natural widths are plotted as functions of frequency or wave vector for each branch, the data for each transverse branch indicate the presence of a pronounced peak in the width at a phonon frequency of around 3 or 4 THz. It is thus apparent that behaviour characteristic of resonance modes persists into the high concentration regime. Calculations based on mass defect theory for isolated defects or small finite concentrations show that well-defined resonances should occur for a mass ratio of 2 to 1. For example, Dawber and Elliott (1963) have calculated the mode amplitude of a defect atom relative to that of a host atom, in a cubic Bravais lattice with a Debye frequency distribution, for several values of the defect to host mass ratio. Their results show that, for a mass ratio of 2 ($M_{Pd}/M_{Ni} = 1.8$), the amplitude at the resonance peak is about half that for a mass ratio of 3 ($M_{Au}/M_{cu} = 3.1$). The resonance frequency is about 25% higher for the lower mass ratio. In other words, the 'strength' of the resonance is much more sensitive to the mass ratio than is its frequency. Our own calculations for Cu(Au) and Ni-Pd, based on low concentration theory, and not assuming a Debye distribution, show similar behaviour for the resonant perturbation (impurity-induced shifts and widths) of the phonon

dispersion curves. That a Pd atom has resonance modes in a Ni host is thus to be expected, but it is rather surprising that such clearly-defined resonances exist at a concentration of 45 atomic percent Pd.

Branch Dependence; Comparison with Cu(Au)

Now turning to consider the details of the experimental results, the most striking feature of the behaviour of the natural widths shown in Fig. III-4 is the pronounced branch dependence, qualitatively very similar to that seen in Cu(Au). The dependence can be seen more clearly in Fig. III-7, where the results have been plotted against unperturbed frequency for each branch. As mentioned before, the unperturbed frequency is the frequency of the corresponding mode (same reduced wave vector) in a lattice with Ni mass and force constants averaged between Ni and Pd. Fig. III-7 should be compared in detail with Fig. II-2 for Cu(9% Au), which has been laid out in a similar manner to permit a direct and easy comparison.

For the four branches which have been studied in both systems, the overall pattern of the resonances in the widths is remarkably similar. The amplitude of the width is largest in the $[\zeta\zeta\zeta]T$ branch, next largest in the $[\zeta\zeta 0]T_1$ branch, smaller in the $[00\zeta]T$ branch, and very small in $[00\zeta]L$. In fact, it was only after the Ni-Pd experiment had been almost completed, and the similarity of the pattern of the resonances

Fig. III-7. The natural widths for Ni(55%)Pd(45%) plotted as a function of reference lattice frequency for each branch. The solid lines represent the predictions of the self-consistent theory, and the dashed lines represent those of low concentration theory.

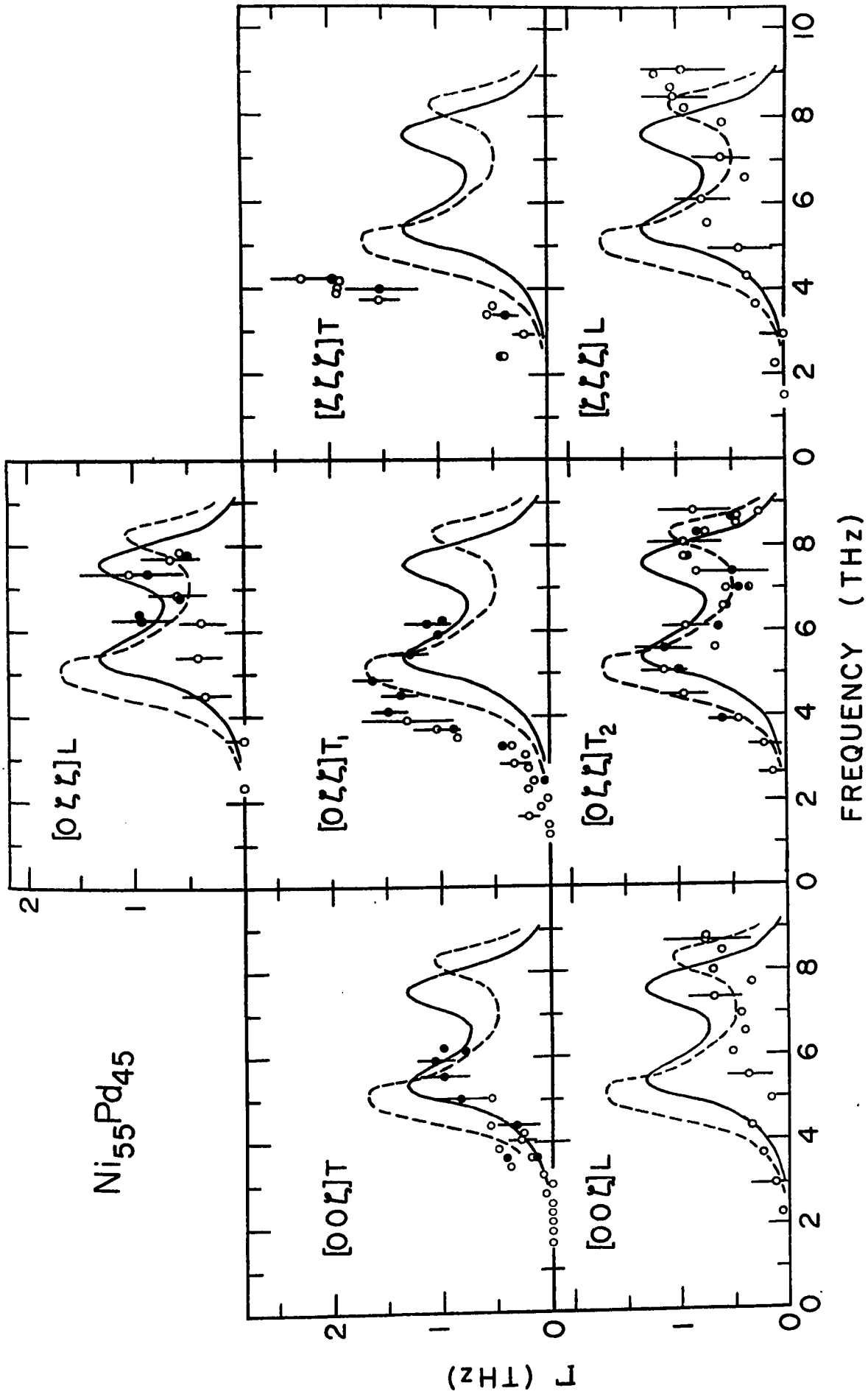
$Ni_{55}Pd_{45}$
[00ζ]T
[00ζ]L
[0ζζ]L
[0ζζ]T₁
[0ζζ]T₂
[ζζζ]T
[ζζζ]L
Γ (THz)
FREQUENCY (THz)

had been noted, that the [ζζζ]T branch was measured in Cu(3% Au) and Cu(9% Au). As anticipated, the resonances were found to be strong and sharp.

As in Cu(Au), the mean frequencies of the resonances in Cu(Au) are related to their amplitude and sharpness. The branches can be listed in order of increasing resonance frequency, and decreasing amplitude and sharpness as follows: [ζζζ]T, [ζζ0]T_1 [ζζ0]T_2, [00ζ]T, [ζζζ]L and [ζζ0]L about equal, and finally [00ζ]L. For the L branches, there are no clearly defined resonances and the amplitude has been used as an indicator to make this ordering. For [ζζζ]T and [00ζ]T, the high frequency side of the resonance peak has not been reached, and the position of steepest slope on the low frequency side of the resonance peak, as well as the sharpness of the rise and the amplitude of the peak, have been used as indicators.

Despite the pronounced similarities, the behaviour of the widths is not identical for the Cu(Au) and Ni-Pd systems. The following differences should be noted:

1) The resonance peaks occur at higher values of the reduced wave vector in Ni-Pd. That is to say, noting that the dispersion curves of the reference lattices (Cu and Ni, with adjusted force constants) are similar, apart from a scaling factor of about 1.25, the resonances occur at higher relative frequency in Ni-Pd than in Cu(Au). By 'relative frequency'

is meant ν/ν_{max}, where ν_{max} is the maximum frequency in the reference lattice. Thus in Ni-Pd, the frequencies corresponding to the high frequency side of the resonance peak have not been reached at the zone boundary in the $[\zeta\zeta\zeta]T$ and $[00\zeta]T$ branches, whereas in Cu(Au), the zone boundary frequencies are obviously well on the high side of the resonance. Even in the $[00\zeta]L$ branch, the widths for Cu(9% Au) show a low, broad peak while the Ni-Pd widths show only a steady increase with frequency, perhaps indicating that the 'resonance' again occurs at a higher relative frequency in Ni-Pd.

2) In $[\zeta\zeta 0]T_1$, which is the only branch where we can compare the width of the resonance for the two systems, the resonance is clearly broader in Ni-Pd than in Cu(9% Au), and much broader than in Cu(3% Au). Whether this is partially caused by the high Pd concentration is hard to say, since some broadening, and higher resonance frequencies as noted in the preceding paragraph 1), must arise from the difference between the Au/Cu and Pd/Ni mass ratios.

3) The amplitude of the width in Cu(Au), per heavy atom, is about twice as large as in Ni-Pd. Again, in the absence of very strong concentration-dependent effects, this is to be expected from the difference in the impurity-host mass ratios.

4) The rise in the width on the low frequency side of the resonance occurs at about the same unperturbed frequency

(approximately 2.6 THz) in the three branches $[\zeta\zeta\zeta]T$, $[\zeta\zeta 0]T_1$, and $[00\zeta]T$ in Cu(9% Au). For Ni-Pd, the rise in the $[00\zeta]T$ branch occurs at about 5 THz, a frequency substantially higher than in $[\zeta\zeta 0]T_1$ or $[\zeta\zeta\zeta]T$; in both of the latter two branches, it occurs at about 3.7 THz.

In the preceding chapter, it was emphasized that the behaviour for Cu(3% Au) is similar to that in Cu(9% Au), although there are significant concentration-dependent effects. Force constant changes were brought forth as the only logical explanation for the pronounced and similar branch dependence of the widths. By extension, force constant changes must also be important for Ni(55%)Pd(45%), unless there is a very unexpected similarity between the effects produced by large concentrations and force constant changes. The changes must have a physical origin that is common to the Cu(Au) and Ni-Pd systems. The most obvious consideration is the increased overlap of the heavy atoms with their nearest neighbours, because of their larger size. The lattice constants of Pd and Au are about 11 and 10 percent larger respectively than those of Ni and Cu. The work of Bruno and Taylor (1971) for Cu(3% Au) appears to indicate that force constant changes to first neighbours are not enough, and further neighbours need to be considered, but it may be worthwhile to recheck this.

Frequencies

So far, we have been able to make a number of significant qualitative observations about the nature of the imperfect

crystal dynamics in Ni(55%)Pd(45%) by considering the natural widths derived from the measurements. It is relatively more difficult to extract meaningful information about disorder effects from the phonon frequencies. As one can see from Fig. III-4 (bottom), the mean crystal model does a reasonable job of describing the general behaviour. The regions of lowered frequency, near $\zeta = 0.45$ in $[\zeta\zeta 0]T_1$, at higher wave vectors in the $[\zeta\zeta\zeta]T$ and $[00\zeta]T$ branches, and less certainly, in the low wave vector part of the $[\zeta\zeta 0]T_2$ branch and near the zone boundary in the $[\zeta\zeta\zeta]L$ branch, indicate a complementarity to regions of large widths. However, it is not correct to regard the difference between the mean crystal model and the measured frequencies as the disorder-induced frequency shifts.

Natural widths that are much larger than those in pure Ni or Pd must be disorder-induced effects. For phonon frequencies, the disorder effects, in the form of frequency shifts, can only be separated out if one can determine appropriate force constants for the reference lattice. As indicated in the preceding chapter, this problem also arises for a low concentration experiment, but in the case of Cu(Au), the disorder-induced frequency shift is about the same size as, or larger than, the reference lattice shift, so that one can still see and comment on details of the behaviour. On the other hand, for Ni(55%)Pd(45%), most of the frequency shift from pure Ni or pure Pd is caused by the change in mean

mass and the unknown changes in the mean force constants; the disorder-induced frequency shift which is superimposed on the reference lattice shift will be relatively small and hard to separate out.

The anomaly in the $[\zeta\zeta 0]T_1$ branch of the dispersion curves in pure Pd (Miiller and Brockhouse, 1968) is another source of uncertainty in how to extract frequency shifts, although the nature of the anomaly is now believed to be a Kohn effect of a sort that would not be present in an alloy of Ni(55%)Pd(45%) (A.P. Miiller, private discussion).

(iii) Comparison with Theory

(1) Perturbation Theory

The simplest realistic approximation to make for high concentrations is one that uses perturbation theory to second order in the mass differences. This is expected to be applicable only in the case of very small mass differences and no force constant changes, essentially restricting the validity to isotopic disorder. It is discussed here because it gives a reasonable first estimate of the size of disorder-induced widths (which was used when this experiment was in its initial stages) and provides a basis for comparing more complicated theories.

The perturbation theory can be done by working directly in terms of the normal modes of the system (Ng, 1967; Ng and Brockhouse, 1968) or by means of Green's functions. The former approach is based on some work by Mattis (1957). The

latter approach will be outlined here, since it gives a more general result with no extra effort. The notation and most of the needed equations have already been introduced in Chapter I.

We start with the generally valid equation for the configurationally averaged Green's function,

$$\underline{\underline{\bar{G}}} = \underline{\underline{P}} + \underline{\underline{P}}\ \underline{\underline{\Sigma}}\ \underline{\underline{\bar{G}}} \qquad \text{(III-1)}$$

where the self-energy $\underline{\underline{\Sigma}}$ is the object to be evaluated.

With a single-site approximation (i.e., no impurity complexes or force constant changes are considered), the self-energy can be written

$$\underline{\underline{\Sigma}} = \sum_s \underline{\underline{T}}_s \qquad \text{(III-2)}$$

where $\underline{\underline{T}}_s$ represents the configuration-averaged t matrix (a matrix of the form of $\underline{\underline{X}}_i$ in Eq. 1-59 that describes multiple scattering from the site s). The summation is over all lattice sites. Before the configuration average, for an atom of type δ at s, the t matrix is given by

$$\underline{\underline{T}}_s^{\delta} = \underline{\underline{C}}_s^{\delta}\ (\underline{\underline{I}} - \underline{\underline{P}}_s\ \underline{\underline{C}}_s^{\delta})^{-1} \quad ,$$

where $\underline{\underline{C}}_s$ is the defect matrix describing the mass change at site s, and $\underline{\underline{P}}_s$ is the perfect lattice Green's function, but with the same extent as $\underline{\underline{C}}_s$. To second order in the mass

differences,

$$\underline{\underline{T}}_s^{\delta} = \underline{\underline{C}}_s^{\delta} \left(\underline{\underline{I}} + \underline{\underline{P}}_s \underline{\underline{C}}_s^{\delta}\right) = \underline{\underline{C}}_s^{\delta} + \underline{\underline{C}}_s^{\delta} \underline{\underline{P}}_s \underline{\underline{C}}_s^{\delta} \quad . \tag{III-3}$$

In the (α,ℓ) representation, we have, by definition,

$$(\underline{\underline{C}}_s^{\delta})_{\alpha\ell;\beta\ell'} = \varepsilon_{\delta} M\omega^2 \delta_{\alpha\beta} \delta_{\ell\ell'} \delta_{s\ell} \tag{III-4}$$

where M is the mass in the reference lattice (asumed to be monatomic for simplicity), and ε_{δ} is the mass defect parameter $(1-M_{\delta}/M)$. We note that $\underline{\underline{C}}_s^{\delta}$ is diagonal and has only three non-zero elements, each of which is $\varepsilon_{\delta} M\omega^2$. Hence the term $\underline{\underline{C}}_s^{\delta}\underline{\underline{P}}_s\underline{\underline{C}}_s^{\delta}$ on the right hand side of Eq. III-4 has non-zero elements in the 3 by 3 block labelled by s. Using Eq. I-39 for the perfect lattice Green's function, the t matrix must then be given by

$$(\underline{\underline{T}}_s^{\delta})_{\alpha\ell;\beta\ell'} = \delta_{\ell\ell'}\delta_{s\ell}\left[\varepsilon_{\delta} M\omega^2 \delta_{\alpha\beta} + \varepsilon_{\delta}^2 M\omega^4 \frac{1}{N} \sum_{j\underline{q}} \frac{\xi_{\alpha}^{j}(\underline{q})\xi_{\beta}^{j*}(\underline{q})}{\omega^2 - \omega_j^2(\underline{q})}\right] . \tag{III-5}$$

The sum is the same one we considered in Chapter I in Eqs. I-44S to I-47S, and by the arguments which were presented there, for a cubic monatomic crystal, the t matrix has only three equal, non-zero elements along the diagonal, given by

$$(\underline{\underline{T}}_s^{\delta})_{\alpha\ell;\beta\ell'} = \delta_{\ell\ell'}\delta_{s\ell}\delta_{\alpha\beta}\left[\varepsilon_{\delta} M\omega^2 + \varepsilon_{\delta}^2 M\omega^4 \frac{1}{N} \sum_{j\underline{q}} \frac{\xi_{\alpha}^{j}(\underline{q})\xi_{\beta}^{j*}(\underline{q})}{\omega^2 - \omega_j^2(\underline{q})}\right] . \tag{III-6}$$

Now since we are concerned with frequencies within the band, we must follow Brout and Visscher's original (1962) prescription, and replace the summation by a principal part integral plus an additional imaginary term, precisely as given in Eq. I-64, so that

$$(\underline{\underline{T}}_s^{\delta})_{\alpha\ell;\beta\ell'} = \delta_{\ell\ell'}\delta_{s\ell}\delta_{\alpha\beta}[\varepsilon_\delta M\omega^2 + \varepsilon_\delta{}^2 M\omega^4 P(\omega)] \tag{III-7}$$

$$\text{where} \quad P(\omega) = \text{p.p.}\int \frac{f(\omega_o)\,d\omega_o}{\omega^2 - \omega_o^2} + i\,\frac{\pi}{2}\,\frac{f(\omega)}{\omega} \tag{III-8}$$

The function $f(\omega)$ is the frequency distribution of the reference lattice, normalized to unity. A configuration average now gives

$$(\underline{\underline{T}}_s)_{\alpha\ell;\beta\ell'} = \sum_s C_\delta\, \underline{\underline{T}}_s^{\delta}$$

$$= \delta_{\ell\ell'}\delta_{s\ell}\delta_{\alpha\beta}[\langle\varepsilon\rangle M\omega^2 + \langle\varepsilon^2\rangle\, M\omega^4 P(\omega)] \quad . \tag{III-9}$$

If the mean crystal is taken as the reference lattice, $\langle\varepsilon\rangle=0$ and the self-energy is

$$(\underline{\underline{\Sigma}})_{\alpha\ell;\beta\ell'} = \sum_s (\underline{\underline{T}}_s)_{\alpha\ell;\beta\ell'} = \delta_{\alpha\beta}\delta_{\ell\ell'}\langle\varepsilon^2\rangle\, M\omega^4 P(\omega) \tag{III-10}$$

or

$$\underline{\underline{\Sigma}} = \langle\varepsilon^2\rangle\, M\omega^4 P(\omega)\underline{\underline{I}} \quad . \tag{III-11}$$

Since this is just a constant times the identity, the form in the $(j,\underline{q})$ representation is the same, except that the mass M drops out because the transormation $\underline{\underline{X}}$ of Eq. I-35a is slightly non-unitary. Hence the elements of the constant matrix $\underline{\underline{\Sigma}}$ are

$$\Sigma(\omega) = \langle\varepsilon^2\rangle\, \omega^4 P(\omega) \tag{III-12}$$

and the line shape in coherent neutron scattering, from a crystal with component atoms of equal scattering length, is proportional to

$$\text{Im}\, G(j,\underline{q};\omega) = \text{Im}\, \frac{1}{\omega^2-\omega_j^2(\underline{q})-\Sigma(\omega)} \quad . \tag{III-13}$$

If the widths are small enough that $\Sigma(\omega)$ does not vary much over the width of the line shape (not really a good assumption for Ni(55%)Pd(45%)), the full width at half maximum is

$$\Gamma = \frac{1}{\omega}\,\text{Im}\,\Sigma(\omega) = \langle\varepsilon^2\rangle\,\frac{\pi}{2}\,\omega^2\, f(\omega) \quad , \tag{III-14}$$

which is the result of Ng(1967; Ng and Brockhouse, 1968). Krivoglaz (1969) has derived the same expression by a somewhat different argument.

The right hand side of Eq. III-14 has been evaluated for Ni(55%)Pd(45%) and is shown in Fig.III-8, together with

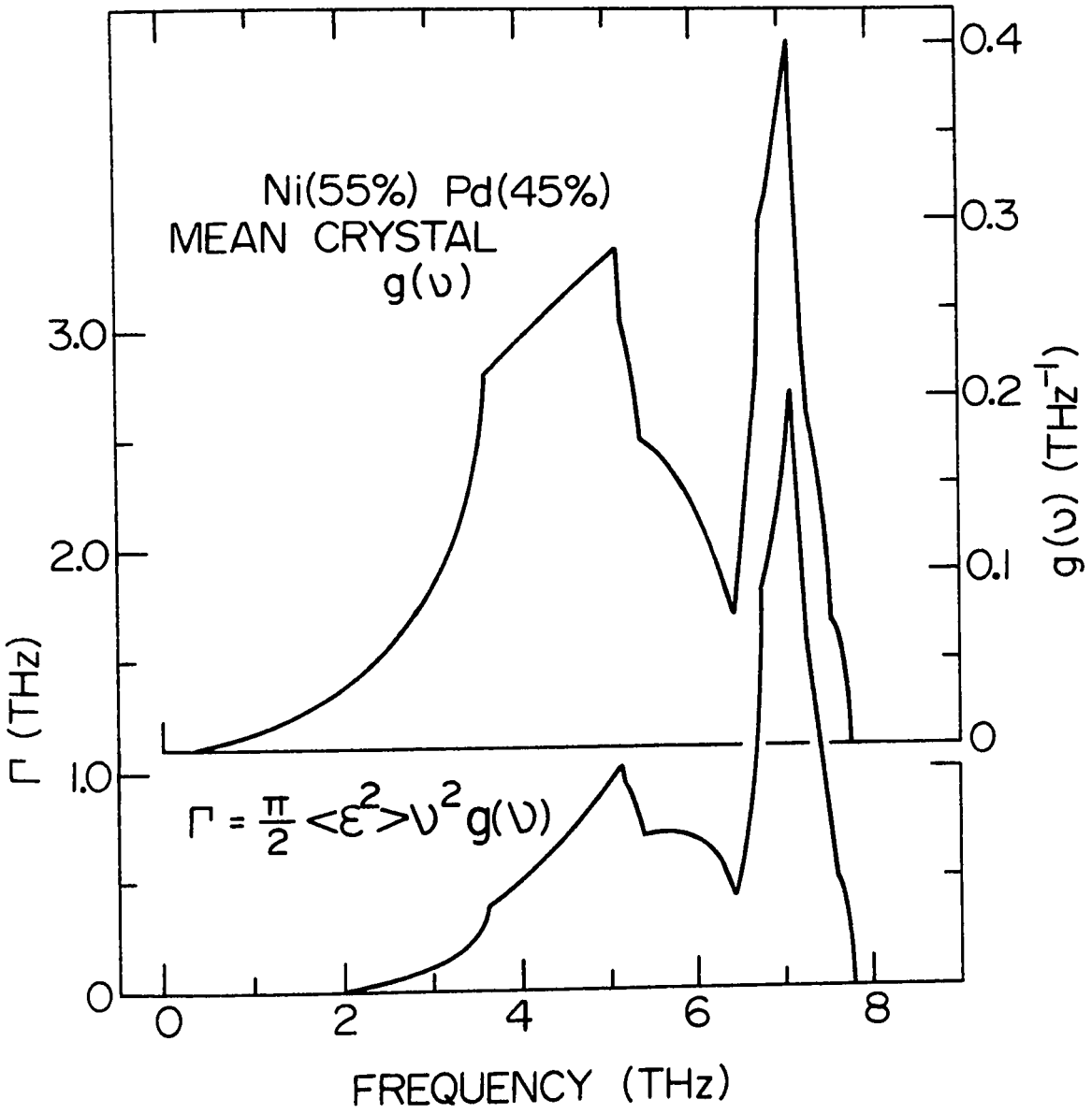

Fig. III-8. Widths Γ for Ni(55%)Pd(45%) predicted by perturbation theory. The top portion of figure shows the reference lattice frequency distribution, g(ν), used in the calculation.

the frequency distribution, $g(\nu) = f(\omega)$, from which it was calculated. The force constants which were used to calculate this frequency distribution are listed in table III-2, and are the averages(55% to 45%) of the force constants of pure Ni and Pd. The same distribution, apart from a scale change on the x-axis to make the distribution appropriate to a Ni mass, and on the y-axis to preserve the normalization at unity,was also used in the calculations for low concentration and self-consistent theory.

A comparison of the experimental widths of Fig.III-7 with the width from perturbation theory in Fig.III-8 shows that this simple calculation gives qualitatively correct results for frequencies below the first minimum in the frequency distribution. (When making the comparison, keep in mind that the x-axis ascale in Fig. III-4 is the reference lattice frequency with a Ni mass, so that 9.05 THz in Fig. III-7 corresponds to 7.75 THz in Fig.III-8. These numbers are the maximum reference lattice frequencies in each case.) The calculated widths in this region are typically about 40 or 50 percent too small for the transverse branches but the agreement is better for longitudinal branches; the calculated widths are certainly of the right order of magnitude. The predictions are qualitatively correct in two other respects. First, the frequency at which the widths should start to become large is predicted to be about 3.5 THz, which is approximately correct. Also, two 'resonances' are

predicted, corresponding to the two major peaks in $g(\nu)$; we observe two resonances in the $[\zeta\zeta 0]T_2$ branch, and there are indications of two resonances in the $[\zeta\zeta\zeta]L$ branch. However, in the calculations, the amplitude of the second resonance is much too large, by about a factor of three.

In Eq. III-14, the width is proportional to the frequency distribution $f(\omega)$. The obvious interpretation of this proportionality is that the disorder allows a mode of frequency ω to decay into modes close to it in frequency, and that this decay is easier if there are many such modes. The large amplitude predicted by the perturbation theory for the second resonance is produced by the large number of modes with frequencies near 7 THz in the reference lattice. However, it seems very reasonable that the reference lattice $f(\omega)$ does not really represent the density of phonon states available for decay, but that since the phonons have become smeared out in frequency, the amplitude of the second peak in $f(\omega)$ has been greatly reduced. What we are really saying here is that the theory lacks self-consistency; the reference lattice $f(\omega)$ should be replaced by the imperfect crystal $f(\omega)$, because the imperfect crystal itself is, for high concentration isotopic disorder, almost certainly a better approximation for the environment of any given atom. One can achieve a sort of self-consistency by iterating Eq. III-14, at each step inserting for $f(\omega)$ the function obtained by giving a width $\Gamma(\omega)$ to each mode in the reference

lattice $f(\omega)$, where $\Gamma(\omega)$ is obtained from the previous step. Actually, it is hard to justify such a procedure except on an intuitive basis, but the argument does point out why the amplitude of the second resonance in the perturbation theory is too large.

(2) Self-Consistent Theory

Among theories that treat imperfect crystal dynamics for high concentrations, the theory of D.W. Taylor (1967) is at present the most realistic attempt for which detailed calculations have been made. Aiyer et. al. (1969) and Leath (1972) have extended the self-consistent theory to include pair scattering, but calculations based on this extended treatment have not yet been carried out. The self-consistent theory has already been described in Chapter I. However, in order to discuss its application to this experiment, it may be useful at this point to list some of the approximations involved and other characteristics.

a) The theory is applicable to substitutionally imperfect crystals, with no long or short range order. Only mass disorder is considered.

b) The crystal has a monatomic cubic structure, or the diamond structure.

c) The environment of any atom is considered to be the imperfect crystal itself. Fluctuations in the environment are neglected. Hence the approximation is most suitable for large concentrations in three dimensions, where it can

be argued that the environment of an atom really does resemble the imperfect crystal. By implication, scattering from 'impurity' pairs, or 'impurity' complexes, is being neglected.

d) The theory treats 'host' and 'impurity' type atoms on an equivalent basis, an essential property of a high concentration theory.

e) In the limit of very small concentrations, the low c theory is correctly obtained, but the initial concentration effects that occur as c is increased, such as the broadening of a local mode, are not being properly described.

The main success of this theory is the agreement obtained with the frequency distributions derived from the computer experiments of Payton and Visscher (1967a). In one and three dimensions, and for fairly large mass ratios (up to 3), the agreement is very good, except that the 'spiky' structure around the local mode for moderate concentrations of light defects (c less than about 0.3 in three dimensions, for a mass ratio of 1/3) is not reproduced. This is to be expected, since the impurity complexes that give rise to this structure have been neglected. The agreement in three dimensions in this regard is better than in one dimension; this is also to be expected, since the approximation c) has become a more reasonable one. For frequencies well within the band, for all cases considered, the agreement is within

the fluctuations of the histograms of the computer experiments.

However, it should be pointed out that a quantity such as a frequency distribution is a relatively insensitive criterion by which to judge a theory that attempts to give a detailed description of the imperfect crystal dynamics. Especially for modes within the band, much of the detailed behaviour of the modes has been averaged out; in particular, one has lost information about the widths of the phonons within the band, or even whether phonons remain a good description. Comparisons of calculations with observations on the behaviour of individual phonons, such as can be seen by neutron scattering, or perhaps by more complicated types of computer experiments, represent more stringent tests of theory.

The dynamics of a disordered binary alloy in which the mass ratio of the components is about 2 or 3 to 1, and in which the composition is about 50 percent light atoms and 50 percent heavy atoms, should then be in the regime where the self-consistent theory might be expected to work in a non-trivial way. For mass ratios much closer to unity, or for very low concentrations, the theory reduces to simpler theories. For intermediate concentrations, of the order of 15 to 30 percent light or heavy atoms, fluctuations in the environment of an impurity atom are expected to play a major role, and no theory presently devised is expected to work in

detail, although in the absence of suitable experimental information, the importance of these fluctuations for modes within the band is not known. The computer experiments indicate that the fluctuations are important for local modes, but the situation for band modes may be different. From these considerations, the self-consistent theory should be applicable to the dynamics of an alloy like Ni(55%)Pd(45%) if it is applicable anywhere. The major obstacle to a critical comparison is the highly probable importance of force constant changes in this alloy. As has been mentioned several times, the experimentally observed widths show very strong indications that force constant changes are present. The branch dependent width that is observed means that the self-consistent theory cannot give quantitative agreement with the experiment.

The solid lines in Fig. III-7 represent the widths calculated for Ni(55%)Pd(45%) from the self-consistent theory, plotted as a function of the reference lattice frequency. Each of the solid lines is the same, since the calculation produces widths that depend only on the reference lattice frequency, and not on branch. This is a consequence of the single site approximation, in which no impurity complexes or force constant changes are considered. The calculated widths are also shown as solid lines in Fig. III-4 (top), where the results are plotted against wave vector. These lines were produced by associating, with each wave vector,

the frequency of the phonon of the same reduced wave vector in the reference lattice (which has Ni mass and force constants averaged between those of Ni and Pd), and then plotting the width corresponding to that reference lattice frequency against wave vector. The plot against frequency, Fig. III-7, permits an easier comparison of the theoretical widths with experiment. The plot against wave vector, however, shows the behaviour of the phonon frequencies at the same time, and summarizes almost all the results of the experiment. The difference between the scattering lengths of Ni and Pd has been accounted for in the calculations. The computer programs to calculate the self-energy and the neutron scattering line shapes were written by Dr. D. W. Taylor; the latter program was modified by the author.

Comparing the experimental points with the theory, we find general agreement for the $[00\zeta]T$ and $[\zeta\zeta 0]T_2$ branches. In the latter case, two resonances are predicted, and both are observed, although the theoretical resonance peaks appear to occur at a slightly higher frequency for the first (low frequency) resonance and at a slightly lower frequency for the second resonance. For $[\zeta\zeta 0]T_1$ and $[\zeta\zeta\zeta]T$, the agreement is not as good. The theory predicts a higher resonance frequency and a smaller amplitude for the resonance in each case. The disagreement between theoretical and experimental widths in the plot against wave vector for the $[\zeta\zeta\zeta]T$ branch is really not as bad as it looks at first sight. As one can

see from the plot against the reference lattice frequency, if the theoretical resonance frequency were only slightly lower, the agreement would improve markedly. For longitudinal branches, the agreement is poorer. The structure predicted by the theory is not observed, there being no well-defined resonances shown in the experimental widths. The calculated widths are generally somewhat too large, especially for [00ζ]L.

The theories for which we have made calculations of the neutron scattering cross sections, i.e., the low concentration and self-consistent mass defect theories, both predict line shapes with pronounced asymmetries for phonons with frequencies in the regions of the resonances. The self-consistent line shapes are shown in Fig. III-9 for several values of the reference lattice frequency ν_o. When ν_o is small, the line shapes are almost delta functions. For values of ν_o/ν_M less than 0.35, the natural widths are less than 0.1 THz. (ν_M is the maximum reference lattice frequency, 9.047 THz.) As ν_o/ν_M reaches about 0.4, a tail starts to develop towards higher frequencies, but the line shapes are still sharply peaked. The line shapes for $\nu_o/\nu_M = 0.5$ and above, for which the widths are large, are shown in Fig. III-9. For frequencies just below the first resonance ($\nu_o/\nu_M = 0.5, 0.55$), there is a pronounced asymmetry to the right, that is to say, the line shapes show a sharp rise on the low frequency side, but decline slowly

Fig. III-9. Line shapes of the coherent neutron scattering cross section for Ni(55%)Pd(45%) predicted by the self-consistent mass defect theory of Taylor. The difference between the scattering lengths of Ni and Pd has been taken into account. ν_M is the maximum reference lattice frequency.

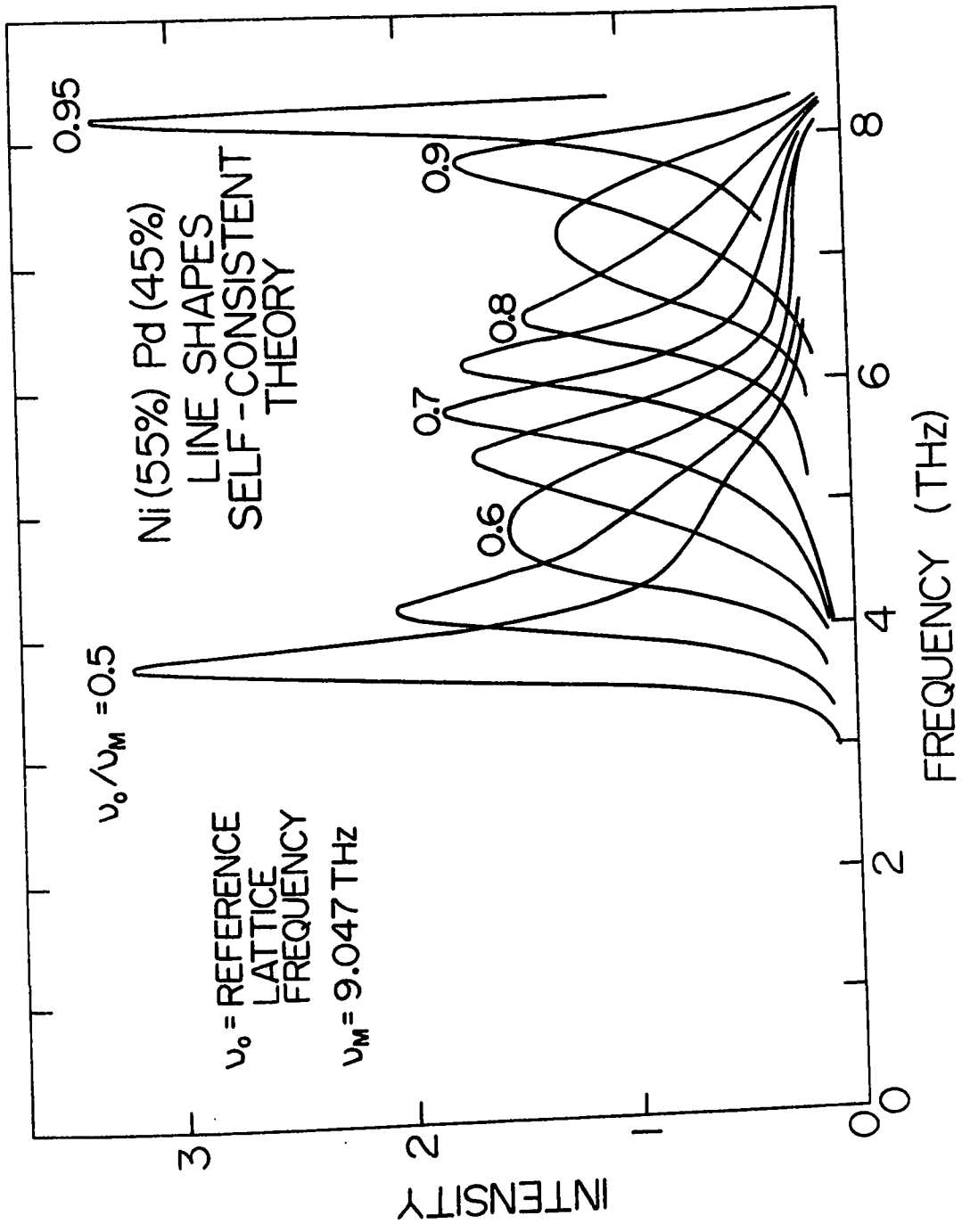
Ni (55%) Pd (45%)
LINE SHAPES
SELF-CONSISTENT
THEORY
ν_0/ν_M =0.5
0.95
0.9
0.8
0.7
0.6
ν_0 = REFERENCE LATTICE FREQUENCY
ν_M = 9.047 THz
INTENSITY
FREQUENCY (THz)
0
1
2
3
4
6
8

on the high frequency side. Near the resonance peak, and past the resonance, the line shapes are nearly symmetric, although varying in shape, until, as the second resonance is approached, the line shapes again show an asymmetry to the right, but to a lesser degree than in the case of the first resonance. (See the line shape for $\nu_o/\nu_M = 0.8$) Past the second resonance, the line shapes show an asymmetry to the left.

Most of the line shapes observed in the experiment were nearly symmetric. For some neutron groups corresponding to transverse phonons with frequencies just below the first resonance, definite asymmetries to the right were observed. Such asymmetries are evident in the groups for $[\zeta\zeta\zeta]T$, $\zeta = 0.35$ in Fig. III-5, and for $[\zeta\zeta 0]T_1$, $\zeta = 0.4$, 0.45 in Fig. III-10. In most cases, the energy resolution of the spectrometer, typically 0.5 THz full width at half maximum, was probably not good enough to detect the other types of asymmetries, even if they are present, especially since the counting statistics for the higher frequency phonons were usually not good enough to define the line shapes accurately. A detailed comparison between the calculated and experimental line shapes has not yet been made, since the disagreement of the widths for most branches, and the fairly poor resolution of the measurements, make it questionable whether such a comparison is warranted. However, on the basis of an indirect visual comparison, the asymmetries of the neutron groups appear to be smaller than predicted.

Fig. III-10. Neutron groups for the $[\zeta\zeta 0]T_1$ branch in Ni(55%)Pd(45%). The structure at around 2.5 THz for ζ = 0.55, 0.6, and 0.7 is not necessarily real, but is an interesting indication. Note the similarity to structure predicted by low concentration mass defect theory - ν_o = 5.5 and 6 THz in Fig. III-11. The rise in intensity at about 7.5 THz for ζ = 0.6 to ζ = 1.0 is caused by a contaminant energy in the incident neutron beam.

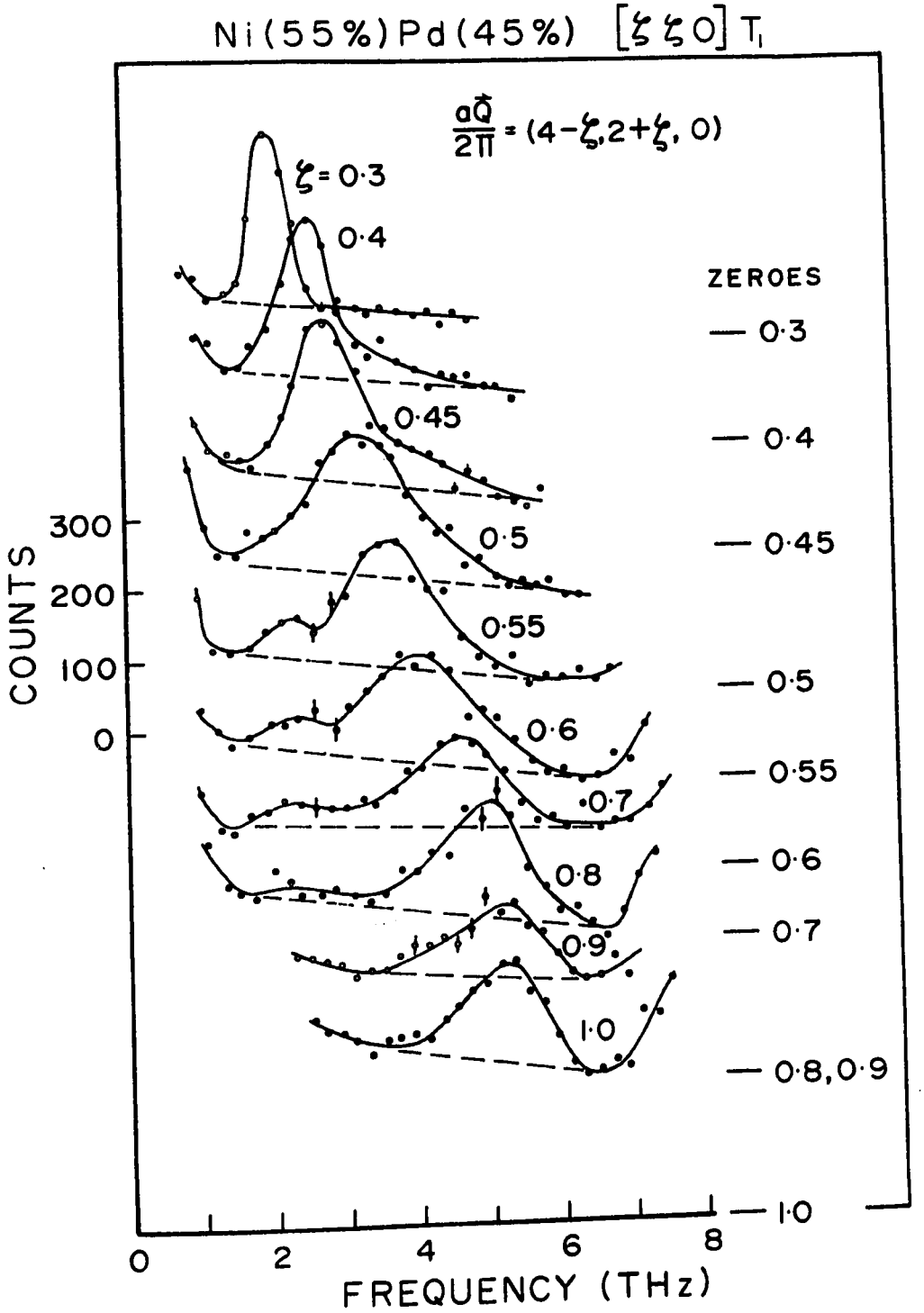
Ni(55%)Pd(45%) [ζ ζ 0] T₁
aQ/2π = (4−ζ, 2+ζ, 0)
ζ = 0·3
0·4
0·45
0·5
0·55
0·6
0·7
0·8
0·9
1·0
ZEROES
— 0·3
— 0·4
— 0·45
— 0·5
— 0·55
— 0·6
— 0·7
— 0·8, 0·9
— 1·0
COUNTS
300
200
100
0
0
2
4
6
8
FREQUENCY (THz)

The self-consistent theory gives better agreement with the experimental widths than the perturbation theory, as might well be expected, since the former is a much more sophisticated theory. The amplitude of the second resonance has come down to a reasonable value, in good accord with the data on the $[\zeta\zeta 0]T_2$ branch. The first resonance has increased in amplitude, again in better general accord with experiment.

In summary, it may be said that the overall qualitative agreement between the self-consistent theory and experiment is fairly good, although a critical comparison is not possible because of the highly probable importance of force constant changes. However, as we shall now discuss, low concentration mass defect theory also seems to give good overall qualitative agreement with the experimental widths.

(3) Low Concentration Theory

Calculations based on Eqs. I-63 to I-65 for 45 atomic percent Pd 'defects' in a Ni host have also been carried out. The derived widths are shown as dotted lines in Fig.III-7. The (1-c) factor that corrects for multiple occupancy of the defect sites was not included; this should have been done since it is probably important in this case. The low concentration theory should in principle not be applicable in this case, but in fact the overall qualitative agreement with the experimental widths is about as good as for the self-consistent theory. The predictions of the two theories are quire similar; both predict resonances at two frequencies. The resonance peaks, which are very nearly of equal amplitude in the self-consistent theory, are shifted apart and become unequal in amplitude in the low concentration theory. The first (low frequency) resonance is shifted to the left (towards lower frequencies) and becomes larger in amplitude and the second resonance shifts to the right and decreases in amplitude. Because the behaviour of the widths predicted by the two theories is otherwise quite similar, most of the comments that were made when the self-consistent theory was compared with experiment apply to the low concentration theory as well. There are some differences. The agreement between theoretical and experimental widths is actually better for the low-c theory for the $[\zeta\zeta\zeta]T$ and $[\zeta\zeta 0]T_1$ branches, about the same for the $[\zeta\zeta 0]T_2$ branch, and worse for the

[00ζ]T branch.

The line shapes are in generally poorer qualitative agreement with experiment than the self-consistent line shapes. The calculated line shapes for the low-c theory, shown in Fig. III-11, exhibit pronounced double peaks in the resonance regions. These were definitely not observed. Neutron groups corresponding to the [ζζζ]T zone boundary phonon, which should be on, or nearly on, the peak of the strongest resonance, failed to show a double peak. This phonon was measured several times, and the resolution and counting statistics should have been adequate to resolve a double peak if it existed. In the $[\zeta\zeta 0]T_1$ branch, the resonance is also strong, but there are again no definite double peaks. However, for phonons with frequencies past the resonance peak, there are some indications of asymmetries to the left in the form of shoulders, or long tails. These asymmetries, if present, resemble the asymmetries predicted by the low-c theory. Compare the neutron groups for ζ = 0.55, 0.6, and 0.7 in Fig. III-10 with the line shapes calculated for ν_o = 5.5, 6.0 and 6.5 THz in fig. III-11. The shoulders drawn on the experimental groups are not shown to be definitely real by the measurements. They are just outside counting statistics and may be caused by an unidentified spurious scattering process. However, they are certainly interesting indications.

It should incidentally be mentioned that the dotted lines

Fig. III-11. Line shapes predicted for Ni(55%)Pd(45%) by low concentration mass defect theory, with 45% Pd 'defects' in a Ni host. The difference between the scattering lengths of Ni and Pd has been taken into account.

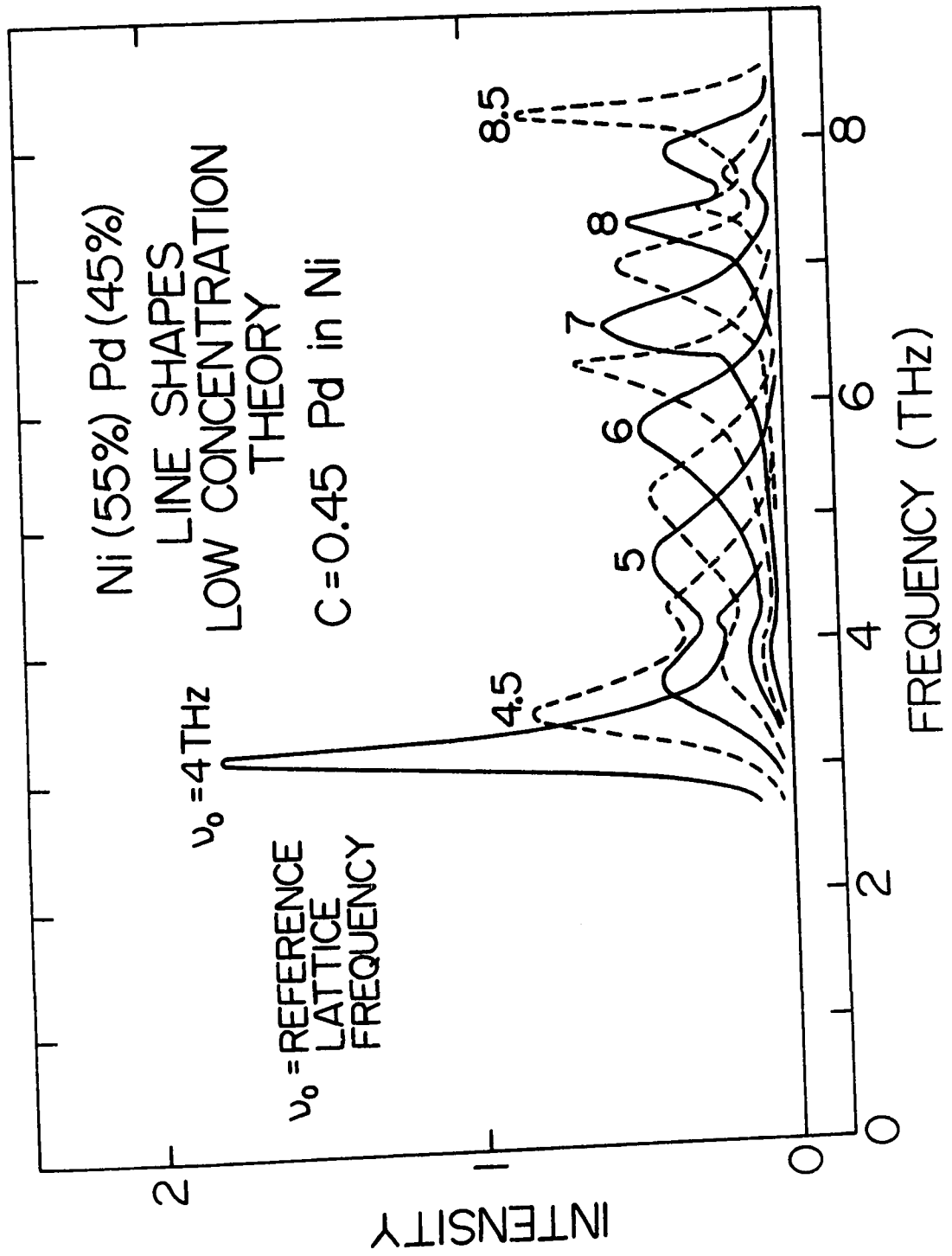
Ni (55%) Pd (45%)
LINE SHAPES
LOW CONCENTRATION
THEORY
C=0.45 Pd in Ni
ν_o =4 THz
ν_o = REFERENCE LATTICE FREQUENCY
4.5
5
6
7
8
8.5
INTENSITY
FREQUENCY (THz)
0
1
2
0
2
4
6
8

in Fig.III-7 include the smoothing effect of the experimental resolution to some extent. The theoretical line shapes were folded with a Gaussian of width 0.7 THz; the Gaussian-Lorentzian resolution extraction procedure which was used to treat the experimental widths was then applied to the widths of the folded line shapes. The experimental resolution was typically somewhat less than 0.7 THz. The effect of the resolution is not severe in any case, however. The structure in the theoretical width, plotted as a function of reference lattice frequency, is smoothed out to some extent. The discontinuities in the width resulting from the double peaks are eliminated, but otherwise the 'shape' of the width plotted against frequency is unchanged. These points were previously discussed in the section on the treatment of experimental resolution, III-B(iii), and are illustrated in Fig. III-3.

The low concentration theory gives about as good overall agreement with the experimental widths as the self-consistent theory. Whether this occurs because of the similarity of the theories or because of the insensitivity of the experiment to the differences between the theories is difficult to say. The low concentration theory lacks the necessary host-defect symmetry of a <u>bona fide</u> high concentration theory. Applying the theory with a concentration of 55 atomic percent Ni 'defects' in Pd would probably not

give sensible results. In this respect, its application to the present experimental situation is less appealing than the application of the self-consistent theory. The limited information revealed by the experiment on line shapes also seems to favour the description given by the self-consistent theory.

(iv) Factors Other Than Force Constant Changes.

As in the relatively low concentration experiment on Cu(Au) described in the previous chapter, the possibilities of structural ordering in the Ni-Pd alloy and of phonon scattering from impurity complexes could be important factors in determining the details of the dynamics in the imperfect crystal. These factors are ignored in the theories described above.

Possibility of non-randomness

Since the composition of the Ni-Pd specimen is

very nearly 50-50, the possibility of ordering needs to be seriously considered. The phase diagram (Hansen 1958) shows no indication of ordered phases in the Ni-Pd system down to 0°C. We have examined our specimen for long range order by neutron diffraction and have found absolutely no evidence of it to within 1 part in 2000 (superlattice peak intensity : fcc peak intensity). All Bragg reflections with indices (h,h,k), $h,k \leq 4$ were examined, using a Ge(111) analyser to eliminate second order effects. (The (222) reflection of the diamond structure has a zero structure factor.) If a certain ordered structure is assumed, we can place an upper limit on the amount of long range order. The amount of ordering in an incomplete state of long range order can be characterized by the long range order parameter S, which is defined by

$$S = \left|\frac{R - W}{R + W}\right|$$

where R = fraction of atoms on right lattice sites
and W = fraction of atoms on wrong lattice sites.
S = 1 for perfect order and S = 0 for no order.
The Cu Au I (tetragonal) structure, for example, has alternate (001) planes consisting of atoms of the same element. If an incompletely ordered structure of this type is assumed for the Ni-Pd specimen, the (001) and (003) superlattice reflections should have a relative intensity (expressed as

a fraction of an F.C.C. peak) of roughly

$$\frac{1}{3}\frac{(b_{Ni} - b_{Pd})^2}{(b_{Ni} + b_{Pd})^2} S^2 = 0.0232\ S^2$$

where b_{Ni} and b_{Pd} are the average coherent scattering lengths of Ni and Pd. The factor $\frac{1}{3}$ enters because we need to allow for the presence of many domains in which the tegragonal axis can be oriented perpendicular to any of the cube faces of the original fcc unit cell.

Therefore, in our specimen, we have

$$0.0232\ S^2 < \frac{1}{2000}$$

hence $$S < 0.147$$

or $$0.43 < W < 0.57$$

For a lattice with no long range order, R=W=0.5 exactly. The effects of extinction and reflectivity of the crystal planes have been neglected in order to make this rough estimate for S, but both these effects, if properly accounted for, would decrease the upper limit on S.

Short range order is still possible; to what extent its presence would influence the widths in Ni-Pd is difficult to guess. The effect of long range order would be to produce apparently large widths in regions where the degeneracy of two branches is lifted by the lowering of the crystal symmetry. The effect of short range order may be qualitatively similar, but one would expect that its influence would

be less pronounced. The calculations of Hartmann (1968) for short range order effects in Cu(9% Au) appear to indicate that not much change in the impurity-induced widths and shifts can be produced by the short range order, but the situation may be different for Ni(55%)Pd(45%). However, it is extremely unlikely that the overall pattern that is observed, i.e., the peaks in the width as a function of wave vector and branch, are a consequence of the tendency to form a particular ordered structure. In order to explain the similarity of the results for Cu(Au) and Ni-Pd,one would have to believe that the ordering tendencies are much the same for Cu(3% Au), Cu(9% Au), and Ni(55%)Pd(45%), but vary slightly in a way such as to produce a shift in the wave vector position of the resonance peaks as the concentration is increased, and the mass ratio is changed. It is far more reasonable to assume that resonance mode behaviour of the heavy atoms, together with similar force constant changes for each case, are the unifying features of the three situations. Short range order may, however, be affecting the details of the behaviour in Ni(55%)Pd(45%). The amount and nature of the short range order could possibly be determined by measuring the elastic diffuse scattering around and between reciprocal lattice points. This would be most conveniently done by X-ray diffraction, but can also be done with neutrons.

Scattering from impurity pairs and impurity complexes

The approximation that has been made in most of the theories discussed so far is to consider only scattering of the lattice waves from single sites, and to treat the total scattering from a single site as the sum of all the multiply-scattered waves. The scattering from an atom is assumed not to depend on its environment. This is a reasonable approximation for low impurity concentrations, where the probability of adjacent impurities is small, and the environment of most defect atoms looks like a lattice with all host atoms. However, it is a questionable assumption for higher impurity concentrations, such as the situation for Ni(55%)Pd(45%). The self-consistent theory says that a single site approximation can still be used for very high concentrations in three dimensions because, in Taylor's words, although the environmental fluctuations are "large in number, they are mainly weak in strength." Aiyer et. al. (1969) have recently extended the self-consistent theory to include scattering from pairs, but to our knowlege, calculations based on this extended treatment have not yet been carried out.

In our experiment, the presence of force constant changes unfortunately does not allow us to make a significant statement about this important aspect of the imperfect crystal problem, except to say that for Ni(55%)Pd(45%), it is unlikely that it has a large effect on the phonon widths.

To speculate, one might expect that the effect of pair and higher-order scattering would be to broaden and to increase the frequency of the resonances. The shift and width would become dependent on branch, even with no force constant changes. In Ni(55%)Pd(45%), it is fairly certain that the pattern of the branch dependence in the widths is coming from force constant changes. If this is the case, clearly the effect of pair and higher-order scattering is not so large as to substantially modify this pattern.

(v) Summary

Coherent inelastic neutron scattering measurements have been carried out on a single crystal of the F.C.C. random alloy Ni(55%)Pd(45%), in which the components have a mass ratio (M_{Pd}/M_{Ni}) of 1.8. The experiment has shown that phonons remain a good description in such a mass-disordered alloy, although many of the modes are observed to have large widths, up to 80% of the mean frequency of the mode.

Natural widths have been extracted from the measurements by means of detailed resolution calculations. When the natural widths are plotted as a function of wave vector or frequency for each branch, peaks in these functions are observed for transverse branches, indicating that resonant mode behaviour is present in this alloy, even though the heavy atom concentration is very high. The natural widths

are found not to be dependent on just the phonon frequency, but a different function (width vs. frequency) is obtained for each branch. This implies that the crystal dynamics cannot be adequately described by a Green's function theory in a single site approximation, which would give a branch-independent width. We have made detailed calculations based on single-site-approximation theories, notably the self-consistent mass-defect theory of D.W. Taylor (1967). We find fairly good qualitative agreement between the theoretical and experimental widths for the self-consistent theory, and, surprisingly, equally good qualitative agreement for calculations based on low concentration mass defect theory. Because of the branch dependent nature of the widths, the agreement is not quantitative.

The pattern of the branch dependence is observed to be very similar to that obtained in the experiment on Cu(Au), described in the preceding chapter. Force constant changes were invoked to explain the results for Cu(Au), and by extension, we infer that force constant changes must also be important for Ni(55%)Pd(45%). If this interpretation is correct, the presence of force constant changes prevents us from making a significant statement on effects dependent on the configuration of pairs or complexes of like atoms, at least within the framework of present theories. However, we note that such effects are not so large as to be dominating the pattern of the disorder-induced widths.

CHAPTER IV

CRYSTAL DYNAMICS OF COPPER-NICKEL ALLOYS

A. INTRODUCTION

The preceding chapters have been concerned with the crystal dynamics of binary disordered alloys in which the atomic masses of the constituents are very different, by factors of 2 or 3 to 1. For random metallic alloys in which the masses differ by only a few percent, but in which the constituents are chemically different, experience has shown that the phonons do not in general possess large widths. Several experiments have been carried out by inelastic neutron scattering on such systems as Nb-Mo (Powell et. al., 1968), Bi-Pb-Tl (Ng and Brockhouse, 1968), and Fe-Ni (Hallman and Brockhouse, 1969). The interest in the crystal dynamics of these alloys lies not so much in the disorder effects, which are surprisingly small, but in the influence of the average electronic structure on the phonon dispersion curves.

Our specific concern with the Cu-Ni system stems largely from an interest in the role of the d electrons in the lattice dynamics of transition metals and noble metals. The d electrons of such metals are known to make a large contribution to the cohesive energy; the contribution is

larger in the middle of a transition element row than at the ends. The mechanism by which this occurs is imperfectly understood and is probably complicated. The large first neighbour force constants of F.C.C. transition metals and alloys arise primarily from core-core interactions, mostly from the d electrons. In contrast to alkali metals and polyvalent metals, there is substantial core overlap for transition and noble metals. The theory of the lattice dynamics of noble metals and transition metals has recently been discussed by Prakash and Joshi (1971) and by Hanke and Bilz (1972).

The electronic structure of alloys can be considered in several approximations of varying complexity. The simplest is the 'rigid band' approximation, in which the band structure is considered to be the same for the constituent pure metals and for each of the alloys, and only the Fermi level is changing with the alloy composition. Clearly disorder effects are being neglected here, as they are in the 'virtual crystal' approximation, in which the electron-ion potential is assumed to be the same for all atoms, but is the average of the potentials for the pure elements. Disorder effects are specifically considered in the 'coherent-potential' approximation (Soven, 1969), which is the formal equivalent for electrons of the self-consistent theory of Taylor (1967) for phonons. The latter was discussed in detail in Chapters I and III.

The applicability of a rigid band model to Cu-Ni alloys is very questionable in view of several experiments, notably photoemission and optical studies by Seib and Spicer (1970). The onset of spontaneous magnetization at about 45 atomic percent nickel was thought in former years to correspond to the filling of the d band on a rigid band model. The substructure of these alloys seems to be a point of dispute (Mozer, Keating, and Moss, 1968; Moss, 1969; Kidron, 1969). The short range order could be characterized by a fairly small tendency to have like atoms on the nearest neighbour shell, or the substructure could consist partially of Cu- and Ni-rich clusters about 10 Å in diameter. The actual electronic structure and crystalline substructure of Cu-Ni alloys are questions on which the author feels unqualified to judge, but comment will be made later on with respect to the possible influence of the different interpretations on the phonon dispersion curves.

In the present measurements on Cu-Ni alloys, the phonon frequencies are found to depend approximately linearly on the Cu or Ni concentration. Significant phonon broadening was not noticed, although the data have not been examined carefully to see if it is present. Certainly the phonon widths are small compared with the difference between phonon frequencies in pure copper and nickel. The experimental findings are presented and discussed in the next two

sections.

The experiment on Cu-Ni alloys is part of an extensive research program carried out at McMaster University on the crystal dynamics of transition metals, noble metals, and their alloys. It is a natural extension of the dispersion curve measurements of Hallman and Brockhouse (1969; Hallman, 1969) on Fe-Ni, Cu(75%) Zn(25%), and Cu(50%)Ni(50%) alloys and is fairly closely related to the work of Ng, Roy, and Brockhouse (Ng, 1967; Ng and Brockhouse, 1968; Roy, 1970) on Bi-Pb-Tl alloys. Less closely related, but still along similar lines, are the experiments on mass disorder in Cu(Au) and Ni-Pd alloys that have been described in detail in Chapters II and III.

B. EXPERIMENT

(i) The Specimen Crystals

Five alloy crystals were used in this experiment; the compositions were nominally 5, 16, 40, 60 and 85 atomic percent nickel. The first two of these crystals were obtained from Research Crystals, Inc. of Richmond, Virginia, and the last three from Monocrystals Company, Cleveland, Ohio. Characterization by neutron diffraction, using the method of Ng *et. al.* (1967), described in Chapter II, revealed the mean compositions to be, for the last four alloys listed above, 20, 41, 81, and 89 atomic percent Ni, with a substantial amount of inhomogeneity present. The non-correspondence of the nominal and measured compositions, and the inhomogeneities, are to be expected from the nature of the Cu-Ni phase diagram (Hansen, 1958, p. 602), which shows that the liquidus and solidus of the continuous series of solid solutions are well separated for non-dilute alloys. The separation is about 70°C at a composition of 40 atomic percent Ni, and a solidus temperature of 1200°C.

The results of the characterization for three of the crystals are shown in Fig. IV-1. As mentioned in previous chapters, the method yields peaks similar to powder diffraction peaks. The position of the peak gives the lattice constant of the alloy. Its width, above the resolution width, gives the spread in lattice constant. If the lattice constant

depends reasonably strongly on composition, the position and width of the peak thereby respectively give the mean composition and inhomogeneity (spread in composition). In Fig. IV-1, the width (FWHM) of the peak for Cu(59%)Ni(41%) corresponds to a composition spread of about 38 atomic percent. The peak for Cu(81%)Ni(19%) shows a shoulder on the lower (smaller ø) side, perhaps indicating that there may be some separation into Cu-rich and Ni-rich parts. The lattice constants, implied compositions and inhomogeneities derived from the neutron characterizations are shown in the following table.

TABLE IV - 1

Characterization of Cu-Ni Alloy Crystals

Specimen Composition (atomic % Ni)	Lattice Constant (Å)	inhomogeneity (atomic % FWHM)
89 ± 2	3.532 ± .001	14 ± 10
81 ± 3	3.539 ± .002	33 ± 7
41 ± 2	3.573 ± .001	38 ± 5
20 ± 1	3.593 ± .001	10 ± 2

(ii) Neutron Scattering Measurements

All measurements were done in constant-Q scans, using the McMaster triple-axis spectrometer at Chalk River,

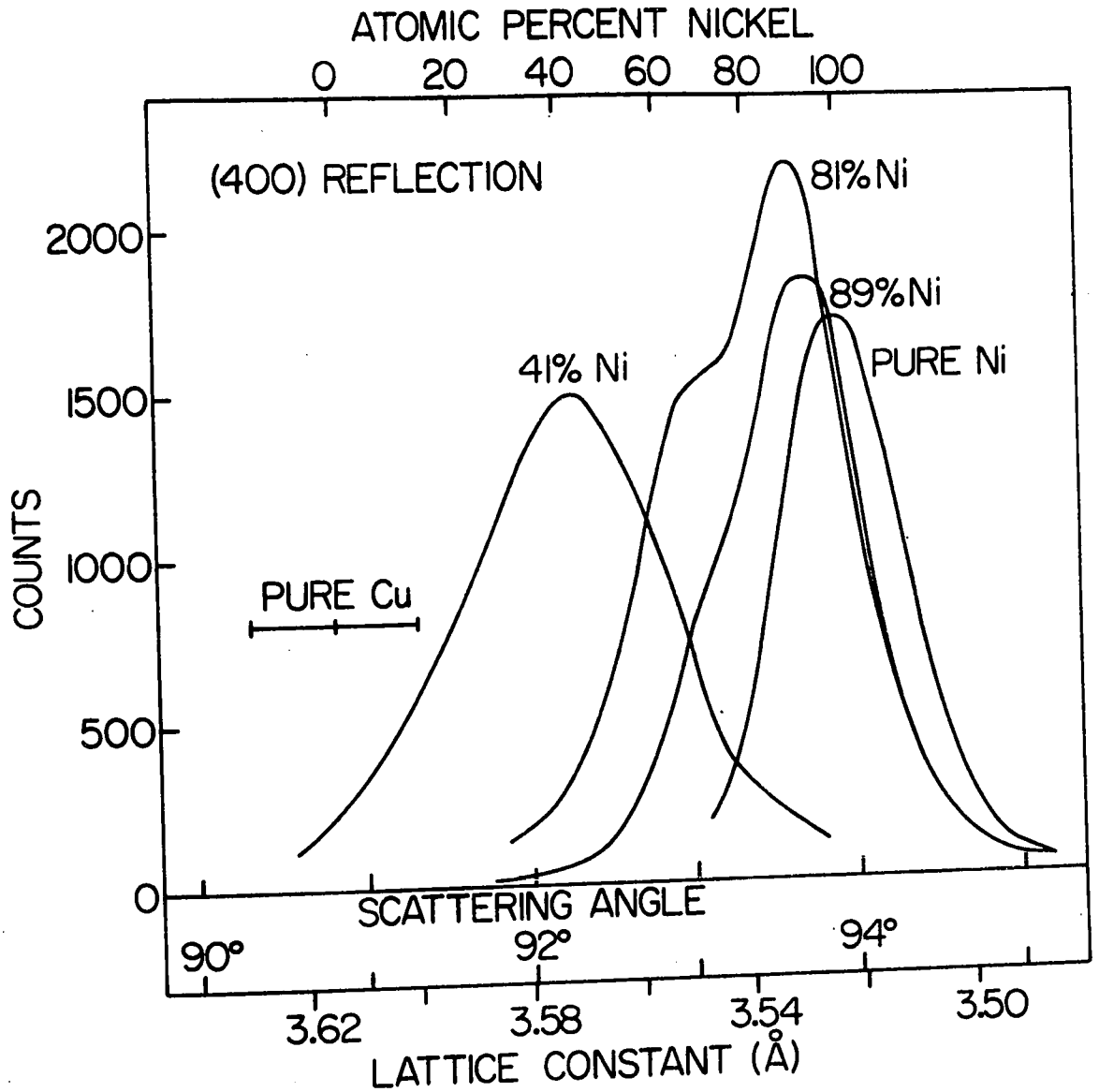

Fig. IV-1. Characterization of three copper-nickel alloy crystals by neutron diffraction.

described in Chapter I, with the specimen crystals at room temperature. Fixed incident-neutron energies, usually in the range from 10 to 15 THz, were used. No serious unexpected difficulties were encountered in this experiment. Apart from the moderately bad mosaic spreads and inhomogeneities of some of the specimen crystals, phonon measurements on crystals such as these are among the easiest experiments that one can do by inelastic neutron scattering, from the standpoints of simple structure, neutron properties, and ease of handling.

Complete dispersion curve measurements along the symmetry directions in the Brillouin zone were made for all specimen crystals, with the exception of Cu(95%)Ni(5%). In the latter case, measurements were made only for the $[\zeta\zeta 0]T_2$ and $[\zeta\zeta 0]L$ branches.

C. RESULTS AND DISCUSSION

(i) General Description of Results

The dispersion curves of nickel (Birgeneau et. al., 1964; de Wit and Brockhouse, 1968) are very similar to those of copper (Svensson, Brockhouse and Rowe, 1967), the phonon frequencies in Ni bearing roughly a constant ratio, about 1.24, to those in Cu. The dispersion curves for each of the Cu-Ni alloys were also found to exhibit very similar behaviour. The phonon frequencies are approximately given by interpolating the frequencies linearly in composition between the frequencies for the pure metals. Fig. IV-2 compares the measurements on Cu(59%)Ni(41%) with the dispersion curves of copper.

No unusual features have been noted in these results. In particular, the very anomalous features reported by Sakamoto and Hamaguchi (1968) for the $[\zeta\zeta 0]T_2$ and $[\zeta\zeta 0]L$ branches in Cu(95%)Ni(5%) and Cu(84%)Ni(16%) appear to be spurious. Perhaps the behaviour observed by them arises from a resolution effect associated with the accidental degeneracy of the $[\zeta\zeta 0]L$ and $[\zeta\zeta 0]T_2$ branches near $\zeta = 0.65$. Fig. IV-3 shows our measurements for these two branches in Cu(95%)Ni(5%) and Cu(80%)Ni(20%).

(ii) Absence of Disorder Broadening

Most of the measurements were taken with resolution that is probably too coarse to detect phonon natural widths,

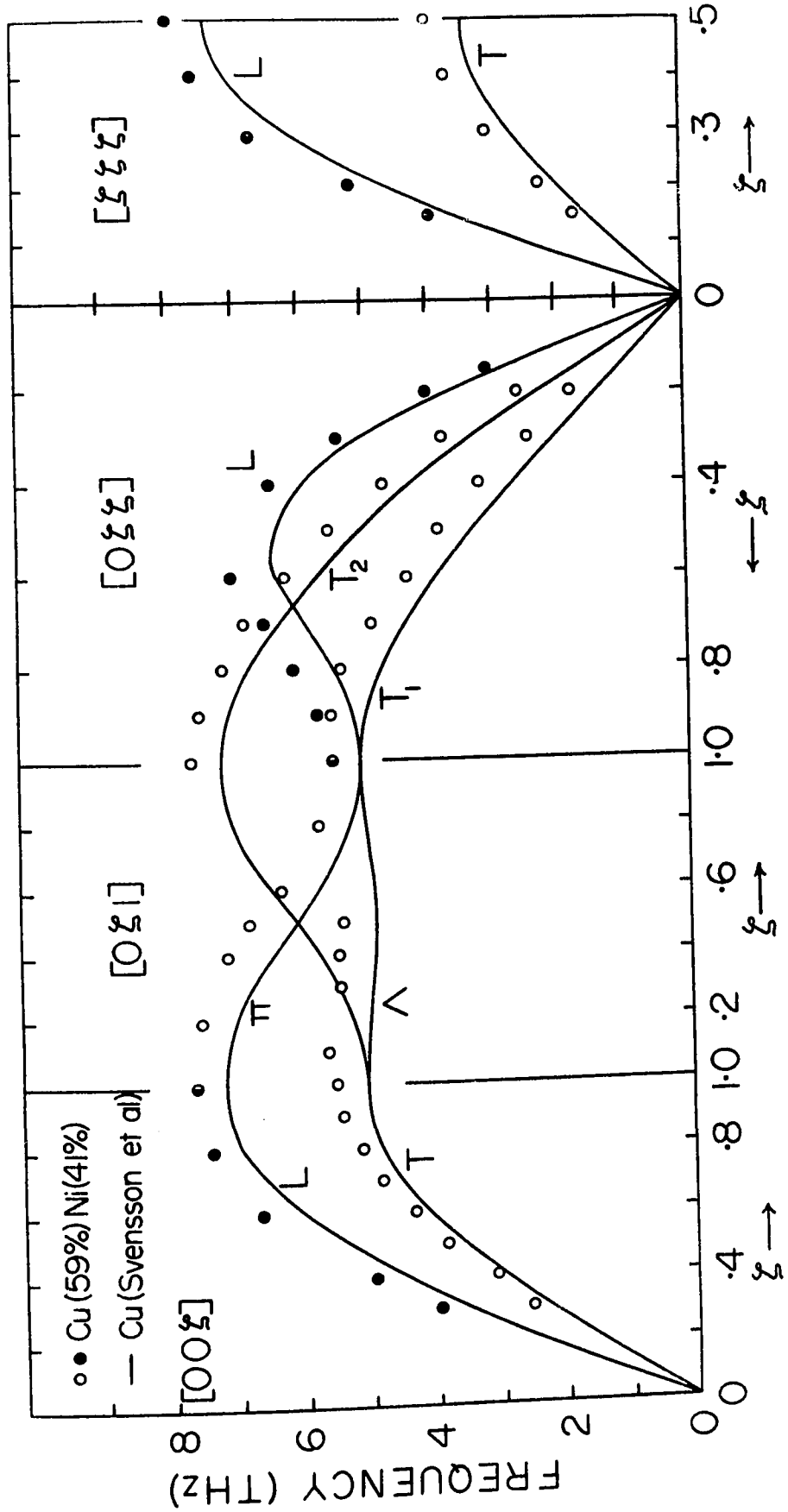

Fig. IV-2. Measured dispersion curves of Cu(59%)Ni(41%) compared with those of copper (Svensson et. al., 1967).

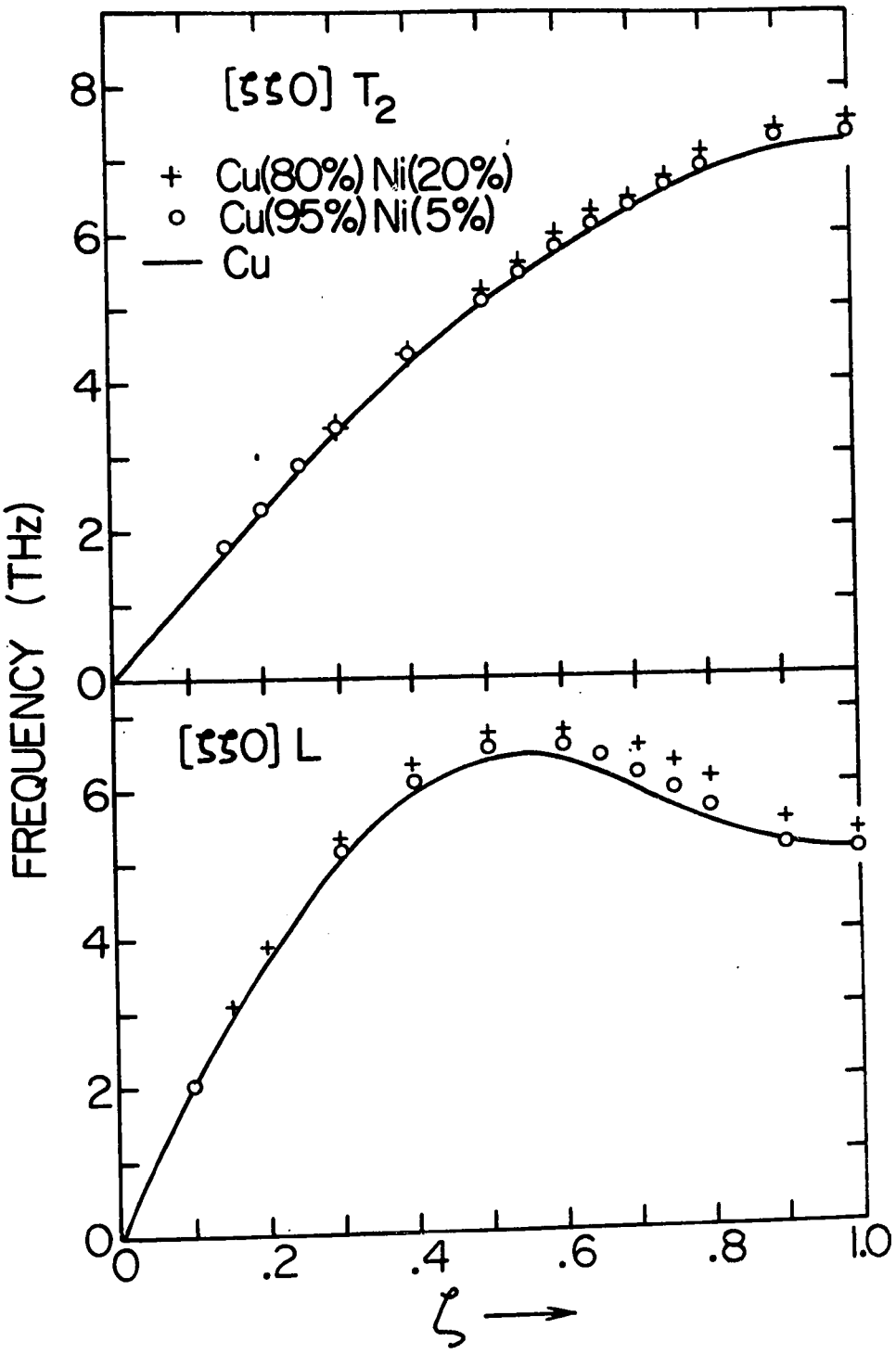

Fig. IV-3. The $[\zeta\zeta 0]T_2$ and $[\zeta\zeta 0]L$ branches of the dispersion curves of Cu(95%)Ni(5%) and Cu(80%)Ni(20%). The anomalous behaviour reported by Sakamoto and Hamaguchi (1968) is not observed. The solid line was smoothly drawn through the points of Svensson et. al. (1967) for pure copper.

if the following estimate of force constant disorder effects is taken to be an indication. The difference between the masses of Cu and Ni, 63.54 and 58.71 a.m.u. respectively, is much too small to produce observable disorder broadening. The perturbation theory result for mass disorder, Eq. III-14, predicts that the widths are proportional to the mean-square deviation of the atomic masses from the average atomic mass in the alloy. The following, rather similar, expression may be derived (Ng and Brockhouse, 1968; Ng, 1967) for force constant disorder.

$$\Gamma(\omega,\underline{q}) \simeq \frac{3\pi}{2}\frac{f(\omega)}{M^2\omega^2}\sum_{\substack{\ell' \\ (\ell'\neq\ell)}} <|\Delta\Phi^{\ell}_{\alpha\beta}(\underline{R}_{\ell\ell'}) \times [\exp(-i\underline{q}\cdot\underline{R}_{\ell\ell'}) - 1]|^2>_{\ell\alpha\beta} \quad . \qquad \text{(IV-1)}$$

As before, $f(\omega)$ is the phonon frequency distribution normalized to unity. The brackets $<\ >_{\ell\alpha\beta}$ denote a configuration average of all types of force constant changes that can occur at site ℓ, and also an average over the Cartesian indices α and β. Equation IV-1 is not as general as Eq. III-14; the situation for force constant disorder is more complicated than for mass disorder and several simplifying assumptions have been made, as detailed by Ng (1967). A few more assumptions allow us to make a rough estimate of Γ for Cu(50%)Ni(50%).

First of all, we assume that the force constants

depend just on the types of atoms at sites ℓ and ℓ' . That is, we have force constants Φ^{AA}, Φ^{AB}, and Φ^{BB} in the lattice between the A and B type atoms, with respective probabilities $c^2 = 1/4$, $2c(1-c)=1/2$, and $(1-c)^2=1/4$. The AB force constants are the most numerous and we assume that they are determining the average behaviour, and are given by the average of the AA and BB force constants, and that the latter are the same as for the pure metals. We consider only the large first neighbour force constants (4 out of 9 for each of the first neighbours), set them equal to each other, and set all the other force constants equal to zero. For Cu and Ni, this is not an unreasonable procedure. The nearest neighbour force constants 1XX and 1XY (see Table III-2 for nickel force constants) differ by less than 10% and are more than an order of magnitude larger than any of the other force constants. Hence we have $(\Delta\phi/\phi) = 0$ between A and B atoms, $(\Delta\phi/\phi) = \delta$ between two A atoms and $(\Delta\phi/\phi) = -\delta$ between two B atoms. At the zone boundary points X: $\underline{q} = \frac{2\pi}{a}(0,0,1)$ and L: $\underline{q} = \frac{2\pi}{a}(1/2,1/2,1/2)$, we can easily determine the value of $[\exp(-i\underline{q}\cdot\underline{R}_{\ell\ell'})-1]$ for each of the neighbours, and carry out the summation in Eq. IV-1. This gives the following values for disorder-induced widths.

$$\Gamma_L(X) = 0.1_3\text{THz} \qquad \Gamma_L(L) = 0.1_3\text{THz}$$

$$\Gamma_T(X) = 0.2_6\text{THz} \qquad \Gamma_T(L) = 0.5_2\text{THz}$$

Except for $\Gamma_T(L)$, the width of the [ζζζ]T zone boundary mode, these widths are too small to be detected with the resolution that we have used (from 0.7 to 1.0 THz FWHM). If we consider how the force constant changes might arise from the microscopic physical situation, as we do in the next section, we can see that these estimates are probably too large.

For the zone boundary modes measured in the experiment, no significant broadening above resolution was observed, nor even tendencies to indicate that natural widths are present. However, with the resolution that we have used, this just sets an upper limit of about 0.3 THz on the widths of the zone boundary modes. Away from the zone boundaries, focussing effects of the crystal spectrometer can give somewhat better resolution, but because of the inhomogeneities and fairly large mosaic spreads of some of the specimens, to check the widths of all the groups that were measured against resolution calculations would be a far more complicated task than is warranted by the information that might be gained. Fig. IV-4 shows the concentration dependence of a well-focussed neutron group of high frequency. It clearly shows that the effect of changing the composition is, for this mode, to smoothly shift a relatively narrow line. The concentration dependence of the phonon frequency is also shown in Fig. IV-4.

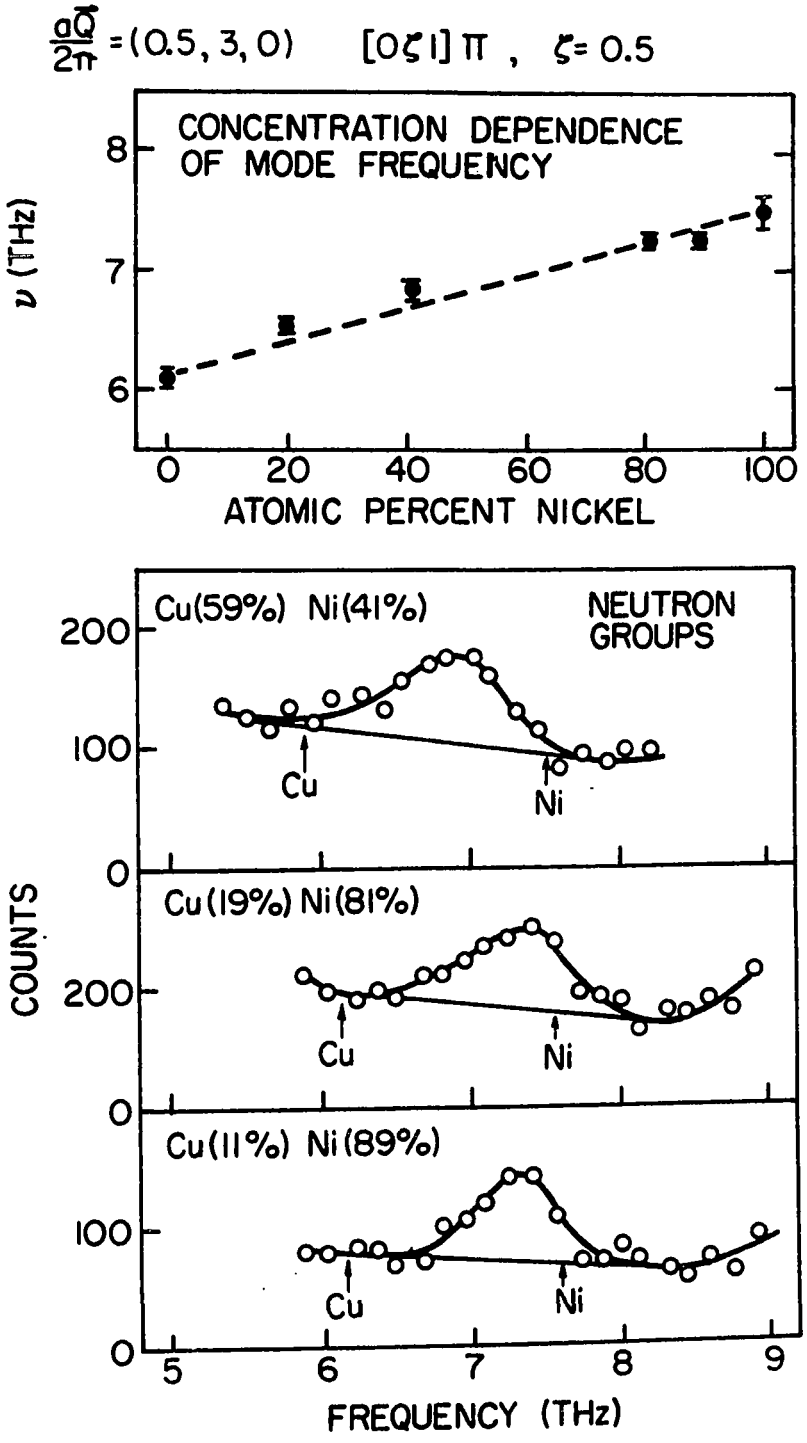

Fig. IV-4. Neutron groups for [0ζ1]Π, ζ = 0.5, in three Cu-Ni alloys. In these neutron groups, which are fairly well-focussed, there is no indication of disorder broadening. The concentration dependence of the mode frequency is almost linear.

From the absence of large phonon widths in the present experiment, the existence of a large fraction of the alloy constituents in clustered form appears to be less probable than a more or less random arrangement, although if the fractional clustered volume were fairly small, we probably would not notice the effect of the clusters in any case. The argument here is that a phonon of a certain wave vector propagating in a Ni cluster would have a higher frequency than one propagating in a Cu cluster.

(iii) Interpretation of Results

The main conclusions to be drawn from this experiment are negative ones. As shown in Fig. IV-5, the concentration dependence of the force constants, derived from fitting to the phonon frequencies, exhibits no features that can definitely be correlated with the changing electronic structure. The anomalous behaviour reported by Sakamoto and Hamaguchi (1968) was found to be spurious. If the lattice dynamics are in fact being primarily determined by the d and s electron concentrations, our data do not favour a rigid band model in which the d band fills at about 40 atomic percent nickel. In the rigid band picture, one would expect that the large first neighbour force constants would be about the same as in pure Ni up to about 40 at.% Ni, and then would start to decrease rapidly with the increasing s electron concentration. However, Fig. IV-5 shows that the force constants 1XX and 1XY decrease nearly linearly with Cu

Fig. IV-5. Composition dependence of first and second neighbour force constants for Fe-Ni, Cu-Ni, and Cu-Zn alloys. Except for the points for Cu-Ni alloys, which are the open circles, this figure has been reproduced from the Ph.D. thesis of E.D. Hallman (1969). The solid lines are just straight lines between the points for Cu (Svensson et. al., 1967) and Ni (Birgeneau et. al., 1964:; deWit and Brockhouse, 1968). Fifth neighbour models were used for the Fe-Ni and Cu-Zn alloys and for the pure metals. Fourth neighbour models were used for the Cu-Ni alloys.

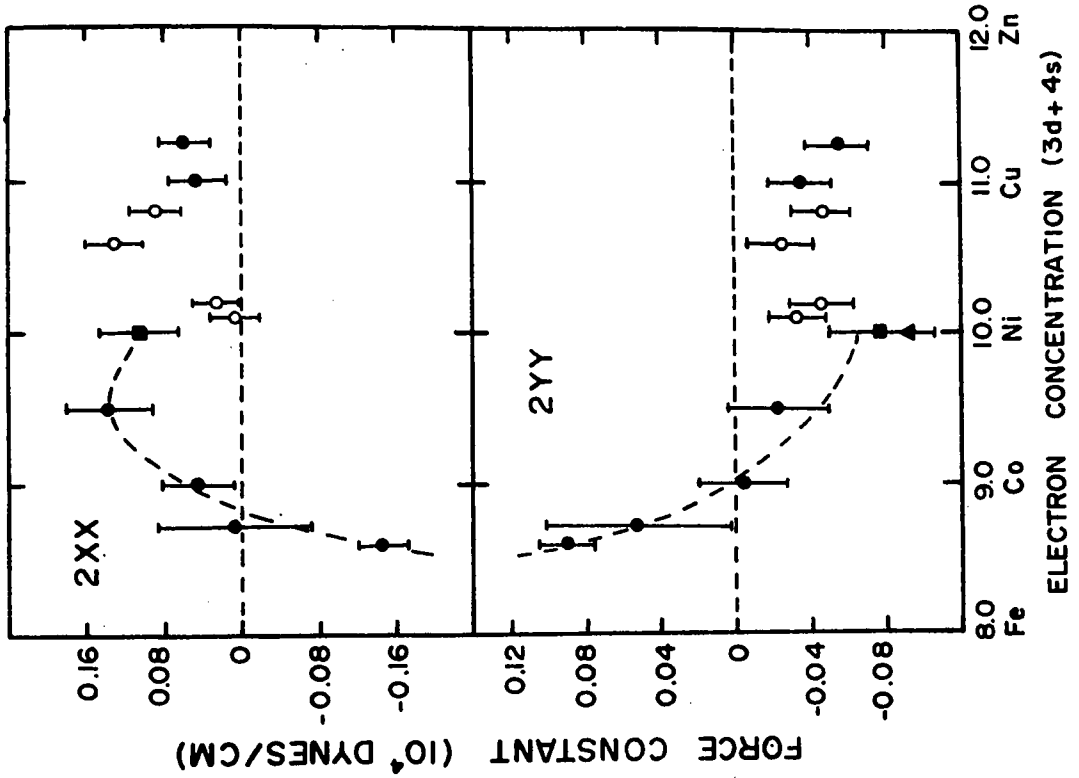
2XX
2YY
FORCE CONSTANT (10⁴ DYNES/CM)
0.16
0.08
0
-0.08
-0.16
0.12
0.08
0.04
0
-0.04
-0.08
8.0 Fe
9.0 Co
10.0 Ni
11.0 Cu
12.0 Zn
ELECTRON CONCENTRATION (3d+4s)

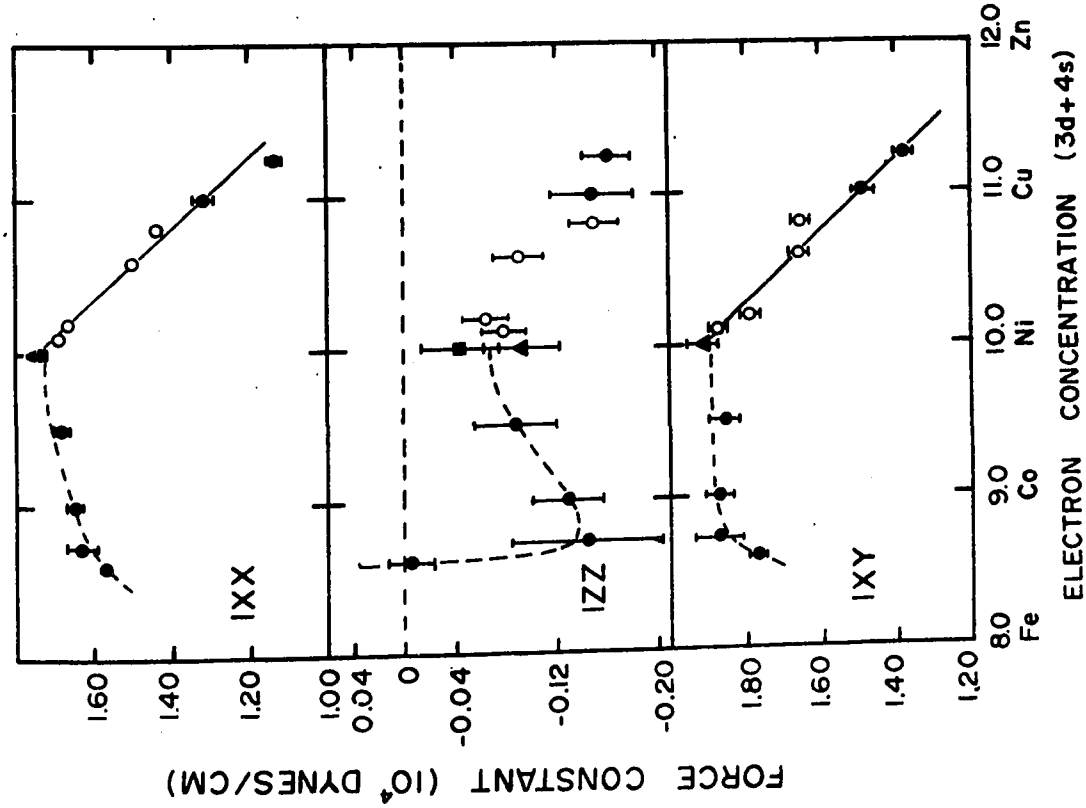
1XX
1ZZ
1XY
FORCE CONSTANT (10⁴ DYNES/CM)
1.60
1.40
1.20
1.00
0.04
0
-0.04
-0.12
-0.20
1.80
1.60
1.40
1.20
8.0 Fe
9.0 Co
10.0 Ni
11.0 Cu
12.0 Zn
ELECTRON CONCENTRATION (3d+4s)

concentration from 0 to 100% copper. We do not attach much significance to the behaviour of 1ZZ, 2XX, and 2YY, which are an order of magnitude smaller, although the Cu-Ni points for 2XX appear not to interpolate smoothly between the points for Cu, Ni, and the other alloys.

The following description provides a plausible but very uncertain explanation for our results. The d electrons are visualized as being localized on the nickel atoms, and to a large extent affect only the overlap forces, which are in themselves not changing much, since the total increase of the d electron concentration through the copper-nickel system is only about 10%, from 10 to 11 electrons per atom, and the effect of the d electrons on the cohesive forces is known to be largest near the middle of a transition metal row. Meanwhile, the s electron concentration is increasing more or less uniformly with copper concentration, repelling the ion cores, decreasing the overlap, and decreasing the large first neighbour force constants. The measurements of Hallman and Brockhouse (1969) show that the phonon frequencies in Fe-Ni alloys do not change much with the d electron concentration, but that the addition of a higher valence component, Zn, to Cu, increasing the s electron concentration, lowers the phonon frequencies. In Fig. IV-5, the points for the first neighbour force constants of Cu_3Zn appear to lie on the same straight lines as the points for Cu-Ni. This

is an indication, although a weak one, that the s electron concentration is the factor that is primarily determining the phonon frequencies. However, most of the above interpretation for the results on Cu-Ni alloys is merely conjecture. A model that considers AA, BB, and AB force constants, as estimated very simply in the preceding subsection (but not restricting the force constants to just first neighbours), with no reference to the electronic structure, must give a reasonable description of the phonon frequencies.

The dispersion curves of F.C.C. transition metal alloys are thus less easily correlated with the electronic structure than those of the F.C.C. polyvalent alloys of Bi, Pb, and Tl which were studied by Ng and Brockhouse (1968; Ng, 1967) and Roy (1970). In the case of Bi-Pb-Tl, alloys of equal electron concentration, such as Pb(40%)Tl(60%) and Bi(20%)Tl(80%), were observed to have very similar dispersion curves. The distortions produced by the electron-phonon interaction were observed to vary with the conduction electron concentration. Some of these distortions could be demonstrated to be Kohn anomalies, and the positions of the anomalies in wave vector could be observed to shift with alloy composition, in accord with the changing dimensions of the Fermi surface. It was also shown that the type of estimate that we have made above for force constant disorder gives phonon widths larger than are actually observed. This is presumably because the response of the conduction electrons

to the motion of the ion cores is such that the effects of the variable ionic charges are minimized. This observation, and the plausible belief that the s electrons are more or less uniformly distributed around the ions, and the very nearly equal size of the ion cores for Cu and Ni, make it appear reasonable that the phonon broadening from force constant disorder in Cu-Ni alloys is smaller than we have estimated above.

APPENDIX I

CRYSTAL DYNAMICS OF SILVER

Next to the alkali metals, the noble metals copper, silver, and gold are perhaps the simplest of metallic substances, in phenomenology if not in theoretical description. In Table AI-1 are listed some physical properties of Cu, Ag and Au relevant to neutron scattering measurements of the phonon dispersion curves.

In contrast to the alkali metals, which show decreasing melting temperatures and elastic constants with increasing atomic mass, the noble metals do not show such clear systematic variation in these properties.

Copper has very favourable neutron properties and its crystal dynamics have been very thoroughly studied (Sinha, 1966; Svensson, Brockhouse, and Rowe, 1967; Nicklow et. al., 1967; Miiller and Brockhouse, 1971). The moderately large absorption cross sections of silver and gold (see the following table) make inelastic neutron scattering measurements on these metals somewhat more difficult and considerably lengthen the experimental running times. In other respects the experiments are straightforward: the structures are simple (F.C.C.) and large single crystal specimens are easily obtainable. Although the ratio of coherent scattering to absorption cross sections is about the same for silver and gold, the latter is a slightly more difficult experimental

TABLE AI-1

Properties of Copper, Silver, and Gold.

	Cu	Ag	Au
Atomic Number	29	47	79
Atomic mass (amu)	63.54	107.87	196.97
Lattice constant[a] at room temperature (Å)	3.6147	4.0862	4.0785
Thermal neutron cross sections[b] (barns):			
$\sigma_{coherent}$	7.25 ± 0.4	4.5 ± 0.5	7.3 ± 0.1
$\sigma_{incoherent}$	$\approx$0.6	$\approx$1.1	—
[d] $\sigma_{absorption}$	3.77 ± 0.03	63.6 ± 0.6	98.8 ± 0.3
Elastic Constants[c] at 300°K (10^{11} dynes/cm):			
C_{11}	16.839 ± 0.2%	12.399 ± 1.5%	19.234 ± 1.5%
C_{12}	12.142 ± 0.44%	9.367 ± 1.5%	16.314 ± 1.5%
C_{44}	7.539 ± 0.25%	4.612 ± 0.5%	4.195 ± 0.5%
Melting temperature (°C)	1083°C		1063°C

[a] Pearson (1967), p.81.

[b] Hughes and Schwartz (1958); Goldberg et. al. (1966).

[c] Cu - Overton and Gaffney (1955);
Ag, Au - Neighbours and Alers (1958).

[d] Absorption cross sections are for a neutron velocity of 2200 m/s.

subject, because of the labour and expense involved in preparing suitable single crystal specimens. Also, the lower phonon frequencies caused by the larger mass of the Au atom make it desirable to carry out the measurements at nitrogen temperatures, in order to observe the dispersion curves in the absence of anharmonic effects. Nitrogen temperature measurements are also probably desirable for silver, but our data were all taken with the specimen at room temperature, in order not to further decrease the already weak scattered-neutron intensity, and also to permit easier handling of the specimen crystal. The cross section is higher at room temperature because of the factor $n(\omega)+1$ in the cross-section equation I-6. Also, the geometry of the crystal relative to the directions of the incident and scattered neutron beams, an important consideration in this experiment, can be more easily seen if the crystal is not enclosed in a cryostat.

In order to obtain adequate counting rates for the neutron groups in this experiment, the measurements were done with the specimen in a reflection geometry, with single crystals that covered a large fraction of the beam area (5 cm x 5 cm), and as large a scattering angle as possible (up to 145°). Two different single crystals were obtained for this experiment. The first was a cylindrical boule, 1" in diameter by 3 1/2" in length, with a (110) plane approximately along the cylinder axis. The boule was cut along this plane, giving two specimen crystals which were separately mounted, one so that the [001] direction was vertical (normal to the

scattering plane), and the other so that the [1$\bar{1}$0] direction was vertical. For some of the branches, the measurements were found to be very difficult with these specimens, and another crystal, slab-shaped, 2" x 2 1/2" x 1/4", with (001) major faces, was obtained to complete the experiment.

The measured dispersion curves are shown in Fig. AI-1. The lines represent a Born-von Kármán model fitted to the points, with force constants extending to fourth nearest neighbours. A third neighbour model was found to fit the data within errors, and in fact the data can be almost fitted with a first neighbour axially-symmetric model, in which there are only two independent parameters ($1XX_{AS} = 1XY_{AS} + 1ZZ_{AS}$). The axially-symmetric model (Lehman, Wolfram, and de Wames, 1962) assumes that the internal energy can be written as a sum of bond-stretching and bond-bending terms which have axial symmetry about the line joining a pair of atoms.

No unusual features are apparent in these dispersion surves. Apart from a scaling factor, they are very similar to the dispersion curves of other F.C.C. noble and transition metlas (Cu, Ni, Pd, Pt). For 68 points measured along the symmetry directions, the mean frequency ratio $\langle \nu(Ag) \rangle / \nu(Cu) \rangle$ is 0.675 with a standard deviation of 0.016 for a single ratio from the mean. This value agrees well with the criterion for homology of forces: $[\nu(Ag)/\nu(Cu)] = [(Ma^2)^{1/2}(Cu)/(Ma^2)^{1/2}(Ag)] = 0.6790$ although the relative splitting between high and low frequency modes is slightly larger in silver than in

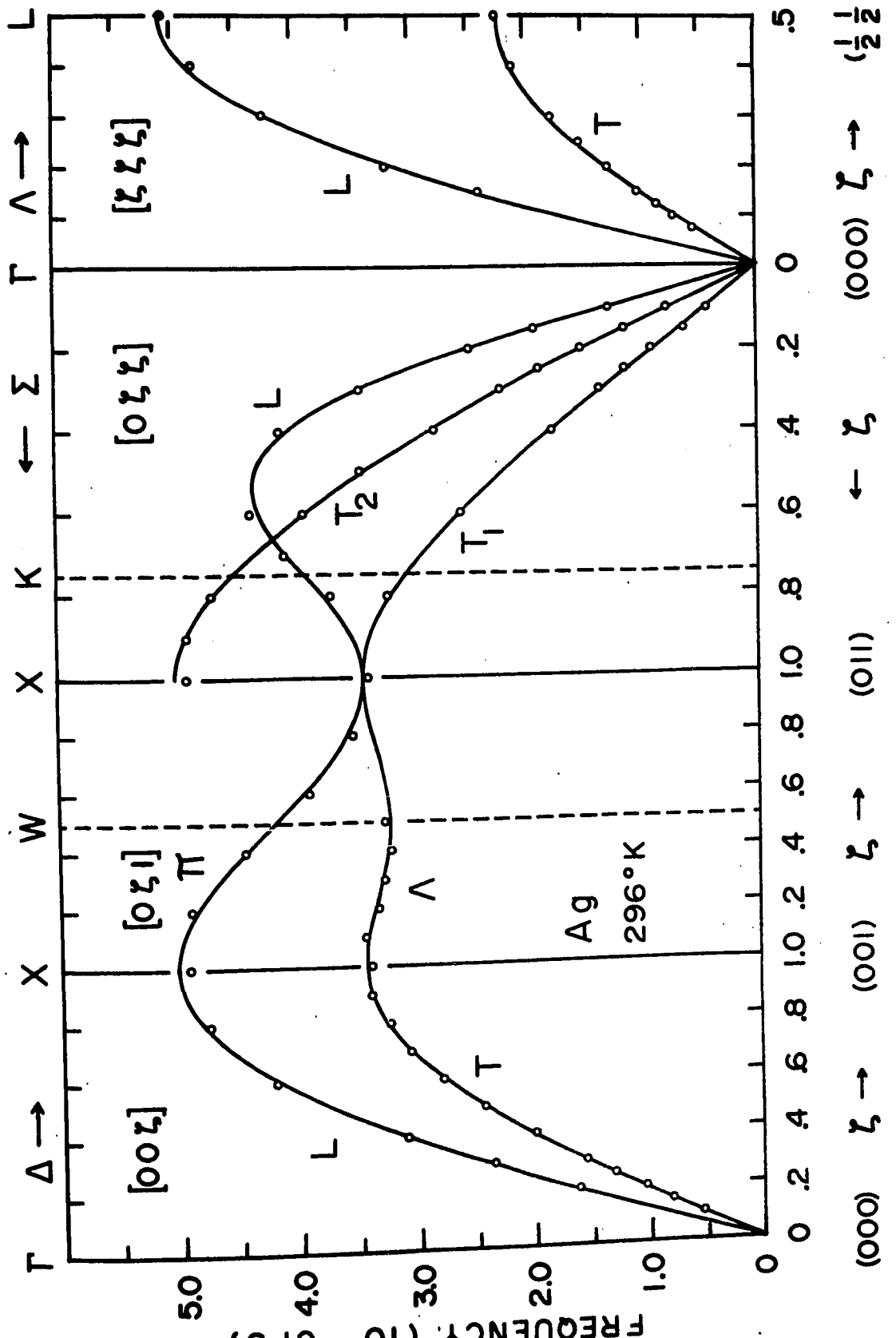

Fig. AI-1. The phonon dispersion curves of silver at room temperature. The solid lines represent a 4-neighbour Born-von Karman model fitted to the measurements.

copper. The homology criterion would hold exactly if the Ag and Cu force systems had the same form relative to their respective lattice constants. Table AI-2 gives the force constants derived from the 4-neighbour Born-von Kármán fit to the data. The force constants of Svensson et. al. for Cu are included for comparison. We note that the force constants of silver are somewhat smaller than those of copper, but otherwise the force systems must be very similar; even the order of the signs on the force constants is the same.

Also included in Table AI-2 are the force constants of Drexel, Gläser, and Gompf (1969), who have also measured the dispersion curves of silver using a time-of-flight neutron spectrometer. Our data, taken with the E2 crystal spectrometer at Chalk River, are almost certainly more accurate. There is reasonable agreement between the two experiments for the lower phonon frequencies, but some discrepancy exists for higher frequencies, where, however, Drexel et. al. have few measurements. The disagreement at higher frequencies is the source of the discrepancy between the force constants listed in Table AI-2.

Recent theoretical calculations of the phonon dispersion curves of silver from fairly basic models have been carried out by Nikulin and Tsarev (1971), Sharma and Singh (1971), and Prasad and Srivastava (1972). The treatment of Nikulin and Tsarev is a first-principles calculation, with no adjustable parameters. Fair agreement with the measured dispersion

TABLE AI-2. ATOMIC FORCE CONSTANTS OF SILVER AND COPPER AT 296°K (Units of 10^4 dynes/cm.).

FORCE CONSTANT	Ag		Cu
	DREXEL et. al.	PRESENT WORK	SVENSSON et. al.
1XX	0.95 ± .04	1.071 ± .017	1.314 ± .011
1ZZ	-0.05 .06	-0.175 .020	-0.123 .015
1XY	1.09 .09	1.232 .032	1.498 .020
2XX	0.12 .10	0.006 .029	0.006 .022
2YY	-0.08 .05	-0.023 .019	-0.011 .014
3XX	0.03 .04	0.052 .010	0.044 .007
3YY	0.01 .01	0.021 .009	0.032 .006
3YZ	0.003 .02	-0.005 .012	-0.018 .008
3XZ	0.03 .02	0.030 .007	0.036 .005
4XX		-0.013 .010	-0.006 .006
4ZZ		-0.014 .015	-0.046 .011
4XY		0.001 .018	0.007 .009

curves is obtained. Slightly better agreement is obtained by Sharma and Singh, who have used the values of the experimental elastic constants in their model.

APPENDIX II

DATA TABLES

All of the data discussed in Chapters II, III, and IV, and in Appendix I, are listed in the following tables. Phonon frequencies and widths are given in THz(10^{12}HZ). Wave vector coordinates are given in units of $2\pi/a$, where a is the lattice constant of the specimen crystal.

TABLE AII-1

Phonon frequency shifts Δ and widths Γ in Cu(9% Au). These data are plotted in Fig. II-2 and II-3. Also listed are the copper phonon frequencies ν(Cu) and the coordinates of the wave vector transfer $\underline{Q}$ used in the measurements. Each set of data is labelled with the name of the experimenter who took the measurements and the spectrometer used.

$[\zeta\zeta\zeta]T$ $\quad \underline{Q} = (2-\zeta, 2-\zeta, 2+\zeta)$ Kamitakahara,E2

ζ	ν(Cu)	Δ=ν(Cu)−ν(Cu(Au))	Γ(natural)
0.1	0.98 ±.02	-0.07 ±.03	0.12 ±.08
0.125	1.21*	-0.11 3	0.09 8
0.15	1.44*	-0.16 4	0.09 8
0.175	1.66*	-0.20 4	0.14 7
0.2	1.91 ±.03	-0.31 5	0.18 7
0.25	2.29*	-0.28 5	0.51 11
0.3	2.65 ±.04	-0.30 8	0.90 15
0.35	2.98*	-0.285 8	1.29 21
0.4	3.20 ±.05	-0.20 10	1.17 22
0.45	3.30*	-0.17 11	0.87 23
0.5	3.32 ±.06	-0.17 10	0.71 25

$[\zeta\zeta 0]T_1$ $\quad \underline{Q} = (2-\zeta, 2+\zeta, 0)$ Kamitakahara,E2

ζ	ν(Cu)	Δ	Γ(natural)
0.2	1.325±.02	-0.145±.05	0.10 ±.10
0.25	1.66 2	-0.195 5	0.20 9
0.3	1.99 2	-0.275 5	0.19 9
0.35	2.345 2	-0.345 6	0.33 10
0.4	2.68 2	-0.385 8	0.75 11
0.45	3.005 2	-0.37 11	1.07 12
0.5	3.305 2	-0.32 11	1.01 20
0.55	3.57*	-0.27 10	0.83 18
0.6	3.84 2	-0.24 10	0.99 15
0.65	4.12 5	-0.22 9	0.59 15
0.7	4.34 5	-0.16 7	0.46 13

*interpolated, not measured

C5 = triple-axis spectrometer at C5 beam facility, NRU reactor, Chalk River (Brockhouse, 1961)

E2 = McMaster University triple-axis spectrometer, NRU reactor, Chalk River (Brockhouse *et. al.*, 1968; see Chapter I).

MS = triple-axis spectrometer at the McMaster Nuclear Reactor, McMaster University, Hamilton, Ontario. (Brockhouse *et.al.*, 1968).

TABLE AII-1 (continued)

[00ζ]T $\underline{Q}$ = (2,ζ, 0) Sevensson,C5

ζ	ν(Cu)	Δ	Γ(natural)
0.2	1.58 ±.04	-0.18 ±.04	0.00 ±.03
0.25	1.93 3	-0.19 4	0.04 4
0.3	2.30 3	-0.24 4	0.075 4
0.35	2.66*	-0.31 8	0.36 6
0.4	3.02 4	-0.31 10	0.555 9
0.45	3.33*	-0.22 9	0.55 8
0.5	3.63 3	-0.23 8	0.45 8
0.6	4.17 4	-0.25 8	0.43 8
0.8	4.84 7	-0.18 11	0.165 13
1.0	5.10 8	-0.16 13	0.195 16

[00ζ]L Q = (0,2+ζ,0) Svensson,C5

ζ	ν(Cu)	Δ	Γ(natural)
0.15	1.90 ±.09	-0.19 ±.12	0.00 ±.06
0.2	2.42 7	-0.15 10	0.055 11
0.25	3.02 8	-0.18 11	0.305 10
0.3	3.56 6	-0.21 9	0.225 12
0.35	4.03*	-0.20 11	0.175 8
0.4	4.47 7	-0.23 11	0.395 13
0.45	4.91*	-0.23 11	0.365 14
0.5	5.32 7	-0.28 11	0.335 16
0.55	5.70*	-0.23 13	0.415 19
0.6	6.05 8	-0.27 11	0.16 22
0.65	6.37 8	-0.28 11	0.125 22
0.7	6.60 8	-0.28 11	0.075 23
0.75	6.77 12	-0.27 15	0.11 28
0.8	6.99 13	-0.39 16	0.00 43
0.9	7.17 12	-0.37 16	0.25 24
1.0	7.19 12	-0.34 16	0.00 20

* interpolated, not measured.

TABLE AII-2

Phonon frequency shifts Δ and widths Γ in Cu(3% Au). These data are plotted in Figs. II-4 and II-5. Both observed and natural widths are listed.

$[\zeta\zeta\zeta]T$ $\underline{Q} = (2-\zeta, 2-\zeta, 2+\zeta)$ Kamitakahara,E2

ζ	ν(Cu)	Δ	Γ(observed)	Γ(natural)
0.075	0.74*	+0.01 ±.04	0.36 ±.05	0.19 ±.07
0.1	0.98 ±.02	0.00 3	0.26 5	0.05 8
0.125	1.21*	+0.01 5	0.27 5	0.08 8
0.15	1.44*	+0.01 5	0.38 7	0.25 9
0.175	1.66*	-0.04 5	0.36 7	0.22 9
0.2	1.91 ±.03	-0.07 4	0.41 7	0.29 9
0.225	2.08*	-0.07 5	0.34 7	0.20 9
0.25	2.29*	-0.09 6	0.40 7	0.28 9
0.275	2.50*	-0.09 6	0.545 8	0.46 9
0.3	2.65 ±.04	-0.03 6	0.60 10	0.52 11
0.325	2.825*	-0.025 6	0.575 10	0.47 12
0.35	2.975*	-0.035 6	0.53 10	0.38 12
0.375	3.10 *	-0.04 6	0.485 10	0.28 14
0.4	3.20 ±.05	-0.03 5	0.53 10	0.30 13
0.425	3.265*	-0.035 6	0.495 10	0.20 15
0.45	3.30 *	-0.03 6	0.50 10	0.15 15
0.475	3.31 *	+0.04 6	0.505 10	0.10 16
0.5	3.32 ±.06	+0.025 6	0.56 10	0.14 16

$[\zeta\zeta 0]T_1$ $\underline{Q} = (2-\zeta, 2+\zeta, 0)$ Svensson,MS

ζ	ν(Cu)	Δ	Γ(observed)	Γ(natural)
0.1	0.69 ±.03	-0.02 ±.03	0.18 ±.03	0.00 ±.06
0.125	0.84 3	-0.01 3	0.215 3	0.015 6
0.15	1.00 3	-0.02 3	0.19 3	0.00 6
0.175	1.17 3	-0.035 3	0.22 3	0.035 5
0.2	1.325 3	-0.045 3	0.20 3	0.00 6
0.225	1.495 3	-0.06 3	0.215 3	0.035 5
0.25	1.66 3	-0.065 3	0.245 3	0.09 5
0.275	1.83 3	-0.09 3	0.27 3	0.13 5
0.3	2.01 3	-0.105 3	0.29 5	0.16 6
0.325	2.18 3	-0.11 3	0.30 7	0.18 8
0.35	2.34 3	-0.085 4	0.39 5	0.30 7
0.375	2.50 3	-0.08 5	0.48 7	0.405 8
0.4	2.67 4	-0.045 5	0.42 7	0.335 8
0.425	2.89 3	+0.02 6	-	
0.45	3.01 3	+0.02 4	0.35 5	0.25 6

*interpolated, not measured

TABLE AII-2 (continuation page 1)

$[\zeta\zeta 0]T_1$ $\underline{Q} = (2-\zeta, 2+\zeta, 0)$ Kamitakahara,E2

ζ	ν(Cu)	Δ	Γ(observed)	Γ(natural)
0.125	0.835±.02	-0.035±.03	0.195±.03	0.00 ±.06
0.15	0.995 2	-0.03 3	0.23 3	0.05 5
0.175	1.155 2	-0.055 3	0.20 3	0.00 6
0.2	1.325 2	-0.065 3	0.21 3	0.02 6
0.225	1.495 2	-0.075 3	0.205 3	0.015 6
0.25	1.66 2	-0.095 3	0.22 3	0.045 5
0.275	1.83 2	-0.11 3	0.25 3	0.10 5
0.3	1.99 2	-0.105 3	0.33 4	0.215 6
0.325	2.17 2	-0.10 4	0.40 5	0.305 6
0.35	2.345 2	-0.11 4	0.405 5	0.315 6
0.375	2.505 2	-0.08 4	0.375 5	0.28 6
0.4	2.68 2	-0.06 4	0.475 5	0.40 6
0.425	2.845 2	-0.01 4	0.345 5	0.24 6
0.45	3.005 2	-0.015 4	0.36 4	0.26 6
0.475	3.155 2	-0.015 4	0.30 4	0.18 6
0.5	3.305 2	-0.015 4	0.29 4	0.165 6
0.525	3.46 2	-0.05 4	0.325 4	0.215 6
0.55	3.57*	-0.03 4	0.30 4	0.175 6
0.6	3.84 2	-0.045 4	0.33 5	0.205 7
0.625	3.945*	-0.025 4	0.275 5	0.12 8

[00ζ]T $\underline{Q} = (2, \zeta, 0)$ Kamitakahara,E2

ζ	ν(Cu)	Δ	Γ(observed)	Γ(natural)
0.15	1.20*	-0.065±.04	0.29 ±.04	0.01 ±.08
0.2	1.605±.02	-0.07 4	0.265 3	0.01 6
0.25	1.985 2	-0.10 3	0.225 3	0.00 4
0.275	2.185 2	-0.115 3	0.28 4	0.08 7
0.3	2.355 2	-0.11 3	0.30 4	0.12 6
0.325	2.55 2	-0.12 3	0.32 4	0.15 6
0.35	2.71 2	-0.09 4	0.355 4	0.21 6
0.375	2.885 2	-0.09 4	0.375 4	0.24 5
0.4	3.06 2	-0.115 4	0.365 4	0.23 5
0.45	3.39 2	-0.09 4	0.33 4	0.19 6
0.6	4.18 2	-0.075 4	0.26 4	0.10 6
0.65	4.395 2	-0.075 4	0.265 4	0.10 6
0.7	4.57 2	-0.07 4	0.30 4	0.16 6

Data set #1

*interpolated, not measured.

TABLE AII-2 (continuation page 2)

[00ζ]T $\underline{Q}$ = (2, ζ, 0) Kamitakahara,E2

ζ	ν(Cu)	Δ	Γ(observed)	Γ(natural)
0.15	1.19 ±.02	-0.065±.03	0.28 ±.03	0.00 ±.06
0.175	1.39 2	-0.065 3	0.255 3	0.00 2
0.2	1.59 2	-0.09 3	0.205 3	0.00
0.225	1.78 2	-0.09 3	0.25 3	0.00 1
0.25	1.96 3	-0.11 4	0.285 3	0.015 6
0.275	2.16 2	-0.13 3	0.25 3	0.00 2
0.3	2.34 2	-0.15 4	0.31 3	0.075 5
0.325	2.52 2	-0.14 4	0.415 6	0.245 8
0.475	3.51 3	-0.13 4	0.31 7	0.185 10
0.5	3.64 3	-0.09 4	0.285 7	0.165 10
0.525	3.78 4	-0.12 4	-	-
0.55	3.91 4	-0.11 4	-	-

Data set #2

TABLE AII-3

Phonon frequency shifts in Cu(1% Au)

[00ζ]T $\underline{Q}$ = (2,ζ,0)

ζ	ν(Cu)	Δ
0.15	1.19 ±.02	-0.045±.03
0.2	1.585 2	-0.062 3
0.25	1.962 2	-0.077 3
0.3	2.339 2	-0.071 3
0.4	3.052 3	-0.066 4
0.45	3.344 2	-0.034 3
0.5	3.65 2	-0.055 3

Data set #2

[00ζ]T $\underline{Q}$ = (2,ζ,0)

ζ	ν(Cu)	Δ
0.2	1.582±.02	-0.039±03
0.225	1.78 2	-0.059 3
0.25	1.962 2	-0.052 3
0.275	2.15 2	-0.069 3
0.3	2.332 2	-0.072 3
0.325	2.519 2	-0.075 3
0.35	2.688 2	-0.049 3
0.375	2.87 2	-0.068 3
0.4	3.03 2	-0.058 3
0.425	3.205 2	-0.053 3
0.575	4.038 2	-0.023 3
0.6	4.152 2	-0.047 3
0.625	4.26 2	-0.024 3

Data set #1

$[\zeta\zeta 0]T_1$ $\underline{Q}$ = (2-ζ,2+ζ,0)

ζ	ν(Cu)	Δ
0.125	0.833±.02	-0.013±03
0.15	0.995 2	-0.025 3
0.175	1.156 2	-0.025 3
0.2	1.325 2	-0.027 3
0.225	1.497 2	-0.047 3
0.25	1.66 2	-0.045 3
0.275	1.83 2	-0.05 3
0.3	1.99 2	-0.04 3
0.325	2.17 2	-0.038 3
0.35	2.345 2	-0.043 3
0.375	2.503 2	-0.046 3
0.4	2.68 2	-0.038 3
0.425	2.845 2	-0.023 3
0.45	3.005 2	-0.02 3
0.475	3.157 2	-0.009 3
0.5	3.305 2	-0.023 3
0.525	3.46 2	-0.03 3
0.55	3.57*	+0.001 3
0.575	3.72 2	-0.02 3
0.6	3.84 2	-0.018 3

*interpolated, not measured

TABLE AII-4

Phonon frequencies ν and natural widths Γ in Ni(55%)Pd(45%). Within the data for each branch, the measurements of data set #1 represent measurements with better resolution than those of data set #2. These data are plotted in Figs.III-4 and III-7.

$[\zeta\zeta\zeta]T$ $\quad \underline{Q} = (2-\zeta, 2-\zeta, 2+\zeta)$

ζ	ν	Γ(set#1)	Γ(set#2)
0.2	1.87±.04	0.40±.10	0.42±.12
0.25	2.17 6	0.21 10	
0.3	2.49 7	0.55 10	0.38 12
0.325	2.64 8	0.50 11	
0.35	2.91 17	1.54 9	
0.375	3.13 22	1.93 23	
0.4	3.17 18	1.92 23	1.53 31
0.45	3.18 22	1.90 27	
0.5	3.42 24	2.25 27	1.96 35

$[\zeta\zeta 0]T_1$ $\quad \underline{Q}(\#1) = (2-\zeta, 2+\zeta, 0) \quad \underline{Q}(\#2) = (4-\zeta, 2+\zeta, 0)$

ζ	ν	Γ (set#1)	Γ (set#2)
0.15	1.12±.03	0.00±.03	
0.175	1.25 3	0.00 8	
0.2	1.43 4	0.19 9	
0.225	1.54 4	0.07 10	
0.25	1.68 4	0.01 11	
0.275	1.83 5	0.19 11	
0.3	2.02 4	0.14 13	0.04±.17
0.325	2.13 5	0.19 16	
0.35	2.20 6	0.32 14	
0.375	2.42 5	0.21 15	
0.4	2.51 6	0.34 14	0.43 19
0.425	2.69 10	0.84 16	
0.45	2.80 11	1.03 21	0.87 18
0.475	2.98 14	1.31 42	
0.5	3.39 16		1.47 16
0.55	3.73 15		1.36 16
0.6	4.11 18		1.62 18
0.7	4.59 15		1.28 17
0.8	4.94 13		1.02 19
0.9	5.09 14		1.12 21
1.0	5.17 13		0.98 16

TABLE AII-4 (continuation page 1)

$[00\zeta]T$	$\underline{Q}$(#1) = (4,ζ,0)		$\underline{Q}$(#2) = (3,3,ζ-1)	
ζ	ν	Γ(set #1)	Γ(set #2)	
0.175	1.35±.04	0.00±.03		
0.2	1.48 5	0.00 16		
0.225	1.67 4	0.00		
0.25	1.85 4	0.00 3		
0.275	2.02 4	0.00 5		
0.3	2.17 5	0.06 19		
0.325	2.31 5	0.00 9		
0.35	2.48 5	0.08 20		
0.375	2.68 7	0.38 10		
0.4	2.82 6	0.19 12	0.41±.14	
0.425	3.04 8	0.49 13		
0.45	3.12 6	0.28 12		
0.475	3.25 6	0.26 10		
0.5	3.45 8	0.57 13	0.32	19
0.6	3.88 12	0.55 19	0.83	23
0.7	4.39 10		0.99	22
0.8	4.82 13		1.07	17
0.9	5.02 11		0.79	19
1.0	5.20 13		0.99	16

$[\zeta\zeta 0]T_2$	$\underline{Q}$ = (-ζ,-ζ,4)			
ζ	ν	Γ(set #1)	Γ(set #2)	
0.2	2.18±.04	0.11±.12		
0.25	2.65 4	0.20 15		
0.3	3.17 6	0.44 19	0.58±.10	
0.35	3.73 10	0.94 22		
0.4	4.29 12	1.12 21	0.99	16
0.45	4.74 8	0.65 22	1.12	27
0.5	5.17 8	0.92 21	0.62	29
0.55	5.54 7	0.57 24	0.54	30
0.6	5.91 7	0.55 24	0.44	38
0.65	6.30 9	0.82 28	0.49	32
0.7	6.56 11	0.94 33	0.93	46
0.75	6.87 11	0.94 34		
0.8	7.15 10	0.73 24	0.84	49
0.85	7.24 10	0.45 35		
0.9	7.32 8	0.45 29	0.48	48
0.95	7.52 10	0.24 30		
1.0	7.48 13	0.84 32		

TABLE AII-4 (continuation page 2)

$[\zeta\zeta 0]_L$ $\quad \underline{Q}(\#1) = (2+\zeta, 2+\zeta, 0) \quad \underline{Q}(\#2) = (4-\zeta, 4-\zeta, 0)$

ζ	ν	Γ(set #1)	Γ(set #2)
0.1	1.99±.04	0.00	
0.15	2.84 5	0.00±.17	
0.2	3.68 7	0.36 22	
0.25	4.41 7	0.42 21	
0.3	5.12 7	0.39 21	
0.35	5.77 9	0.61 25	
0.4	6.07 13	1.05 45	
0.45	6.46 10	0.68 25	
0.5	6.65 10	0.59 26	
0.6	6.73 20		0.53±.54
0.7	6.15 20		0.88 54
0.8	5.75 10		0.59 27
0.9	5.46 13		0.94 38
1.0	5.14 13		0.92 25

$[00\zeta]_L$ $\quad \underline{Q} = (1, 1, 3+\zeta)$

ζ	ν	Γ
0.15	1.95±.04	0.07±.23
0.2	2.56 5	0.12 23
0.25	3.12 5	0.24 23
0.3	3.65 6	0.34 21
0.35	4.12 4	0.16 22
0.4	4.64 6	0.37 20
0.45	5.24 7	0.51 18
0.5	5.68 6	0.40 25
0.55	5.93 6	0.43 26
0.6	6.32 9	0.68 24
0.65	6.64 6	0.34 22
0.7	6.84 9	0.69 31
0.8	7.22 10	0.61 27
0.9	7.31 12	0.77 39
1.0	7.41 12	0.76 40

TABLE AII-4 (continuation page 3)

$[\zeta\zeta\zeta]_L$ $\quad\quad \underline{Q} = (2+\zeta, 2+\zeta, 2+\zeta)$

ζ	ν	Γ
0.05	1.25±.10	0.01±.49
0.075	1.81 7	0.09 32
0.1	2.43 6	0.00 23
0.125	3.02 8	0.26 30
0.15	3.64 8	0.35 30
0.175	4.11 8	0.42 30
0.2	4.67 9	0.71 25
0.225	5.10 11	0.76 25
0.25	5.52 7	0.36 27
0.275	5.90 9	0.59 27
0.325	6.66 9	0.57 27
0.35	6.90 12	0.92 24
0.375	7.10 13	1.02 30
0.4	7.34 13	1.04 35
0.45	7.47 15	1.20 60
0.5	7.51 14	0.95 39

TABLE AII-5

Phonon frequencies in copper-nickel alloys.

(1) Cu(95%) Ni(5%)

$[\zeta\zeta 0]T_2$

ζ	ν
0.15	1.82±.05
0.2	2.33 5
0.25	2.91 5
0.3	3.42 4
0.4	4.39 5
0.5	5.12 6
0.55	5.49 5
0.6	5.84 5
0.65	6.16 6
0.7	6.41 6
0.75	6.70 7
0.8	6.93 7
0.9	7.32 8
1.0	7.36 7

$[\zeta\zeta 0]L$

ζ	ν
0.3	5.15±.07
0.4	6.07 7
0.5	6.52 10
0.6	6.54 9
0.65	6.40 9
0.7	6.17 8
0.75	5.92 8
0.8	5.68 10
0.9	5.14 9
1.0	5.04 9

(2) Cu(80%) Ni(20%)

$[00\zeta]T$

ζ	ν
0.3	2.44±.05
0.4	3.13 4
0.5	3.86 7
0.6	4.36 6
0.7	4.72 6
0.8	5.02 8
0.9	5.24 8

$[00\zeta]L$

ζ	ν
0.15	1.94±.04
0.2	2.58 6
0.4	4.70 7
0.5	5.47 10
0.6	6.39 7
0.7	6.94 9
0.8	7.27 10

$[\zeta\zeta\zeta]T$

ζ	ν
0.2	2.09±.07
0.3	2.90 7
0.4	3.37 7
0.5	3.61 8

$[\zeta\zeta\zeta]L$

ζ	ν
0.1	2.58±.07
0.2	4.77 10
0.3	6.40 7
0.4	7.49 9
0.5	7.73 8

$[0\zeta 1]\Lambda$

ζ	ν
0.0	5.32±.08
0.1	5.40 8
0.2	5.36 11
0.3	5.21 10
0.4	5.18 11
0.5	5.15 11

$[0\zeta 1]\Pi$

ζ	ν
0.2	7.49±.06
0.4	6.85 6
0.5	6.53 7
0.6	6.19 14
0.8	5.67 11

TABLE AII-5 (continuation page 1)

$[\zeta\zeta 0]T_2$

ζ	ν
0.2	2.38±.05
0.3	3.34 7
0.4	4.39 6
0.5	5.23 6
0.55	5.62 5
0.6	6.00 5
0.65	6.32 7
0.7	6.55 6
0.75	6.82 8
0.8	7.10 8
0.9	7.41 8
1.0	7.60 8

$[\zeta\zeta 0]L$

ζ	ν
0.1	2.04±.04
0.15	3.09 6
0.2	3.96 8
0.3	5.36 7
0.4	6.33 7
0.5	6.72 15
0.6	6.76 15
0.65	6.54 10
0.7	6.32 7
0.75	6.10 7
0.9	5.51 12
1.0	5.35 12

$[\zeta\zeta 0]T_1$

ζ	ν
0.2	1.55±.04
0.3	2.21 3
0.4	2.92 4
0.5	3.60 5
0.6	4.12 7
0.7	4.56 8

(3) Cu(59%) Ni(41%)

$[00\zeta]T$

ζ	ν
0.3	2.57±.08
0.4	3.12 10
0.5	3.88 8
0.6	4.38 8
0.7	4.87 8
0.8	5.17 9
0.9	5.46 7
1.0	5.50 10

$[00\zeta]L$

ζ	ν
0.3	4.01±.06
0.4	4.99 5
0.6	6.69 7
0.8	7.44 7
1.0	7.57 9

$[\zeta\zeta\zeta]T$

ζ	ν
0.15	1.67±.07
0.2	2.20 6
0.3	3.02 7
0.4	3.64 8
0.5	3.93 8

$[\zeta\zeta 0]T_2$

ζ	ν
0.2	2.61±.10
0.3	3.78 10
0.4	4.71 10
0.5	5.56 7
0.6	6.23 8
0.7	6.86 8
0.8	7.20 8
0.9	7.55 7
1.0	7.67 9

$[\zeta\zeta 0]L$

ζ	ν
0.15	3.08±.06
0.2	4.02 5
0.3	5.41 7
0.4	6.51 7
0.5	7.11 10
0.6	7.07 7
0.7	6.58 7
0.75	6.40 6
0.8	6.12 6
0.9	5.75 7
1.0	5.56 8

$[\zeta\zeta 0]T_1$

ζ	ν
0.2	1.71±.12
0.3	2.42 8
0.4	3.20 8
0.5	3.85 9
0.6	4.35 11
0.7	4.90 10
0.8	5.38 8
0.9	5.54 11
1.0	5.52 11

TABLE AII-5 (continuation page 2)

[ζζζ]L

ζ	ν
0.15	3.90±.15
0.2	5.14 20
0.3	6.67 10
0.4	7.54 10
0.5	7.89 10

[0ζ1]Λ

ζ	ν
0.0	5.61±.09
0.1	5.67 10
0.3	5.48 10
0.4	5.48 9
0.5	5.41 10

[0ζ1]Π

ζ	ν
0.0	7.81±.15
0.2	7.58 10
0.4	7.18 10
0.5	6.83 9
0.6	6.34 8
0.8	5.77 11
1.0	5.53 10

(4) Cu(19%) Ni(81%)

[00ζ]T

ζ	ν
0.2	1.95±.05
0.3	2.81 4
0.4	3.60 4
0.5	4.34 4
0.6	4.91 4
0.7	5.40 4
0.8	5.74 6
0.9	6.01 6
1.0	6.06 7

[00ζ]L

ζ	ν
0.2	2.93±.05
0.3	4.17 9
0.4	5.37 6
0.6	7.12 6
0.8	8.01 10
1.0	8.24 10

[ζζζ]T

ζ	ν
0.15	1.90±.06
0.2	2.33 6
0.3	3.25 5
0.4	3.84 7
0.5	4.07 5

[ζζ0]T_2

ζ	ν
0.2	2.76±.05
0.3	4.04 5
0.4	5.14 6
0.5	6.06 4
0.6	6.81 5
0.7	7.40 8
0.75	7.63 9
0.8	7.96 7
0.9	8.17 7
1.0	8.29 10

[ζζ0]L

ζ	ν
0.15	3.41±.08
0.2	4.30 7
0.3	5.91 5
0.4	6.98 6
0.6	7.39 7
0.7	7.08 6
0.75	6.96 5
0.8	6.67 4
0.9	6.15 5
1.0	5.92 7

[ζζ0]T_1

ζ	ν
0.2	1.80±.07
0.3	2.65 8
0.4	3.44 7
0.5	4.14 7
0.6	4.84 8
0.7	5.37 8
0.8	5.70 8
0.9	5.95 9
1.0	6.02 10

TABLE AII-5 (continuation page 3)

[ζζζ]L

ζ	ν
0.15	4.17±.09
0.2	5.44 6
0.3	7.15 9
0.4	8.15 9
0.5	8.34 8

[0ζ1]Λ

ζ	ν
0.0	5.94±.09
0.1	5.98 8
0.3	5.89 10
0.4	5.91 10
0.5	5.99 10

[0ζ1]Π

ζ	ν
0.0	8.37±.07
0.2	8.17 7
0.4	7.55 7
0.5	7.26 8
0.6	6.88 10
0.8	6.21 9
1.0	5.95 10

(5) Cu(11%) Ni(89%)

[00ζ]T

ζ	ν
0.2	1.93±.03
0.3	2.86 3
0.4	3.67 3
0.5	4.42 3
0.6	5.05 3
0.7	5.54 4
0.8	5.93 5
0.9	6.05 8
1.0	6.23 8

[00ζ]L

ζ	ν
0.2	2.97±.07
0.3	4.31 7
0.4	5.49 7
0.6	7.24 6
0.8	8.22 7
1.0	8.39 12

[ζζζ]T

ζ	ν
0.15	1.97±.05
0.2	2.45 5
0.3	3.33 5
0.4	3.96 5
0.5	4.19 7

[ζζ0]T_2

ζ	ν
0.2	2.82±.03
0.3	4.11 3
0.4	5.20 3
0.5	6.14 3
0.6	6.88 5
0.7	7.54 6
0.75	7.80 7
0.8	8.06 6
0.9	8.36 8
1.0	8.36 8

[ζζ0]L

ζ	ν
0.15	3.41±.08
0.2	4.44 7
0.3	6.00 5
0.4	7.03 7
0.6	7.57 10
0.7	7.26 9
0.75	7.09 5
0.8	6.84 5
0.9	6.42 6
1.0	6.12 6

[ζζ0]T_1

ζ	ν
0.2	1.83±.06
0.3	2.69 6
0.4	3.43 5
0.5	4.12 6
0.6	4.79 7
0.7	5.39 8
0.9	5.93 11
1.0	6.01 9

TABLE AII-5 (continuation page 4)

[ζζζ]	
ζ	ν
0.15	4.25±.09
0.2	5.49 7
0.3	7.27 8
0.4	8.35 6
0.5	8.52 10

[0ζ1]Λ	
ζ	ν
0.0	6.10±.10
0.1	6.06 9
0.3	5.88 10
0.4	5.94 8
0.5	5.99 8

[0ζ1]Π	
ζ	ν
0.0	8.37±.12
0.2	8.24 13
0.4	7.67 12
0.5	7.26 13
0.6	7.09 12
0.8	6.58 16
1.0	6.13 15

TABLE AII-6

Phonon frequencies in silver at 296°K

[0ζζ]T_1

ζ	ν	
0.1	0.43±.03	
0.15	0.62	5
0.2	0.91	6
0.25	1.14	4
0.3	1.36	4
0.4	1.78	4
0.6	2.58	5
0.8	3.21	5
1·0	3.37	6

[0ζζ]T_2

ζ	ν	
0.1	0.77±.03	
0.15	1.14	3
0.2	1.52	3
0.25	1.89	5
0.3	2.22	6
0.4	2.80	5
0.5	3.44	5
0.6	3.92	6
0.8	4.71	8
0.9	4.92	8
1.0	4.93	11

[0ζζ]L

ζ	ν	
0.1	1.28±.07	
0.15	1.93	7
0.2	2.50	5
0.3	3.44	7
0.4	4.12	8
0.5	4.38	10
0.7	4.09	7
0.8	3.70	8

[ζζζ]T

ζ	ν	
0.075	0.54±.04	
0.1	0.71	3
0.125	0.85	3
0.15	1.02	3
0.2	1.27	6
0.25	1.53	7
0.3	1.76	5
0.4	2.10	5
0.5	2.24	5

[ζζζ]L

ζ	ν	
0.15	2.40±.07	
0.2	3.20	7
0.3	4.24	7
0.4	4.82	9
0.5	5.07	5

[00ζ]T

ζ	ν	
0.1	0.54±.03	
0.15	0.81	3
0.2	1.04	2
0.25	1.31	3
0.3	1.56	3
0.4	2.00	4
0.5	2.45	3
0.6	2.80	3
0.7	3.08	3
0.8	3.25	5
0.9	3.40	6

[00ζ]L

ζ	ν	
0.2	1.63±.12	
0.3	2.36	10
0.4	3.11	10
0.6	4.21	8
0.8	4.77	10

[0ζ1]π

ζ	ν	
0.2	4.91±.08	
0.4	4.45	8
0.6	3.90	7
0.8	3.53	6
1.0	3.42	6

[0ζ1]Λ

ζ	ν	
0.1	3.44±.06	
0.2	3.33	6
0.3	3.27	6
0.4	3.21	6
0.5	3.26	7

BIBLIOGRAPHY

J. G. Adler, J. E. Jackson and B. S. Chandrasekhar, Phys. Rev. Lett. 16, 53(1966).

R. L. Agacy, Proc. Phys. Soc. 83, 591(1964).

R. N. Aiyer, R. J. Elliott, J. A. Krumhansl and P. L. Leath, Phys. Rev. 181, 1006(1969).

G. A. Alers, J. R. Neighbours, and H. J. Sato, J. Phys. Chem. Solids 13, 40(1960).

J. Als-Nielsen, in Neutron Inelastic Scattering, Vol. I (IAEA, Vienna,1968), p.35.

R. J. Birgeneau, J. Cordes, G. Dolling and A.D.B. Woods, Phys. Rev. 136, A1359(1964).

H. Bjerrum Møller and A. R. Mackintosh, Phys. Rev. Lett. 15, 623(1965).

B. N. Brockhouse, in Inelastic Scattering of Neutrons in Solids and Liquids (IAEA, Vienna, 1961),p.113; in Phonons and Phonon Interactions, edited by T. A. Bak (W. A. Benjamin, Inc., New York, 1964), p.221; in Phonons in Perfect Lattices and in Lattices with Point Imperfections, edited by R.W.H. Stevenson (Oliver and Boyd, Edinburgh, 1966), p. 110.

B. N. Brockhouse, G. A. deWit, E. D. Hallman and J.M. Rowe, in Neutron Inelastic Scattering, Vol. II (IAEA, Vienna, 1968), p.259.

B. N. Brockhouse, S. Hautecler and H. Stiller, in The Interaction of Radiation with Solids, edited by R. Strumane, J. Nihoul, R. Gevers and S. Amelinckx (North-Holland Publishing Co., Amsterdam, 1964), p.580.

R. Brout and W. M. Visscher, Phys. Rev. Lett. 9, 54(1962).

R. Bruno and D. W. Taylor, Can. J. Phys. 49, 2496(1971).

W.J.L. Buyers and R.A. Cowley, in Neutron Inelastic Scattering, Vol. I (IAEA, Vienna, 1968), p.43.

B. S. Chandrasekhar and J. G. Adler, in Localized Excitations in Solids, edited by R. F. Wallis (Plenum Press, New York, 1968), p.694.

I. F. Chang and S. S. Mitra, Phys. Rev. 172, 924(1968).

N. A. Chernoplekov, G.Kh. Panova, M. G. Zemlyanov, B. N. Samoilov, and V. I. Kutaitsev, Phys. Stat. Sol. 20, 767(1967).

N. A. Chernoplekov and M. G. Zemlyanov, Soviet Physics JETP 22, 315(1966).

N. A. Chernoplekov, M. G. Zemlyanov, E. G. Brovman, and A. G. Chicherin, Soviet Physics Solid State 5, 78 (1963); also in Inelastic Scattering of Neutrons in Solids and Liquids, Vol. II (IAEA, Vienna, 1963), p.173 (in Russian).

B. P. Clayman and A. J. Sievers, in Localized Excitations in Solids, edited by R. F. Wallis (Plenum Press, New York, 1968),p.54.

M. F. Collins, Brit. J. Appl. Phys. 14, 805 (1963).

M. J. Cooper and R. Nathans, Acta Cryst. 23, 357(1967).

R. A. Cowley, in Neutron Inelastic Scattering, Vol. I (IAEA, Vienna, 1968), p.89 (discussion).

R. A. Cowley and W. J. L. Buyers, Rev. Mod. Phys. 44, 406(1972).

R. M. Cunningham, L. D. Muhlestein, W. M. Shaw and C. W. Tompson, Phys. Rev. B 2, 4864(1970).

R. W. Davies and J. S. Langer, Phys. Rev. 131, 163(1963).

P. G. Dawber and R. J. Elliott, Proc. Roy. Soc. A273, 222(1963).

P. Dean, Proc. Phys. Soc. 73, 413(1959); Proc. Roy. Soc. A254, 507(1960); ibid. A260, 263(1961); Rev. Mod. Phys. 44, 127(1972).

P. Dean and M. D. Bacon, Proc. Roy. Soc. A283, 64(1965).

P. Dean and J. L. Martin, Proc. Roy. Soc. A259, 409(1960).

G. A. deWit and B. N. Brockhouse, J. Appl. Phys. 39, 451(1968).

G. Dolling and A. D. B. Woods, in Thermal Neutron Scattering, edited by P. A. Egelstaff (Academic Press, New York, 1965) pp.205ff.

C. Domb, A. A. Maradudin, E. W. Montroll and G. H. Weiss, Phys. Rev. 115, 18(1959); ibid. 115, 24(1959).

W. Drexel, W. Gläser and F. Gompf, Phys. Lett. 28A, 531(1969).

R. C. Dynes, Phys. Rev. B 2, 644(1970); ibid. 4, 3255(1971) (erratum).

F. J. Dyson, Phys. Rev. 92, 1331(1953).

R. J. Elliott, Argonne National Laboratory report ANL-7237 (1966).

R. J. Elliott, Comments on Solid State Physics 1, 177(1969).

R. J. Elliott and A. A. Maradudin, in Inelastic Scattering of Neutrons, Vol. I (IAEA, Vienna, 1965), p.231.

R. J. Elliott and D. W. Taylor, Proc. Roy. Soc. A296, 161(1967).

R. Englman, Nuovo Cimento 10, 615(1958).

P. A. Flinn, G. M. McManus, and J. A. Rayne, J. Phys. Chem. Solids 15, 189(1960).

G. Gilat, Solid State Commun. 7, 55(1969).

M. D. Goldberg, S. F. Mughabghab, B. A. Magurno and V. M. May, Neutron Cross Sections, Brookhaven National Laboratory report BNL-325, 2nd Edition, Suppl. No. 2, Vols. IIA and IIC (1966).

E. D. Hallman, Ph.D. Thesis, McMaster University, 1969 (unpublished).

E. D. Hallman and B. N. Brockhouse, Can. J. Phys. 47, 1117(1969).

W. Hanke and H. Bilz, to be published in the Proceedings of a Symposium on Neutron Inelastic Scattering (IAEA, Vienna, 1972), held at Grenoble, France, March 6-10, 1972.

M. Hansen, Constitution of Binary Alloys (McGraw-Hill, New York, 1958).

W. M. Hartmann, Phys. Rev.172, 677(1968).

D. J. Hughes and R. B. Schwartz, Neutron Cross Sections, Brookhaven National Laboratory report BNL-325, 2nd Edition (1958).

Instrumentation for Neutron Inelastic Scattering Research, Proceedings of a panel, Vienna, 1-5 December 1969 (IAEA, Vienna, 1970).

Yu. M. Kagan and Ya. A. Ioselevskii, Soviet Physics JETP 15, 182(1962); ibid 17, 925(1963).

W. A. Kamitakahara and B. N. Brockhouse, Phys. Lett. 29A, 639(1969).

A. Kidron, Phys. Lett. 30A, 304(1969).

M. A. Krivoglaz, Theory of X-ray and Thermal Neutron Scattering by Real Crystals (Plenum Press, New York, 1969),p.341.

K. Lakatos and J. A. Krumhansl, Phys. Rev. 175, 841(1968); ibid 180, 729(1969).

J. S. Langer, J. Math. Phys. 2, 584(1961).

M. Lax, Rev. Mod. Phys. 23, 287(1951).

P. L. Leath, Phys. Rev. 171, 725(1968); Phys. Rev. B 5, 1643(1972).

P. L. Leath and B. Goodman, Phys. Rev. 148, 968(1966); ibid. 175, 963(1968); ibid. 181, 1062(1969).

G. W. Lehman, T. Wolfram and R. E. DeWames, Phys. Rev. 128, 1593(1962).

I. M. Lifshitz, Nuovo Cimento Suppl. 3, 716(1956).

A. R. Mackintosh and H. Bjerrum Møller, in Localized Excitations in Solids, edited by R. F. Wallis (Plenum Press, New York, 1968), p.721.

S. V. Maleev, Soviet Physics JETP 12, 617(1961).

A. A. Maradudin, Solid State Physics, Vol. 18, edited by F. Seitz and D. Turnbull (Academic Press, New York, 1966 a), p.273; Solid State Physics, Vol. 19, edited by F. Seitz and D. Turnbull (Academic Press, New York, 1966 b), p.1.

W. Marshall and S. W. Lovesey, Theory of Thermal Neutron Scattering (Oxford University Press, Oxford, 1971), p.38ff.

D. L. Martin, Phys. Rev. 141, 576(1966).

J. L. Martin, Proc. Roy. Soc. A260, 139(1961).

D. C. Mattis, Phys. Rev. 106, 721(1957); ibid. 107, 1736(1957) (erratum).

W. L. McMillan and J. M. Rowell, Phys. Rev. Lett. 14, 108(1965).

A. P. Miiller and B. N. Brockhouse, Phys. Rev. Lett. 20, 798(1968); Can. J.Phys. 49, 704(1971).

E. W. Montroll and R. B. Potts, Phys. Rev. 100, 525(1955); ibid. 102, 72(1956).

S. C. Moss, Phys. Rev. Lett. 23, 381(1969).

B. Mozer, in Neutron Inelastic Scattering, Vol. I (IAEA, Vienna, 1968), p.55.

B. Mozer, D. T. Keating, and S. C. Moss, Phys. Rev. 175, 868(1968).

B. Mozer, K. Otnes and V. W. Myers, Phys. Rev. Lett. 8, 278(1962).

B. Mozer, K. Otnes and H. Palevsky, in Lattice Dynamics, edited by R. F. Wallis (Pergamon Press, London, 1965), p.63.

B. Mozer, K. Otnes and C. Thaper, Phys. Rev. 152, 535(1966).

L. D. Muhlestein, E. Gürmen and R. M. Cunningham, to be published in the Proceedings of a Symposium on Neutron Inelastic Scattering (IAEA, Vienna, 1972), held at Grenoble, France, March 6-10, 1972; also see W. M. Shaw and L. D. Muhlestein, Phys. Rev. B 4, 969(1971).

V. Narayanamurti and R. O. Pohl, Rev. Mod. Phys. 42, 201(1970).

I. Natkaniec, K. Parliński, A. Bajorek and M. Sudnik-Hrynkiewicz, Phys. Lett. 24A, 517(1967).

I. Natkaniec, K. Parliński, J. A. Janik, A. Bajorek, and M. Sudnik-Hrynkiewicz, in Neutron Inelastic Scattering, Vol. I (IAEA, Vienna, 1968), p.65.

J. R. Neighbours and G. A. Alers, Phys. Rev. 111, 707(1958).

S. C. Ng, Ph.D. Thesis, McMaster University, 1967 (unpublished).

S. C. Ng and B. N. Brockhouse, in Neutron Inelastic Scattering, Vol. I (IAEA, Vienna, 1968), p.253.

S. C. Ng, B. N. Brockhouse and E. D. Hallman, Materials Research Bull. 2, 69(1967).

R. M. Nicklow, G. Gilat, H. G. Smith, L. J. Raubenheimer and M. K. Wilkinson, Phys. Rev. 164, 922(1967).

R. M. Nicklow, P. R. Vijayaraghavan, H. G. Smith, and M. K. Wilkinson, Phys. Rev. Lett. 20, 1245(1968a).

R. M. Nicklow, P. R. Vijayaraghavan, H. G. Smith, G. Dolling, and M. K. Wilkinson, in Neutron Inelastic Scattering, Vol. I (IAEA, Vienna, 1968b), p.47.

V. K. Nikulin and Yu. N. Tsarev, Phys. Lett. 36A, 337(1971).

G. Nilsson, in Neutron Inelastic Scattering, Vol. I (IAEA, Vienna, 1968), p.187.

I. G. Nolt, R. A. Westig, R.W. Alexander,Jr., and A. J. Sievers, Phys. Rev. 157, 730(1967).

S. G. O'Hara and B. J. Marshall, Phys. Rev. B 3, 4002(1971).

W. C. Overton, Jr. and J. Gaffney, Phys. Rev. 98, 969(1955).

D. N. Payton and W. M. Visscher, Phys. Rev. 154, 802(1967a); ibid. 156, 1032(1967b); ibid. 175, 1201 (1968).

W. B. Pearson, A Handbook of Lattice Spacings and Structures of Metals and Alloys (Pergamon Press, New York, 1958); ibid.,Vol. 2 (Pergamon Press, New York, 1967).

G. Placzek and L.Van Hove, Phys. Rev. 93, 1207(1954).

R. O. Pohl, in Localized Excitations in Solids, edited by R. F. Wallis (Plenum Press, New York, 1968), p.434.

B. M. Powell, G. Dolling, L. Piseri and P. Martel, to be published in the Proceedings of a Symposium on Neutron Inelastic Scattering (IAEA, Vienna,1972), held at Grenoble, France, March 6-10, 1972.

B. M. Powell, P. Martel and A. D. B. Woods, Phys. Rev. 171, 727(1968).

J. L. Powell and B. Crasemann, Quantum Mechanics, (Addison-Wesley, Reading, Mass.,1961), p.408ff.

S. Prakash and S. K. Joshi, Phys. Rev. B 4, 1770(1971).

B. Prasad and R. S. Srivastava, J. Phys. F. 2, 247(1972).

Lord Rayleigh, Theory of Sound, (Dover, New York, 1945).

J. A. Rayne, Phys. Rev. 118, 1545(1960).

J. M. Rowell, W. L. McMillan and P. W. Anderson, Phys. Rev. Lett. 14, 633(1965).

A. P. Roy, Ph.D. Thesis, McMaster University, 1970 (unpublished).

R. Rubin, J. Peretti, G. Verdon and W. Kley, Phys. Lett. 14, 100(1965).

M. Sakamoto and Y. Hamaguchi, in Neutron Inelastic Scattering, Vol. I (IAEA, Vienna, 1968), p.181.

G. Schaefer, J. Phys. Chem. Solids 12, 233(1960).

H. Schmidt, Phys. Rev. 105, 425(1957).

D. H. Seib and W. E. Spicer, Phys. Rev. B 2, 1676(1970); ibid. 2, 1694(1970).

P. K. Sharma and N. Singh, Phys. Rev. B 4, 4636(1971).

A. J. Sievers, Phys. Rev. Lett. 13, 310(1964).

S. K. Sinha, Phys. Rev. 143, 422(1966).

P. Soven, Phys. Rev. 156, 809(1967); also see Phys. Rev. 178, 1136(1969).

A. T. Stewart and B. N. Brockhouse, Rev. Mod. Phys. 30, 250(1958).

E. C. Svensson, Ph.D. Thesis, McMaster University, 1967 (unpublished).

E. C. Svensson and B. N. Brockhouse, Phys. Rev. Lett. 18, 858(1967).

E. C. Svensson, B. N. Brockhouse and J. M. Rowe, Solid State Commun. 3, 245(1965); Phys. Rev. 155, 619(1967).

E. C. Svensson, W. J. L. Buyers, T. M. Holden, R. A. Cowley, and R. W. H. Stevenson, in Magnetism and Magnetic Materials - 1971, AIP Conference Proceedings, No. 5, part 2 (American Institute of Physics, 1972), p.1315.

E. C. Svensson and W. A. Kamitakahara, Can. J. Phys. 49, 2291(1971).

S. Takeno, Progr. Theoret. Phys. (Kyoto) 29, 191(1963).

D. W. Taylor, Ph.D. Thesis, Oxford University, 1965 (unpublished).

D. W. Taylor, Phys. Rev. 156, 1017(1967).

D. W. Taylor and P. Vashishta, Phys. Rev. B 5, 4410(1972).

L. Van Hove,Phys. Rev. 95, 249(1954a).

L. Van Hove,Phys. Rev. 95, 1374(1954b).

L. Van Hove,Physica's Grav. 24, 404(1958).

W. M. Visscher, in Proceedings of the Second Mössbauer Conference, Paris, 1961, edited by D.M.J. Compton and A. H. Schoen (Wiley and Sons, New York, 1962), p.30.

N. Wakabayashi, R. M. Nicklow and H. G. Smith, Phys. Rev. B 4, 2558(1971).

M. G. Zemlyanov, S. P. Mironov and G. F. Syrykh, in Neutron Inelastic Scattering, Vol. I (IAEA, Vienna, 1968), p.79.

D. N. Zubarev, Soviet Physics Uspekhi 3, 320(1960).